

# **INTRAMOLECULARLY SENSITIZED PRECIPITONS**

by

**Mark R. Ams**

B.A., Albion College, 2002

M.S., University of Pittsburgh, 2005

Submitted to the Graduate Faculty of  
University of Pittsburgh in partial fulfillment  
of the requirements for the degree of  
Doctor of Philosophy

University of Pittsburgh

2007

UNIVERSITY OF PITTSBURGH  
FACULTY OF ARTS AND SCIENCES

This dissertation was presented

by

Mark R. Ams

It was defended on

March 26, 2007

and approved by

Billy W. Day, Ph.D., Professor, Pharmaceutical Sciences

Joe Grabowski, Ph.D., Associate Professor, Chemistry

Stephane Petoud, Ph.D., Assistant Professor, Chemistry

Dissertation Advisor: Craig S. Wilcox, Ph.D., Professor, Chemistry

## **INTRAMOLECULARLY SENSITIZED PRECIPITONS**

Mark R. Ams, Ph.D.

University of Pittsburgh, 2007

This dissertation describes the first intramolecularly activated precipitons. The isomerization process is induced by intramolecular triplet energy transfer from a covalently attached sensitizer. The intramolecular sensitization leads to a more rapid isomerization than can be achieved by intermolecular sensitization at accessible concentrations. Two different types of intramolecularly sensitized precipitons were investigated. The first precipiton receives intramolecular sensitization from a covalently attached metal complex ( $\text{Ru}(\text{bpy})_3\text{Cl}_2$ ). It was used in a model study for the sequestration of metal contaminants. The second precipiton receives intramolecular sensitization from a covalently attached organic compound (benzil). The preparation, photophysical properties, and photoisomerization kinetics of these precipitons, as well as the precipitation event, are discussed.

## TABLE OF CONTENTS

TABLE OF CONTENTS.....	iv
LIST OF TABLES.....	vii
LIST OF FIGURES.....	viii
LIST OF SCHEMES.....	xiv
ACKNOWLEDGMENTS.....	xvi
1.0 INTRODUCTION.....	1
1.1 THE PRECIPITON APPROACH.....	2
1.2 PRECIPITON ISOMERIZATION METHODS.....	3
1.3 INTRAMOLECULARLY SENSITIZED PRECIPITONS.....	9
1.3.1 Design Strategies for Intramolecular Energy Transfer.....	10
1.3.2 Design of Intramolecularly Sensitized Precipitons.....	14
1.4 DISSERTATION OVERVIEW.....	20
2.0 PRECIPITONS FOR METAL SEQUESTRATION.....	22
2.1 INTRODUCTION.....	23
2.2 AN ENERGY DRIVEN SEQUESTRATION PROCESS.....	25
2.3 PRECIPITON DESIGN.....	26
2.4 RESULTS AND DISCUSSION.....	27
2.4.1 Synthesis.....	27

2.4.2	Absorption and Emission Spectroscopy .....	30
2.4.3	Photoisomerization Reactivity.....	33
2.4.3.1	Electronic Absorption Studies.....	33
2.4.4	Kinetics.....	36
2.5	CONCLUSION: RUTHENIUM TETHERED PRECIPITONS AS A MODEL SYSTEM FOR METAL SEQUESTRATION.....	39
2.6	ADDITIONAL PRECIPITONS FOR METAL SCAVENGING.....	40
2.6.1	Tetraethyldiethylenetriamine (TEDETA) Functionalized Precipitons .....	40
2.6.2	Bipyridine Functionalized Precipiton with a Rigid Phenylene.....	42
3.0	BENZIL TETHERED PRECIPITONS FOR CONTROLLING SOLUBILITY .....	47
3.1	INTRODUCTION.....	48
3.2	PRECIPITON DESIGN.....	48
3.3	RESULTS AND DISCUSSION.....	51
3.3.1	Synthesis.....	51
3.3.2	Absorption and Emission Spectroscopy .....	53
3.3.3	Photoisomerization Kinetics.....	57
3.4	INVESTIGATION OF THE ENERGY TRANSFER PATHWAY .....	61
3.4.1	Proposal of a Round-Trip Energy Transfer Pathway.....	63
3.4.2	Effect of the Attached Benzil on the Precipiton Photostationary States.....	67
3.5	CONCLUSION.....	67
4.0	THE PRECIPITATION EVENT .....	69
4.1	INTRODUCTION.....	70
4.2	RESULTS AND DISCUSSION.....	71

4.3	CONCLUSION.....	79
5.0	SUMMARY AND FUTURE DIRECTIONS .....	81
6.0	EXPERIMENTAL .....	84
6.1	GENERAL.....	85
6.2	EXPERIMENTAL PROCEDURES.....	87
6.2.1	Synthesis and Characterization.....	87
6.2.2	<sup>1</sup> H NMR Spectra, <sup>1</sup> H- <sup>1</sup> H COSY, and <sup>13</sup> C NMR Spectra.....	104
6.2.3	Photoisomerization Experiments .....	135
6.2.3.1	<sup>1</sup> H NMR Monitored Isomerizations.....	135
6.2.3.2	UV-Vis Monitored Isomerizations of 17Z/E .....	135
6.2.3.3	UV-Vis Monitored Isomerizations of 28Z/E and 29Z/E.....	136
	REFERENCES .....	137

## LIST OF TABLES

<b>Table 1.</b> Some representative examples of precipitons prepared in the Wilcox laboratory.....	20
<b>Table 2.</b> Spectroscopic and photophysical data (CH <sub>3</sub> CN, 298 K). .....	31
<b>Table 3.</b> Isomerization rate constants and photostationary state ratios for the photoisomerization process of <b>16Z/E</b> and <b>17Z/E</b> upon irradiation at $\lambda \geq 400$ nm. ....	38
<b>Table 4.</b> The results of photochemical isomerizations of <b>19Z</b> . .....	41
<b>Table 5.</b> Summary of isomerization rates after 30 min of irradiation. ....	44
<b>Table 6.</b> Spectroscopic data in THF at 298 K. ....	55
<b>Table 7.</b> Isomerization rate constants, half-lives, and photostationary state ratios for the photoisomerization process of <b>16Z</b> , <b>16E</b> , <b>28Z</b> , <b>28E</b> , <b>29Z</b> , and <b>29E</b> upon irradiation at 10 $\mu$ M. ....	59
<b>Table 8.</b> Summary of <b>13Z</b> $\rightarrow$ <b>13E</b> isomerization rates after 4 min ( <b>[13Z]</b> = 20 mM,.....	79

## LIST OF FIGURES

<b>Figure 1.</b> Radical catalyzed isomerization of stilbene. ....	3
<b>Figure 2.</b> Triplet energy transfer to stilbene.....	5
<b>Figure 3.</b> Energy diagram showing the photoisomerization of stilbene. ....	6
<b>Figure 4.</b> Photostationary states of stilbene as a function of the sensitizer triplet energy $E_T$ . ....	7
<b>Figure 5.</b> <i>Z</i> -Stilbene ( <b>1Z</b> ) and 2,3-diphenylnorbornene ( <b>2Z</b> ). ....	8
<b>Figure 6.</b> Dexter intramolecular triplet energy transfer in the carbazole-naphthalene system 3. .....	11
<b>Figure 7.</b> Förster triplet energy transfer across a rigid calix[4]arene “bridge.” ....	12
<b>Figure 8.</b> A Ru-Os complex exhibiting Dexter-type intramolecular energy transfer. ....	12
<b>Figure 9.</b> A.) Superexchange can occur in a steroid bridge. B.) Through-bond coupling of p orbitals in a hydrocarbon bridge. ....	13
<b>Figure 10.</b> A.) Superexchange can occur a norbornylogous bridge. B.) Through-bond coupling of $\pi$ orbitals interacting with the $\sigma$ orbitals of a hydrocarbon bridge. ....	13
<b>Figure 11.</b> Rhenium(I) complexes linked by isomerizable stilbene-like ligands.....	15
<b>Figure 12.</b> Ru(2,2'-bpy) <sub>2</sub> ( <i>cis</i> -4-stilbazole) <sub>2</sub> <sup>2+</sup> <b>5</b> .....	15
<b>Figure 13.</b> A phenylene linker extends conjugation from the anthracene donor to the precipiton acceptor of <b>6</b> .....	18

<b>Figure 14.</b> $7Z \rightarrow 7E$ olefin photoisomerization by a through-bond energy transfer. ....	18
<b>Figure 15.</b> Potential rigid hydrocarbon linkers 8-11 for facilitation of energy transfer between a pyrene donor and a precipiton acceptor. ....	19
<b>Figure 16.</b> Alkylation of precipiton <b>13Z</b> by a commercially available pyrene sensitizer. ....	20
<b>Figure 17.</b> Polystyrene (PS) ethylenediamine scavengers and silica (Si) bound scavengers. ....	24
<b>Figure 18.</b> Ru-pyrene complex 15 exhibiting Förster-type intramolecular energy transfer. ....	27
<b>Figure 19.</b> Precipitons covalently linked and unlinked to a $Ru(bpy)_3^{2+}$ unit. ....	28
<b>Figure 20.</b> The room temperature absorption spectra <sup>a</sup> of <b>16Z</b> , <b>16E</b> <sup>b</sup> , <b>17Z</b> , <b>17E</b> , and $Ru(bpy)_3^{2+}$ . <sup>a</sup> Degassed 10 $\mu$ M acetonitrile solutions. <sup>b</sup> Recorded in $CH_2Cl_2$ . ....	32
<b>Figure 21.</b> The room temperature emission spectra <sup>a</sup> of <b>17Z</b> , <b>17E</b> and $Ru(bpy)_3Cl_2$ . <sup>a</sup> Degassed 10 $\mu$ M acetonitrile solutions. ....	32
<b>Figure 22.</b> The UV-Vis spectral changes observed with complex <b>16E</b> upon irradiation at $\lambda \geq 400$ nm at 0, 50, 100, 210, 300, 410, and 565 min (a-g, respectively) in 10 $\mu$ M 7:3 THF:CH <sub>3</sub> CN. ....	34
<b>Figure 23.</b> The UV-Vis spectral changes observed with complex <b>17Z</b> (8.2 $\mu$ M in degassed acetonitrile) upon irradiation at $\lambda \geq 400$ nm at 0, 20, 40, 60, 80 and 100 min (a-f, respectively). ....	35
<b>Figure 24.</b> The UV-Vis spectral changes observed with complex <b>17E</b> (7.4 $\mu$ M in degassed acetonitrile) upon irradiation at $\lambda \geq 400$ nm at 0, 20, 40, 60, 80, and 100 min (a-f, respectively). ....	35
<b>Figure 25.</b> Photochemical production of photostationary state concentrations upon irradiation at $\lambda \geq 400$ nm of <b>16Z/E</b> starting from pure <b>16Z</b> ( $\blacktriangle$ ) and <b>16E</b> (X). ....	37
<b>Figure 26.</b> Photochemical production of photostationary state concentrations upon irradiation at	

$\lambda \geq 400$ nm of <b>17Z</b> ( $\blacktriangle$ ) and <b>17E</b> (X): (top) [ <b>17E</b> ] vs time; (bottom) [ <b>17Z</b> ] vs time.	38
<b>Figure 27.</b> Dexter-type precipiton <b>20Z</b> .	42
<b>Figure 28.</b> Plot of photoisomerization reactions 1-7 ([ <b>13Z</b> ], [ <b>20Z</b> ] = 1mM; .....	43
<b>Figure 29.</b> Plot of photoisomerization reactions 8-11. Reactions 8 and 9 were performed.....	44
<b>Figure 30.</b> Absorbance spectra of the dilution of a 1/1 2,2'-bipyridine/Ru(bpy) <sub>2</sub> <sup>2+</sup> .....	45
<b>Figure 31.</b> A comparison of room-temperature absorption spectra of <b>13Z</b> (---) and <b>20Z</b> (—) (10 $\mu$ M, air-equilibrated CH <sub>3</sub> CN). .....	46
<b>Figure 32.</b> <i>Para</i> and <i>meta</i> benzil precipiton esters and their unbound analogs. ....	51
<b>Figure 33.</b> Room-temperature absorption spectra for degassed 10 $\mu$ M THF solutions of <b>16Z</b> , <b>16E</b> , <b>28Z</b> , <b>28E</b> , <b>29Z</b> , <b>29E</b> , and benzil. ....	54
<b>Figure 34.</b> Emission spectra for degassed 10 $\mu$ M THF solutions of <b>16Z</b> , <b>16Z</b> , <b>28Z</b> , <b>28E</b> , <b>29Z</b> , <b>29E</b> at 25 °C.....	56
<b>Figure 35.</b> The approximate coefficients for the LUMO state of Z-stilbene. ....	57
<b>Figure 36.</b> Reaction progress upon irradiation of 10 $\mu$ M THF solutions of <b>16Z</b> ( $\times$ ) and <b>16E</b> ( $\blacktriangle$ ) in the presence of one equivalent of benzil.....	58
<b>Figure 37.</b> (a) Reaction progress upon irradiation of 10 $\mu$ M THF solutions of <b>28Z</b> ( $\times$ ) and <b>28E</b> ( $\blacktriangle$ ). (b) Reaction progress upon irradiation of 10 $\mu$ M THF solutions of <b>29Z</b> ( $\times$ ) and <b>29E</b> ( $\blacktriangle$ ). .....	61
<b>Figure 38.</b> Fluorescence emission spectra of 10 $\mu$ M <b>16Z</b> and <b>16E</b> compared to a solution of <b>16Z/E</b> + benzil at the same concentration in THF; $\lambda_{exc} = 320$ nm. ....	62
<b>Figure 39.</b> Energy diagram illustrating the “round-trip” precipiton/benzil energy transfer pathway. Radiationless transitions are represented by wavy arrows. P <sub>E</sub> <sup>0</sup> -benzil <sup>0</sup> and P <sub>Z</sub> <sup>0</sup> -benzil <sup>0</sup> represent the ground states of the precipiton-benzil bichromophore.	

Changes in superscripts identify changes in localized electronic excited states (1 = singlet, 3 = triplet). T <sup>3</sup> represents the minimum energy conformer of the precipiton triplet. ....	64
<b>Figure 40.</b> A step-wise depiction of the “round-trip” precipiton/benzil energy transfer pathway: 1) formation of the precipiton singlet state, 2) singlet excitation transfer from the precipiton unit to the benzil, 3) benzil centered intersystem crossing to the localized benzil triplet state, 4) triplet energy transfer from the benzil moiety back to the precipiton, and 5) isomerization. ....	65
<b>Figure 41.</b> The excitation energies of the relevant excited levels (excited singlet (S), excited triplet (T)) of benzophenone and naphthalene. Radiationless transitions are represented by wavy arrows, possible radiative transitions by straight arrows. Changes in superscripts identify changes in localized electronic excited states (1 = singlet, 3 = triplet).....	66
<b>Figure 42.</b> Schematic representation of the concentration of molecularly dissolved sulfur before and after nucleation as a function of time. Based on a figure presented by Lamer and Dinegar in reference 59.....	71
<b>Figure 43.</b> Reaction progress of <b>13Z</b> → <b>13E</b> isomerization with/out <b>13E</b> ([ <b>13Z</b> ] = 20 mM,.....	74
<b>Figure 44.</b> Reaction progress of <b>13Z</b> + <b>13E</b> (([ <b>13Z</b> ] = 20 mM, [ <b>13E</b> ] = saturated; [Ru(bpy) <sub>3</sub> <sup>2+</sup> ] = 50 μM, solvent = 1/1 CD <sub>3</sub> CN/CD <sub>2</sub> Cl <sub>2</sub> ) plotted according to an irreversible first-order rate law (k <sub>obs</sub> = 0.028 s <sup>-1</sup> ) and a reversible first-order rate law (k <sub>obs</sub> = 0.035 s <sup>-1</sup> ). ....	75
<b>Figure 45.</b> Reaction progress of <b>13Z</b> → <b>13E</b> isomerization with/out <b>13E</b> and Ru(bpy) <sub>3</sub> <sup>2+</sup> .....	76
<b>Figure 46.</b> Reaction progress of <b>13Z</b> → <b>13E</b> isomerization using Method A and .....	77

<b>Figure 47.</b> $^1\text{H}$ NMR spectra of compound <b>13Z</b> .....	104
<b>Figure 48.</b> $^1\text{H}$ NMR spectra of compound <b>16Z</b> .....	105
<b>Figure 49.</b> $^{13}\text{C}$ NMR spectra of compound <b>16Z</b> .....	106
<b>Figure 50.</b> $^1\text{H}$ NMR spectra of compound <b>16E</b> .....	107
<b>Figure 51.</b> $^1\text{H}$ - $^1\text{H}$ COSY of 5-bromomethyl-2,2'-bipyridine.....	108
<b>Figure 52.</b> $^1\text{H}$ NMR spectra of compound <b>17Z</b> .....	109
<b>Figure 53.</b> $^1\text{H}$ - $^1\text{H}$ COSY of compound <b>17Z</b> .....	110
<b>Figure 54.</b> $^{13}\text{C}$ NMR spectra of compound <b>17Z</b> .....	111
<b>Figure 55.</b> $^1\text{H}$ NMR spectra of compound <b>17E</b> .....	112
<b>Figure 56.</b> $^1\text{H}$ - $^1\text{H}$ COSY of compound <b>17E</b> .....	113
<b>Figure 57.</b> $^{13}\text{C}$ NMR spectra of compound <b>17E</b> .....	114
<b>Figure 58.</b> $^1\text{H}$ NMR spectra of compound <b>18Z</b> .....	115
<b>Figure 59.</b> $^1\text{H}$ - $^1\text{H}$ COSY of compound <b>18Z</b> .....	116
<b>Figure 60.</b> $^{13}\text{C}$ NMR spectra of compound <b>18Z</b> .....	117
<b>Figure 61.</b> $^1\text{H}$ NMR spectra of compound <b>18Z</b> .....	118
<b>Figure 62.</b> $^1\text{H}$ - $^1\text{H}$ COSY of compound <b>20Z</b> .....	119
<b>Figure 63.</b> $^1\text{H}$ - $^1\text{H}$ COSY of compound <b>22</b> .....	120
<b>Figure 64.</b> $^1\text{H}$ NMR spectra of compound <b>24</b> .....	121
<b>Figure 65.</b> $^{13}\text{C}$ NMR spectra of compound <b>24</b> .....	122
<b>Figure 66.</b> $^1\text{H}$ NMR spectra of compound <b>25</b> .....	123
<b>Figure 67.</b> $^{13}\text{C}$ NMR spectra of compound <b>25</b> .....	124
<b>Figure 68.</b> $^1\text{H}$ NMR spectra of compound <b>31</b> .....	125
<b>Figure 69.</b> $^{13}\text{C}$ NMR spectra of compound <b>31</b> .....	126

<b>Figure 70.</b> $^1\text{H}$ NMR spectra of compound <b>34</b> .	127
<b>Figure 71.</b> $^{13}\text{C}$ NMR spectra of compound <b>34</b> .	128
<b>Figure 72.</b> $^1\text{H}$ NMR spectra of compound <b>28Z</b> .	129
<b>Figure 73.</b> $^{13}\text{C}$ NMR spectra of compound <b>28Z</b> .	130
<b>Figure 74.</b> $^1\text{H}$ NMR spectra of compound <b>28E</b> .	131
<b>Figure 75.</b> $^1\text{H}$ NMR spectra of compound <b>29E</b> .	132
<b>Figure 76.</b> $^{13}\text{C}$ NMR spectra of compound <b>29E</b> .	133
<b>Figure 77.</b> $^1\text{H}$ NMR spectra of compound <b>29E</b> .	134

## LIST OF SCHEMES

<b>Scheme 1.</b> The precipiton approach for achieving product isolation. ....	2
<b>Scheme 2.</b> Photocyclization of <i>Z</i> -stilbene to dihydrophenanthrene followed by oxidation to phenanthrene. ....	5
<b>Scheme 3.</b> Energy transfer from a sensitizer donor to a precipiton acceptor. ....	10
<b>Scheme 4.</b> Time-controlled tactical isomerization by reaction of the target molecule with a sensitizer precursor. ....	16
<b>Scheme 5.</b> Time-controlled tactical isomerization after amine scavenging by reaction of a presensitizer reagent with a sensitizer precursor. ....	17
<b>Scheme 6.</b> Negishi coupling to produce PDE472. ....	24
<b>Scheme 7.</b> An energy activated precipitation process to remove metal impurities. ....	25
<b>Scheme 8.</b> Intermolecular sensitization of <i>E</i> -stilbene by Ru(bpy) <sub>3</sub> <sup>2+</sup> ....	26
<b>Scheme 9.</b> Synthesis of compound <b>16Z</b> . ....	28
<b>Scheme 10.</b> Synthesis of ruthenium complex <b>17Z</b> . ....	29
<b>Scheme 11.</b> Synthesis of ruthenium complex <b>17E</b> . ....	30
<b>Scheme 12.</b> <sup>1</sup> H NMR spectroscopic changes of <b>17Z</b> and <b>17E</b> in CD <sub>3</sub> CN at 298 K. ....	36
<b>Scheme 13.</b> Synthesis of precipiton <b>20Z</b> . ....	42
<b>Scheme 14.</b> Modes of ring opening that can result in the formation of photosubstitution. ....	46
<b>Scheme 15.</b> Reactions of 4-(bromomethyl)benzil <b>23</b> . ....	49

<b>Scheme 16.</b> Synthesis of <b>28Z</b> and <b>28E</b> .....	52
<b>Scheme 17.</b> Synthesis of <b>29Z</b> and <b>29E</b> .....	53
<b>Scheme 18.</b> Intermolecular sensitization of precipiton <b>13Z</b> by $\text{Ru}(\text{bpy})_3^{2+}$ .....	72
<b>Scheme 19.</b> Method A for kinetic data collection.....	72
<b>Scheme 20.</b> Method B for kinetic data collection.....	73

## ACKNOWLEDGMENTS

The completion of my Ph.D. could not have been accomplished without the tremendous help of many people. I would like to thank my advisor, Professor Craig S. Wilcox, for allowing me to join his group and advising me through my graduation. I thank Prof. Wilcox for his patience, mentorship, and help with my career after graduate school.

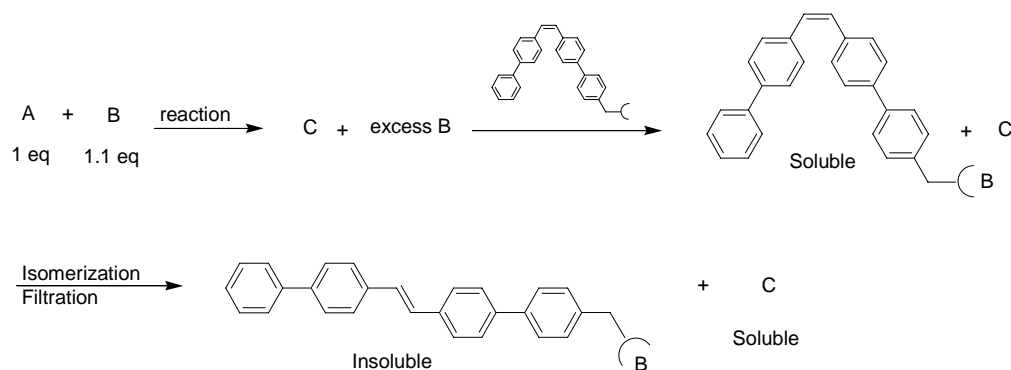
The road toward a Ph.D. in chemistry can be very trying, and my path was no exception. I spent four years and seven months as a full time graduate student at the University of Pittsburgh. I could not have made it through to the end without the emotional and moral support of many dear classmates. I am very grateful to Benjamin Stevens for not only being a constant source of moral support for me, but also for his constant willingness help me with chemistry problems. Many thanks also go to Brijesh Bhayana. I could always count on Brijesh to make me smile and listen to any kind of personal issue that I was battling. I must thank Valerie McCarthy and Wendy Lampart for providing any support that I needed. I would also like to thank Prof. David Crouch, who joined the Wilcox group for one year while he was on sabbatical leave from Dickenson College. His mentorship was extremely helpful and appreciated as I prepared for my proposal and Ph.D. oral defenses.

Finally, I must thank my dear family. My mother (Rose), father (Rudy), brother (Paul), and sister (Alisha) were always there to support me. They were endless sources of love, and for that I am forever grateful.

## **1.0 INTRODUCTION**

## 1.1 THE PRECIPITON APPROACH

Beginning with the Wilcox group's first precipiton publication in 2001, the stilbene-derived approach to precipitons has been successfully applied to purification challenges such as product isolation, reagent scavenging, metal scavenging, and by-product removal. The general approach (shown in Scheme 1) involves the use of a precipiton that contains a functional group that is capable of scavenging a particular reagent in solution.



**Scheme 1.** The precipiton approach for achieving product isolation.

If compound **A** and excess compound **B** are reacted together to form product **C**, the reaction mixture will contain unreacted compound **B**. A precipiton (of the *Z* isomer) that is tailored to react with compound **B** can then be added to the reaction mixture to scavenge excess **B**. Once reacted, the precipiton tag (which is attached to **B**) can be isomerized to its *E* form and precipitated from solution. Only product **C** is left in solution.

## 1.2 PRECIPITON ISOMERIZATION METHODS

Several methods have been employed to induce precipitation. Chemical catalysts can be used to induce stilbene isomerization. Catalysts such as diphenyl disulfide and diphenyl diselenide react by a reversible free radical addition mechanism, where the free radical can cause  $Z \rightarrow E$  isomerization of the double bond (Figure 1).<sup>1</sup> The reactions are clean and inert toward a variety of functional groups. Non-dichalcogen chemical catalysts such as iodine with and without the presence of benzoyl peroxide cause  $Z \rightarrow E$  isomerization in the presence of a 250 W sunlamp as well.<sup>2</sup> However, the disadvantage of using a separate chemical catalyst to induce isomerization is that it reduces the practicality of the precipiton approach because its addition (1) requires an extra step to the reaction setup, (2) introduces an extra reagent to the reaction mixture, and (3) requires a strategy for removing the catalyst once the reaction is complete.

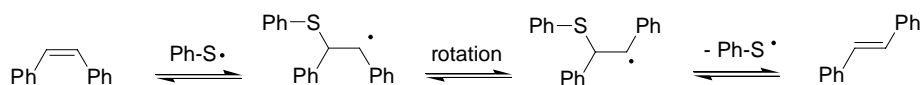


**Figure 1.** Radical catalyzed isomerization of stilbene.

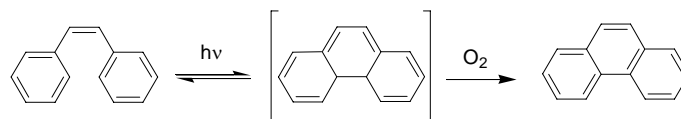
The most desirable method for isomerization is the direct use of light, because it is traceless and does not require the addition of more reagents to the reaction mixture. Induction of isomerization from a direct irradiation process requires that the wavelengths of light used to be in the absorbance region of the precipiton. It is possible to find a wavelength of light in which only one isomer absorbs, providing a method for driving the  $Z \leftrightarrow E$  isomerization in one direction. In the case of stilbene-based precipitons, however, the absorption wavelengths of the  $Z$  and  $E$  isomers are usually below 400 nm ( $\lambda_{\text{max}} = 345$  nm), and somewhat overlapping (although not

identical). The result of extensive ultraviolet irradiation is the production of a photostationary state, where the ratio of *Z/E* isomers does not vary upon further irradiation. The final photostationary state (pss) for direct irradiation is determined by equation 1, where the *Z/E* ratio depends on their efficiencies of absorption at the particular wavelength used,  $\epsilon$ , and their quantum yield for conversion to the other isomer,  $\Phi$ .<sup>3</sup>

**Equation 1.**

$$\frac{[Z]_{\text{pss}}}{[E]_{\text{pss}}} = \frac{\epsilon_E}{\epsilon_Z} \cdot \frac{k_Z}{k_E}$$

A significant disadvantage to using ultraviolet direct irradiation for precipiton isomerization is that high energy light can cause undesirable side reactions, both to the precipiton and the scavenged substrate. It is known that isomerization of stilbene upon direct photoexcitation proceeds through a singlet excited state and not through a triplet excited state. Even though the singlet state lifetime of *Z*-stilbene is very short (1 ps) compared to *E* (70 ps), it can still undergo a reversible electrocyclic ring closure to produce dihydrophenanthrene. Dihydrophenanthrene can react further with oxygen to produce phenanthrene (Scheme 2).<sup>4</sup> Singlet excited *E*-stilbene, due to its comparably longer excited state lifetime, can also undergo a bimolecular [2+2] cycloaddition to produce cyclobutanes. The formation of these byproducts are often soluble in the reaction solvent, thus adding new impurities to the mixture.



**Scheme 2.** Photocyclization of *Z*-stilbene to dihydrophenanthrene followed by oxidation to phenanthrene.

An alternative to achieving photochemical isomerization through singlet excited state processes is to proceed through a triplet state process. Triplet state stilbene cannot be accessed through direct irradiation, but can be accessed indirectly through the use of a sensitizer molecule. Triplet energy sensitizers are molecules that, upon photochemical excitation through direct irradiation, undergo rapid and efficient singlet  $\rightarrow$  triplet intersystem crossing to form a long-lived triplet state. Triplet energy sensitizers are an attractive option because many absorb in the visible light range. The mechanism for triplet-sensitized stilbene isomerization has been studied extensively over the years, beginning with pioneering efforts of Hammond, Saltiel and coworkers in the 1960's (Figure 2).<sup>5</sup>

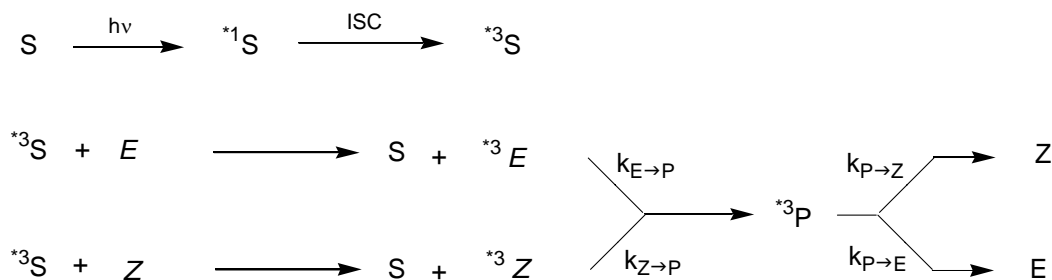


**Figure 2.** Triplet energy transfer to stilbene.

In the model developed by Hammond, a sensitizer **S** acts by absorbing light, then undergoes intersystem crossing to its triplet state  $^3\text{S}$ , after which it takes part in an energy transfer process with stilbene (*E* or *Z*). Triplet energy transfer to ground state stilbene results in triplet excited stilbene. Both excited state isomers relax in a decay pathway to a common phantom triplet state  $^3\text{P}$ . This process is depicted in the energy diagram shown in Figure 3. It is believed that in the case of stilbene the phantom triplet decays to produce an equal ratio of *Z* and *E* ground state isomers.<sup>6</sup> The final isomeric ratio of the photosensitized isomerization produced at the photostationary state is expressed as Equation 2, where  $k_{t \rightarrow p}$ ,  $k_{c \rightarrow p}$ ,  $k_{p \rightarrow c}$ , and  $k_{p \rightarrow t}$  are the rates of the reactions in Figure 2.

**Equation 2.**

$$\left( \frac{Z}{E} \right)_{\text{pss}} = \left( \frac{k_{E \rightarrow P}}{k_{Z \rightarrow P}} \right) \left( \frac{k_{P \rightarrow Z}}{k_{P \rightarrow E}} \right)$$

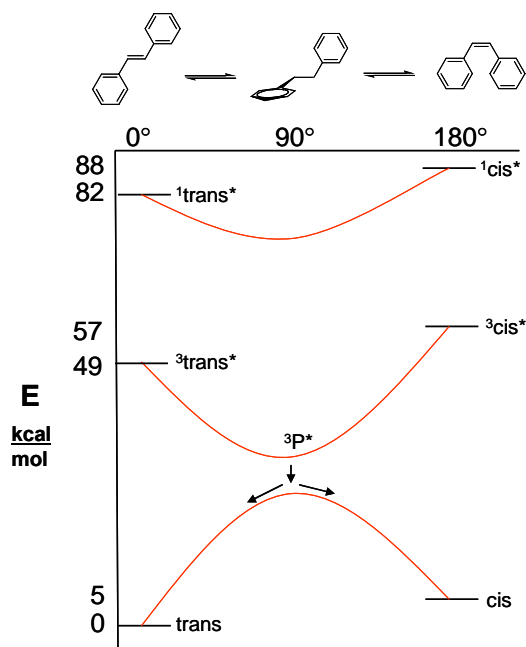


**Figure 3.** Energy diagram showing the photoisomerization of stilbene.

Hammond and Saltiel have demonstrated that final photostationary state mixtures rich in *Z* or *E*-stilbene can be obtained by selecting the proper sensitizer (Figure 4).<sup>5b</sup> The results of their survey showed that sensitizers whose triplet energies are higher than the triplet energies of the both *Z* and *E* isomers results in an approximately equal mixture of *E/Z* at the photostationary state. Sensitizers with triplet energy between 49 kcal/mol and 59 kcal/mol transfer their triplet energy exothermically to only the *E*-stilbene, resulting in a mixture rich in the *Z* isomer. However, when the sensitizer has a triplet energy even lower than *E*-stilbene, its triplet energy is transferred primarily to the *Z* isomer. An explanation for this observation has been the subject of extensive debate for several decades, and non-vertical triplet energy transfer has emerged as a widely accepted theory.

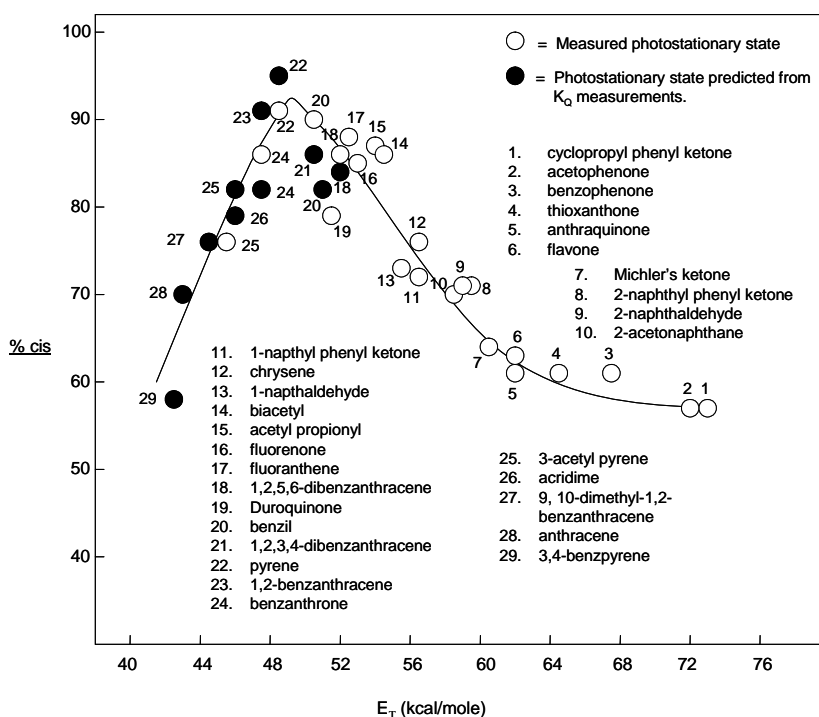


**Figure 4.** Photostationary states of stilbene as a function of the sensitizer triplet energy  $E_T$ .

The concept of “nonvertical” triplet energy transfer, which refers to the process in which triplet energy transfer occurs from donors (D) with triplet energy  $E_T$  that is “insufficient to provide isothermal or exothermic formation of the spectroscopically observed acceptor (A) triplet,”<sup>7</sup> has been used to account for the triplet sensitization of stilbene by sensitizers of lesser triplet energy. The original evidence for nonvertical energy transfer came from studies of *Z*-stilbene, and discussions of its origin were centered on mechanisms involving torsions about the formal double bond of the  $\pi$  system.<sup>8</sup> However, more recent studies by Gorman et al. that compare the sensitized triplet energy transfer rates of 2,3-diphenylnorbornene to *Z*-stilbene (Figure 5) strongly support a single-bond torsional mechanism.<sup>9</sup> 2,3-Diphenylnorbornene, which has essentially the same  $\pi$ -system geometry as *Z*-stilbene but with a central double bond that cannot undergo significant torsion on either the ground state or triplet state surfaces, exhibits virtually identical “nonvertical” triplet excitation behavior as *Z*-stilbene. Thus the key torsional coordinate resulting in nonvertical behavior by these systems is not that involving the central double bond, but is better explained on the basis of single-bond torsion.

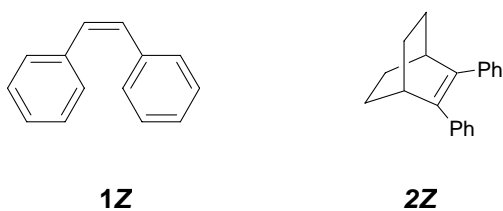


**Figure 5.** *Z*-Stilbene (**1Z**) and 2,3-diphenylnorbornene (**2Z**).

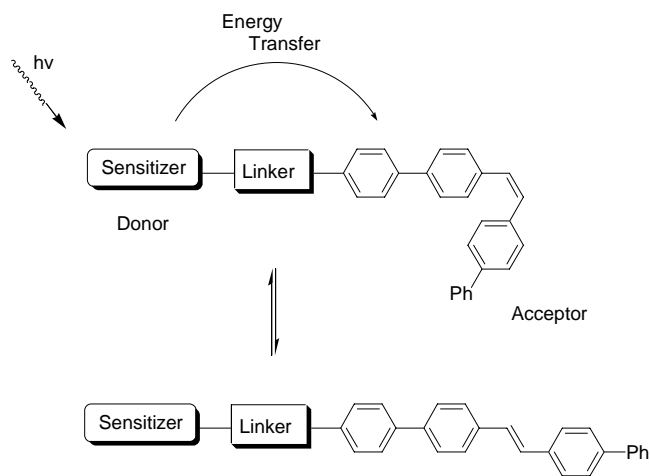
Reduced vertical triplet excitation energy of the acceptor as a consequence of ground-state geometric distortion during sensitization is the only requirement for non-vertical behavior. 2,3-Diphenylnorbornene and *Z*-stilbene possess  $\pi$  systems with non-planar equilibrium

geometries, but single-bond torsions toward a more planar geometry occurs during sensitization. This increases  $\pi$  conjugation and in turn lowers the vertical triplet energy requirement (i.e., nonvertical behavior). An interesting corollary that Gorman et al. notes is that flexible  $\pi$  systems with essentially planar equilibrium geometries do not exhibit nonvertical behavior because single-bond torsion from a planar to a non-planar arrangement will only raise the vertical triplet energy requirement. This has been observed with simple dienes and trienes.<sup>10</sup>

### 1.3 INTRAMOLECULARLY SENSITIZED PRECIPITONS

Although the methods previously described will successfully isomerize precipitons, each method has significant limitations when considering its usefulness to precipitons as purification agents. Direct irradiation of stilbene causes unwanted side reactions such as stilbene dimerization and electrocyclic ring closure. The addition of a chemical catalyst such as diphenyl disulfide or a triplet energy sensitizer compromises a precipiton's practicality due to extra purification steps necessary to remove the catalyst. A solution to this problem is the chemical attachment of a triplet sensitizer to the precipiton moiety. Isomerization may then occur by using mild visible light conditions without sensitizer additives.

My Ph.D dissertation focuses on the development of the first intramolecularly activated precipitons. The isomerization process is induced by intramolecular triplet energy transfer, as illustrated in Scheme 3. In a simple system, a triplet energy sensitizer is covalently attached to a precipiton by an inert linking group. The sensitizer absorbs visible light irradiation and becomes excited to its triplet state (see Figure 3 for mechanism). Triplet energy is then transferred from the sensitizer (donor) to the precipiton (acceptor) to cause isomerization.



**Scheme 3.** Energy transfer from a sensitizer donor to a precipiton acceptor.

### 1.3.1 Design Strategies for Intramolecular Energy Transfer

Prior scholars have shown that there is a clear structure-function relationship between bichromophores and their photochemical behaviors, and their work provides a valuable guide for the design of new systems. Interest in intramolecular energy transfer has increased significantly as shown by the amount of publications on the subject in recent years. Energy transfer processes have been applied to molecular wires,<sup>11</sup> switches,<sup>12</sup> shuttles,<sup>13</sup> and machines.<sup>14</sup> In all examples, the molecular architectures of multichromophoric systems have an influential role on the rate, efficiency and mechanism of energy transfer from donor to acceptor.

The degree of flexibility of the linker, along with its chemical and conformational composition, have fundamental roles in the mechanism of energy transfer.<sup>15</sup> It is known that two types of mechanisms may govern triplet energy transfer: an electron exchange mechanism (Dexter) or a dipole-induced dipole mechanism (Förster). No clear-cut method exists for determining a system's mechanism simply founded on molecular structure analysis alone, and it is possible for both mechanisms to be operative at the same time. The question is “which

predominates for a particular molecular structure?” Predictions can be made based on the linker composition.

A flexible linker may accommodate multiple energy transfer pathways. Dexter electron exchange transfer requires a close approach of the donor and acceptor (essentially a collision) in order to achieve high efficiency,<sup>16</sup> and the model assumes that the transfer rate decreases exponentially as the distance between D and A increases. Shorter, flexible linkers tend to undergo Dexter transfer, such as the carbazole-naphthalene system studied by Yamamoto et al.<sup>17</sup> (Figure 6). Increasing the flexible bridge length allows the overall structure to occupy many conformations, only a small number of which may result in chromophore collision. Barigelletti et al. found the energy transfer of a ruthenium-pyrene bichromophore linked by a long and flexible poly(ethylene glycol) chain (21 Å long in the fully extended conformation) to fit the parameters of a Forster mechanism.<sup>18</sup> Increasing the length of a flexible linker does not necessarily alter the distance between the chromophores because the flexibility of the chain can allow for overlap.<sup>19</sup>

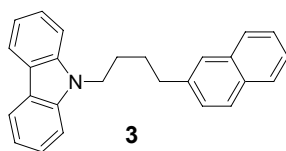


**Figure 6.** Dexter intramolecular triplet energy transfer in the carbazole-naphthalene system **3**.

Increasing the flexibility of the bridge by increasing its length may decrease the probability of collision between the connected chromophores. In the case of Rebek and coworker’s rigid calix[4]arene capsules equipped with FRET pair chromophores, intramolecular

collision is less likely.<sup>20</sup> However, favorable overlap between the emission profile of the donor and the absorption profile of the linked acceptor allowed Förster energy transfer to occur (Figure 7).

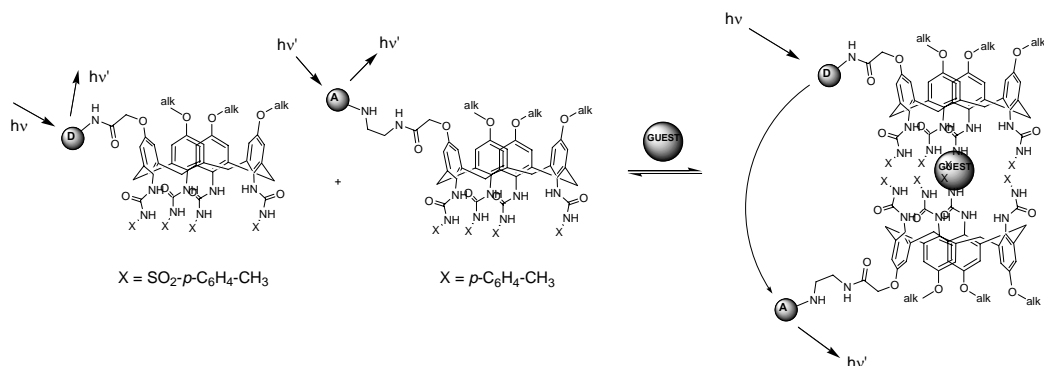


**Figure 7.** Förster triplet energy transfer across a rigid calix[4]arene “bridge.”

If the arrangement of atoms in the rigid spacer overlap favorably, an electronic coupling interaction between a donor and acceptor can occur through the bonds of the spacer. Chemists classify the mechanism as “superexchange”, where overlapping orbitals ( $\sigma$ ,  $\sigma^*$ ,  $\pi$ ,  $\pi^*$ ) provide a medium for electrons to migrate between the chromophores. Superexchange can occur through fully conjugated bridges, as reported by Balzani and Belser et al. in the heterodinuclear [Ru(bpy)<sub>3</sub>-(ph)<sub>3</sub>-Os(bpy)<sub>3</sub>]<sup>4+</sup> complex **4** (Figure 8).<sup>21</sup> They reported a dual Dexter energy transfer and an electron superexchange mechanism to be operative due to the phenylene linker.

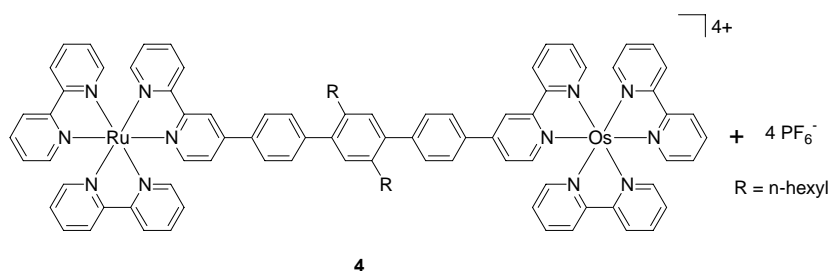


**Figure 8.** A Ru-Os complex exhibiting Dexter-type intramolecular energy transfer.

It is interesting to note that a rigid bridge does not have to contain conjugation in order to facilitate through-bond transmission of electronic excitation. Chemists differ on their opinions of whether the mechanism is superexchange or energy transfer, and sometimes the terms are used together. Closs and Miller, in their pioneering studies of the interactions between chromophores across steroid bridges, provided supportive evidence for efficient through-bond-mediated electron transfer (Figure 9).<sup>22</sup> Other examples of frameworks capable of through-bond transmission of electronic excitation include bicyclo[2.2.2]octanes,<sup>23</sup> oligo[1.1.1]-propellanes,<sup>24</sup> triptycene, polyspirocyclobutanes,<sup>25</sup> and norbornylogous bridges comprising of a mixture of linearly fused norbornyl and bicycle[2.2.0]hexyl groups (Figure 10).<sup>26</sup>

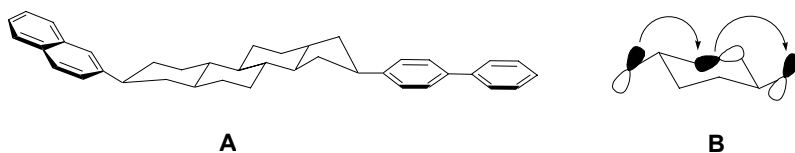


**Figure 9.** A.) Superexchange can occur in a steroid bridge. B.) Through-bond coupling of p orbitals in a hydrocarbon bridge.

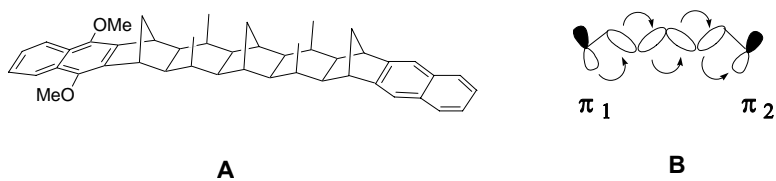


**Figure 10.** A.) Superexchange can occur a norbornylogous bridge. B.) Through-bond coupling of  $\pi$  orbitals interacting with the  $\sigma$  orbitals of a hydrocarbon bridge.

### 1.3.2 Design of Intramolecularly Sensitized Precipitons

If we view the precipiton moiety as one partner in a bichromophoric pair, extending the design strategies discussed above to our stilbene-based precipiton systems is straightforward. Selection of the proper precipiton-chromophore pair and the bridge that connects them together can be accomplished by determining the type of characteristics the precipiton is intended to have.

An essential requisite for the linked sensitizer is that it must have triplet energy in the range of the accepting precipiton (40-70 kcal) in order to cause isomerization. The most straightforward approach for isomerization is achieved unselectively, where exposure to proper irradiation wavelengths is the only required “reagent.” For instance, azo- and stilbene-containing rhenium(I) complexes can undergo reversible photoisomerization upon irradiation at  $\lambda = 480$  nm (Figure 11). Trinuclear *fac*-(diimine)Re(CO)<sub>3</sub> complexes bridged by a stilbene-like ligand also exhibits visible light photoisomerization (Figure 11).<sup>27,28</sup> Ruthenium complexes also undergo intramolecular isomerization processes. Visible irradiation ( $\lambda_{\text{exc}} = 436$  nm and  $\lambda_{\text{exc}} = 570$  nm) of Ru(2,2'-bpy)<sub>2</sub>(*cis*-4-stilbazole)<sub>2</sub><sup>2+</sup> **5** lead to *Z* → *E* isomerization of the stilbazole ligand (Figure 12).<sup>29</sup> In these systems, attachment of an appropriate light-absorbing metal complex (such as Re(CO)<sub>3</sub>(bpy)<sup>+</sup>) to stilbene can allow sensitization to occur due to an efficient energy transfer process from the <sup>3</sup>MLCT excited state to the lowest <sup>3</sup> $\pi^*$  excited state localized on the bipyridine ligand.

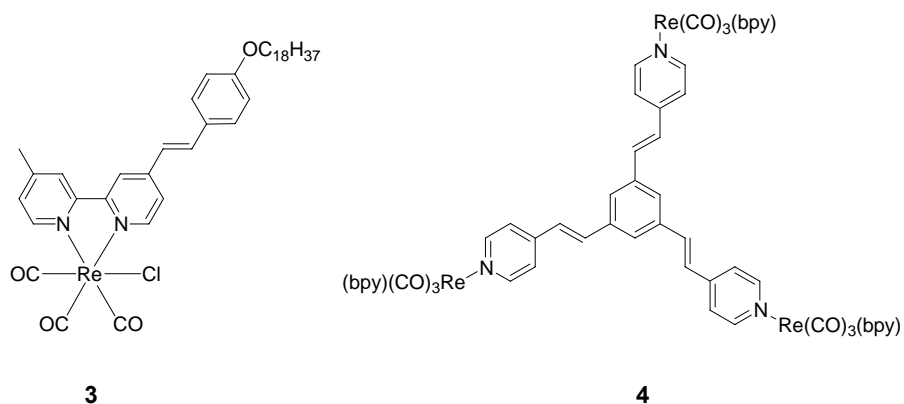


**Figure 11.** Rhenium(I) complexes linked by isomerizable stilbene-like ligands.

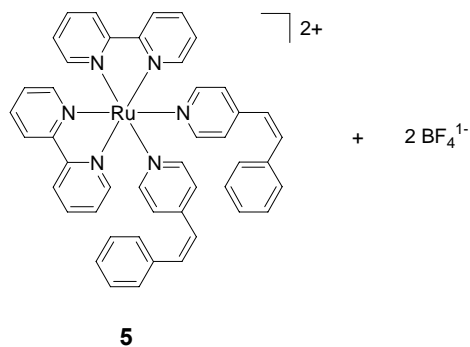
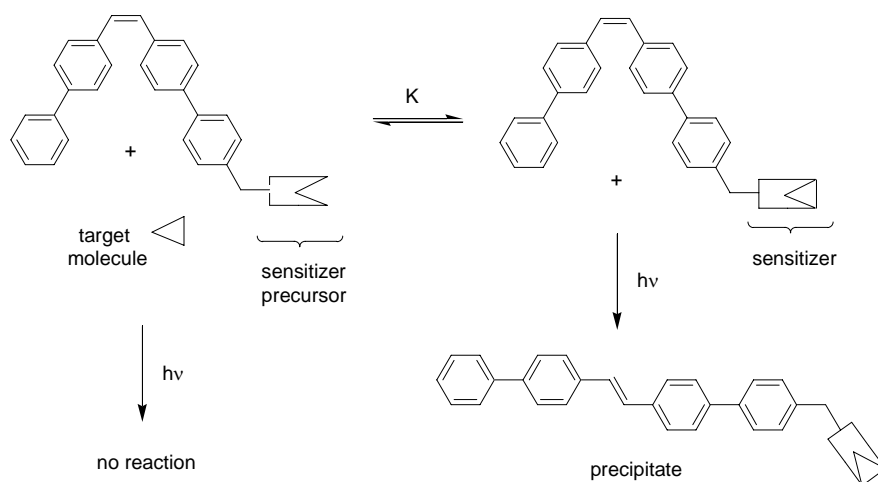


**Figure 12.**  $\text{Ru}(2,2'\text{-bpy})_2(\text{cis-4-stilbazole})_2^{2+}$  **5**.

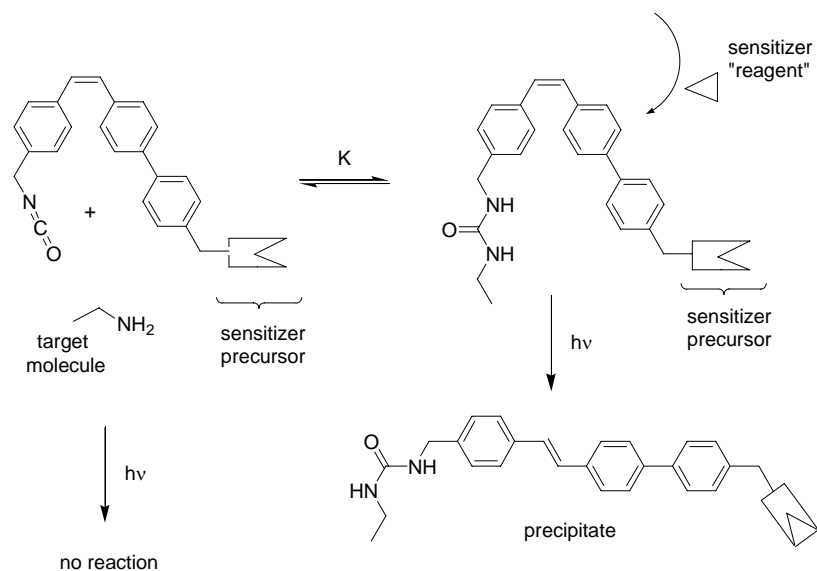
The ability to tactically control the initiation of isomerization is actually advantageous. One possible application of this would be an energy driven separation process, wherein the target molecule would activate isomerization and cause precipitation. In every event where the target molecule reacts with the precipiton in the *Z* form, and if the resulting compound can absorb light,

an isomerization process is “triggered” via intramolecular sensitization to produce the *E* isomer (Scheme 4). The *E* isomer then precipitates along with target molecule.



**Scheme 4.** Time-controlled tactical isomerization by reaction of the target molecule with a sensitizer precursor.

For those target molecules that cannot be transformed into sensitizers upon reaction with the sensitizer precursor, a possible variation of this system is shown in Scheme 5. Here the precipiton contains a sensitizer precursor on one end, and a functional group on the other. After the target molecule reacts with the functional group, a presensitizer “reagent” could then be added to react with the precursor and complete the sensitizer structure. Precipitation then follows.



**Scheme 5.** Time-controlled tactical isomerization after amine scavenging by reaction of a presensitizer reagent with a sensitizer precursor.

The chemical composition and length of the linker used to bridge the precipiton and the sensitizer can affect the system's photochemical properties (singlet and triplet lifetimes, energy transfer rate constants) and predispose the system to undergo Dexter, Förster, or superexchange mechanisms (or a combination). Precipitons react differently to sensitization than simpler static bichromophores, because the energy transfer event to the precipiton is accompanied by a dynamic isomerization event. Ideally, the isomerization event is triggered by intramolecular energy transfer from the attached sensitizer, and not through a direct irradiation process. Incorporation of a conjugated linker, like that used by Balzani and Belser et al (Figure 8), can be problematic because it extends the conjugation of the precipiton, causing a shift in its absorption. If the new absorption includes the visible light region (400-700 nm), as typically used at the chemist's bench top, direct irradiation will be an undesired competing isomerization pathway (Figure 13).

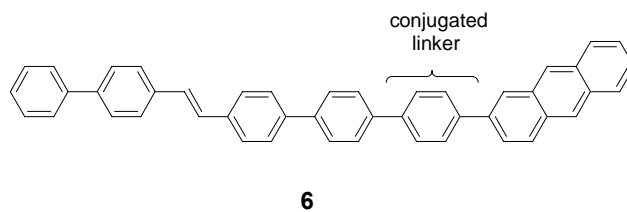


**Figure 13.** A phenylene linker extends conjugation from the anthracene donor to the precipiton acceptor of **6**.

Reports of stilbene linked to triplet energy sensitizers by a rigid hydrocarbon bridge, such as norboronyl or steroid groups, have been absent in the literature. Sensitized isomerization, however, has been achieved for olefins bonded steroids.<sup>30</sup> A dimethylphenylsiloxy (DPSO) group served as a light-absorbing “antenna” and a nearby ketone served as an energy “relay” for the triplet energy transfer to the olefin (Figure 14). The photoisomerization was described as being a through-bond energy transfer.<sup>30(b)</sup> It seems reasonable that the well-defined steroid, bicyclo[2.2.2]octane, oligo[1.1.1]-propellane, polyspirocyclobutane, and norbornylogous bridges could be used to bridge precipitons to sensitizers as well (Figure 15). Hydrocarbon bridges such as these can be advantageous because they do not contain heteroatoms that are easy to oxidize or reduce and/or possess low-energy electronic levels, which can act as quenchers of the donor excited state.

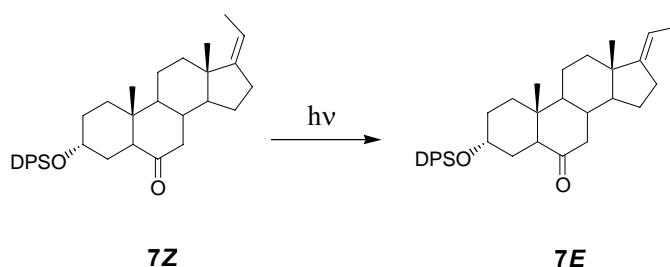


**Figure 14.** **7Z**  $\rightarrow$  **7E** olefin photoisomerization by a through-bond energy transfer.

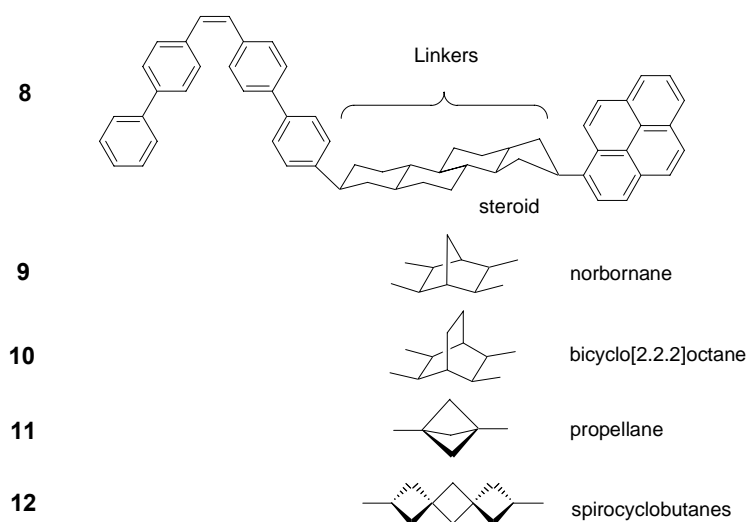


**Figure 15.** Potential rigid hydrocarbon linkers **8-11** for facilitation of energy transfer between a pyrene donor and a precipiton acceptor.

From a synthetic standpoint, perhaps the simplest and most practical bridges to synthesize are flexible, where the sensitizer donor and the precipiton acceptor are connected by a functional group. Significant literature precedent exists for energy transfer in bichromophores linked by ester, ether, amine, and amide functionalities. The strategy is attractive because many triplet energy sensitizers equipped with linking functionalities are commercially available, and the coupling of two chromophores usually requires only one synthetic step (Figure 16). Precipiton synthesis is versatile and allows for many functional options on its terminal end(s). A large library of precipiton syntheses has been established, and several potentially useful structures are shown in Table 1.

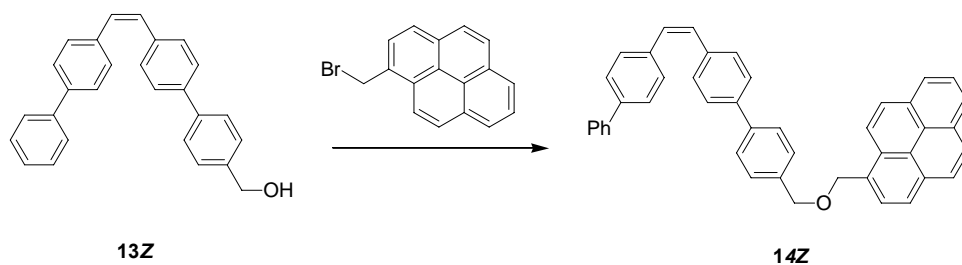
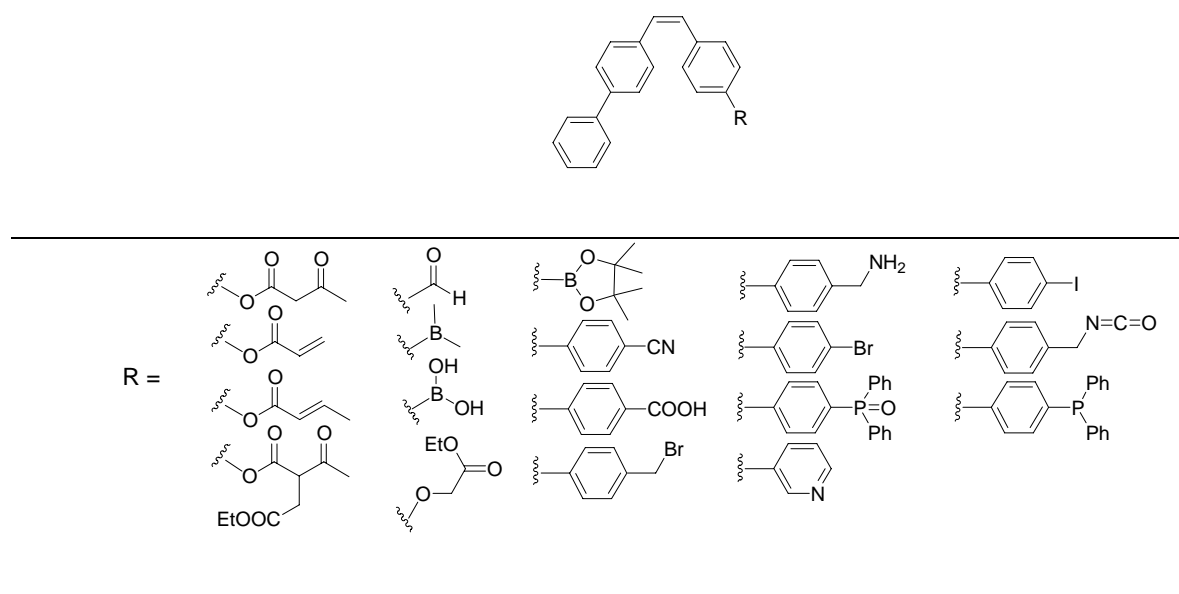


**Figure 16.** Alkylation of precipiton **13Z** by a commercially available pyrene sensitizer.

**Table 1.** Some representative examples of precipitons prepared in the Wilcox laboratory.



## 1.4 DISSERTATION OVERVIEW

Precipiton studies by the Wilcox group and the extensive literature reporting on the subject of stilbene photochemistry provide the basis of understanding intermolecularly sensitized precipitons. The goal of my graduate work has been to develop the area of intramolecularly

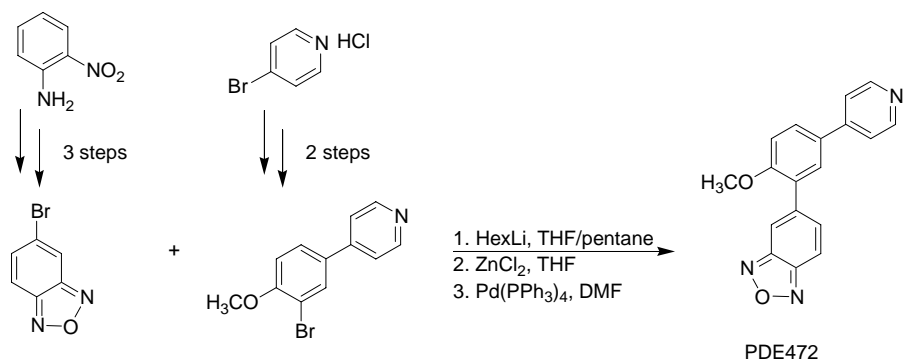
sensitized precipitons. Proper design of these new agents will require integrating our understanding of the intermolecular systems with what is known about bichromophoric energy transfer. The broader scope of this project is to develop intramolecularly sensitized precipitons for practical applications. Consequently, the following precipiton systems presented here were studied within that context.

## **2.0 PRECIPITONS FOR METAL SEQUESTRATION**

## 2.1 INTRODUCTION

The necessity for uncontaminated aqueous and organic media as it relates to public health and the environment cannot be over emphasized.<sup>31</sup> However, effective purification techniques continue to be a challenge. In the area of medicinal chemistry, for example, adequate purification is a challenge in the production of new drugs. Reducing toxic metal impurities in active pharmaceutical ingredients (APIs) to the parts per million (ppm) level is required for the pharmaceutical industry,<sup>32</sup> and this increases production costs.

The most common sources of metal contaminants in APIs are the catalysts used in synthesis. These catalysts are of great importance in reducing the costs of production and there are no good alternatives that would allow them to be replaced. Commonly observed contaminants are palladium, platinum, ruthenium, and rhodium. Many pharmaceutical intermediates and final drugs, because of their heterocyclic structures, have good affinities for these metals, a fact that exacerbates the challenge. For example, Novartis Pharma AG produces 5-[2-methoxy-5-(4-pyridinyl)phenyl]-2,1,3-benzoxadiazole (PDE472) on a multikilogram scale for the treatment of asthma.<sup>33</sup> The final synthetic step is a Negishi aryl-aryl coupling (Scheme 6). Even after chromatography and crystallization, the final product remains contaminated with high amounts of palladium (300 – 800 ppm). Novartis scientists suggested this may be due to strong complexation of PDE472 with Pd(0). The 4-(4-methoxyphenyl)pyridine substructure is a good candidate ligand for Pd(0), and 4-methoxypyridines are well-known to ligate palladium. Treating PDE472 with maleic acid to produce the hemi-maleate salt solved the problem. However, the salt had to be converted back to the free base, treated with active charcoal, and recrystallized again.



**Scheme 6.** Negishi coupling to produce PDE472.

Scavenging methods to remove these trace metal impurities have been reported. For example, silica and synthetic-polymer derived supports have been used to carry thiol and amine ligands so that expended catalysts, if sufficiently sequestered by these ligating groups, can be removed (scavenged) from a reaction mixture by filtration (Figure 17).<sup>32c, 34</sup> The disadvantage of these methods is that they rely on passive binding events. When a binding agent is used in stoichiometric amounts, in order for such a binding agent or scavenger to be effective at removing a metal impurity, the scavenger ligands must have a much stronger affinity for the metal than the drugs and APIs that are also present. For example, to remove 99% of a contaminant metal from 20 kg of an API, one would need 20 grams of a ligand that has an affinity for the metal 100,000 times greater than the API. Although such ligands can certainly be prepared, their use may be prohibitively expensive.

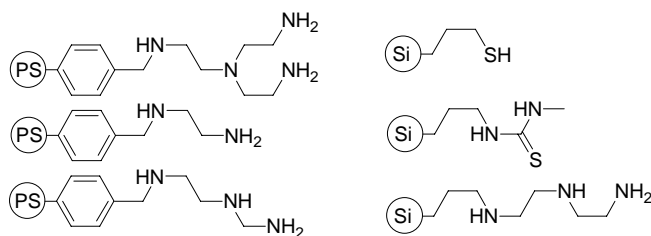
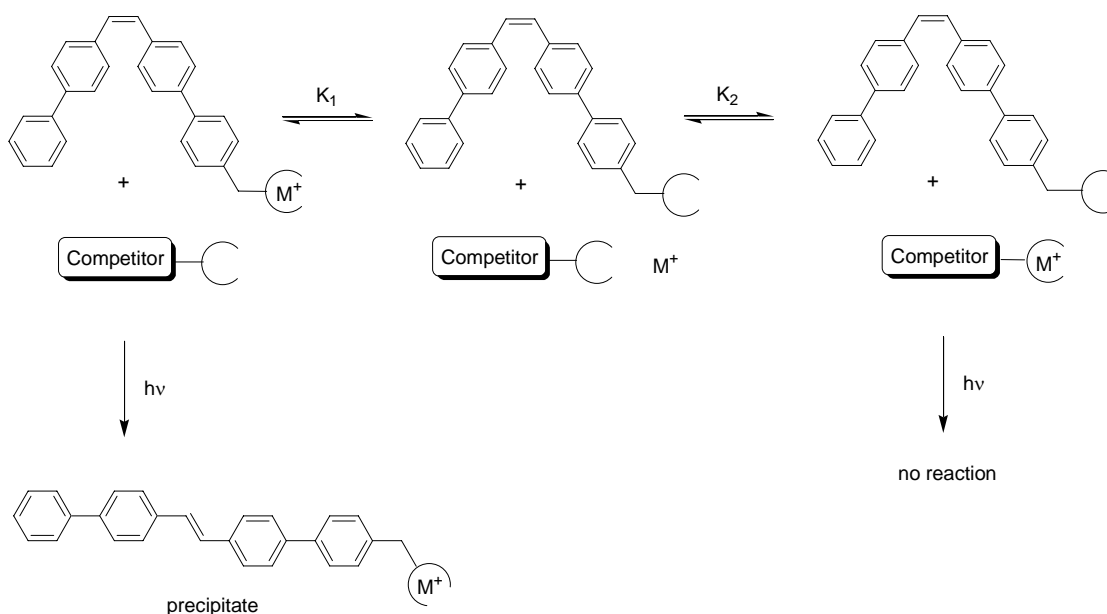


**Figure 17.** Polystyrene (PS) ethylenediamine scavengers and silica (Si) bound scavengers.

## 2.2 AN ENERGY DRIVEN SEQUESTRATION PROCESS

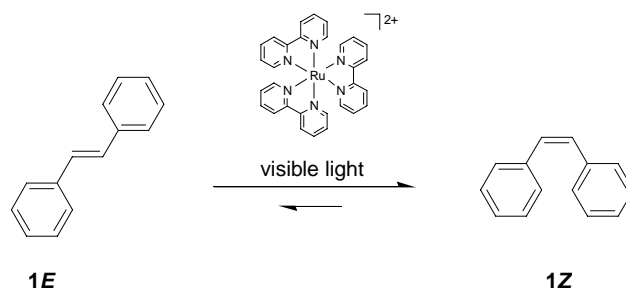
One way in which the problem of ligand competitors in metal scavenging may be overcome is through the use of an energy-driven separation process, wherein the ligated metal would activate isomerization and cause precipitation. In every event that the metal does bind to the precipiton in the *Z* form, if the resulting complex can absorb light, an isomerization process is “triggered” via intramolecular sensitization to produce the *E* isomer. At any time after the point at which the *E* precipiton has reached saturation, the *E* precipiton would precipitate together with the metal, thus decreasing the amount of metal in solution. In short, only a “loaded” ligand will precipitate.<sup>35</sup> The amount of metal bound to scavenger, originally limited by the equilibrium constants for binding to the precipiton ligand ( $K_1$ ) and competitors ( $K_2$ ), is increased due to precipitation (Scheme 7). The energy to drive the process is stored in the structure of the scavenging ligand, and is released by light absorption.



**Scheme 7.** An energy activated precipitation process to remove metal impurities.

## 2.3 PRECIPITON DESIGN

A large number of transition metal complexes containing polyimine ligands are capable of visible light absorption and formation of metal-to-ligand charge transfer (MLCT) triplet states.<sup>36</sup> Within this group, polypyridyl Ru(II) complexes have been widely used as photosensitizers for a variety of reactions, including photoisomerization. In the 1970's, the Wrighton lab demonstrated intermolecular energy transfer from the triplet excited states of Ru(bpy)<sub>3</sub><sup>2+</sup> complexes to *E*-stilbene (Scheme 8).<sup>37</sup> At the photostationary state, 95% *Z*-stilbene had formed. The result was attributed to the isoenergetic triplet energy values for Ru(bpy)<sub>3</sub><sup>2+</sup> and *E*-stilbene of 49 kcal/mol. Photoinduced *Z* → *E* isomerization of stilbene was also examined for Cu(I) complexes with 2,2'-bipyridine, and 1,10-phenanthroline ligands.<sup>38</sup> These sensitizers were similar to Ru(bpy)<sub>3</sub><sup>2+</sup> in terms of their *Z*-stilbene/*E*-stilbene mole ratios at the photostationary state.



**Scheme 8.** Intermolecular sensitization of *E*-stilbene by Ru(bpy)<sub>3</sub><sup>2+</sup>.

Since then, intramolecular energy transfer processes from the <sup>3</sup>MLCT state of Ru(II) complexes to stilbene-containing ligands have also been investigated.<sup>39</sup> Studies of related bichromophoric receiver-antenna systems have demonstrated that Ru(bpy)<sub>3</sub><sup>2+</sup> complexes are

capable of intramolecular energy transfer processes with covalently linked organic chromophores.<sup>40</sup> Barigelletti, Ward and coworkers reported Förster energy transfer that occurs in a bichromophoric species containing a  $\text{Ru}(\text{bpy})_3^{2+}$  and pyrene unit linked together by an ether spacer (Figure 18).<sup>41</sup> Selective excitation at  $\lambda_{\text{exc}} = 532 \text{ nm}$  of the  $\text{Ru}(\text{bpy})_3^{2+}$  unit lead to a Ru-based luminescence and a pyrene-based absorption.

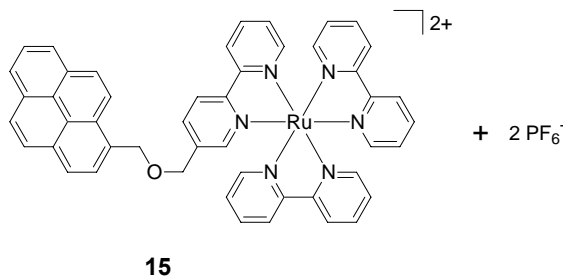


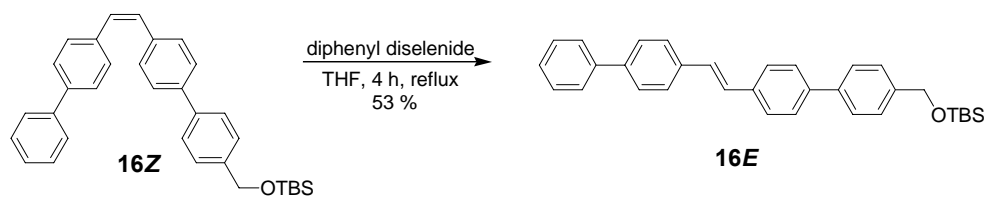
**Figure 18.** Ru-pyrene complex **15** exhibiting Förster-type intramolecular energy transfer.

The greater part of this chapter focuses on the most successful aspects of this project, where the photophysical properties and photoisomerization kinetics of precipitons<sup>42</sup> covalently linked and unlinked to a  $\text{Ru}(\text{bpy})_3^{2+}$  unit were studied. The structures of these compounds are shown in Figure 19. Section 2.6 addresses additional precipiton approaches for metal scavenging and examines their shortcomings.

## 2.4 RESULTS AND DISCUSSION

### 2.4.1 Synthesis

The synthesis of complex **16E** is outlined in Scheme 9. Chemical isomerization of TBS ether **16E**<sup>42g</sup> with 0.1 equiv of diphenyl diselenide in THF afforded the *E* isomer in 59% yield.



**Scheme 9.** Synthesis of compound **16Z**.

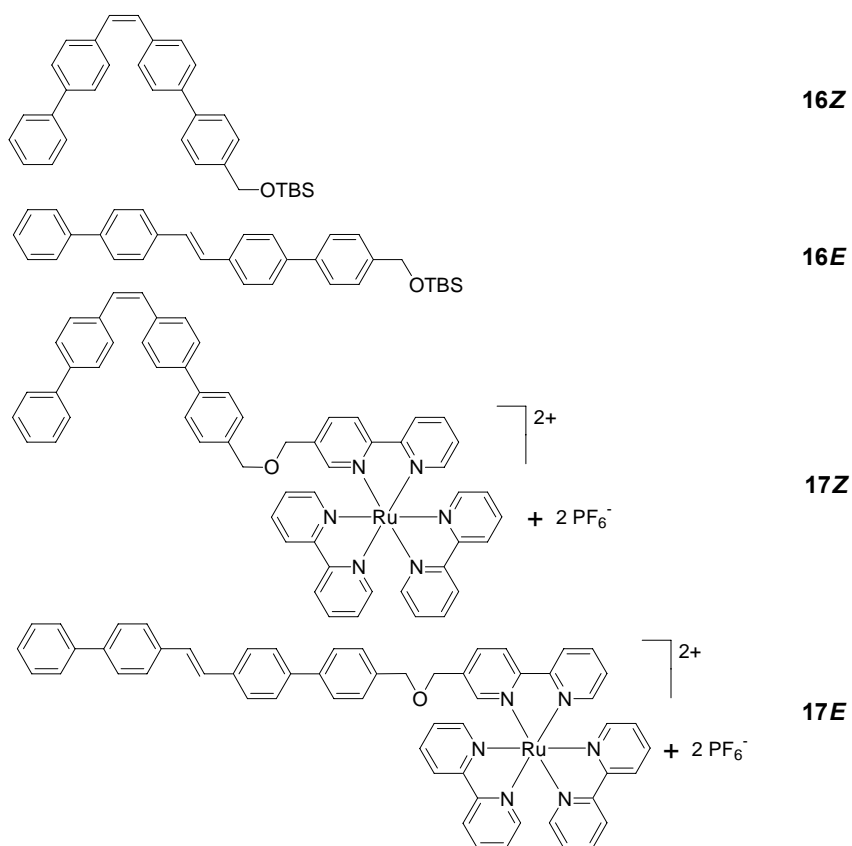
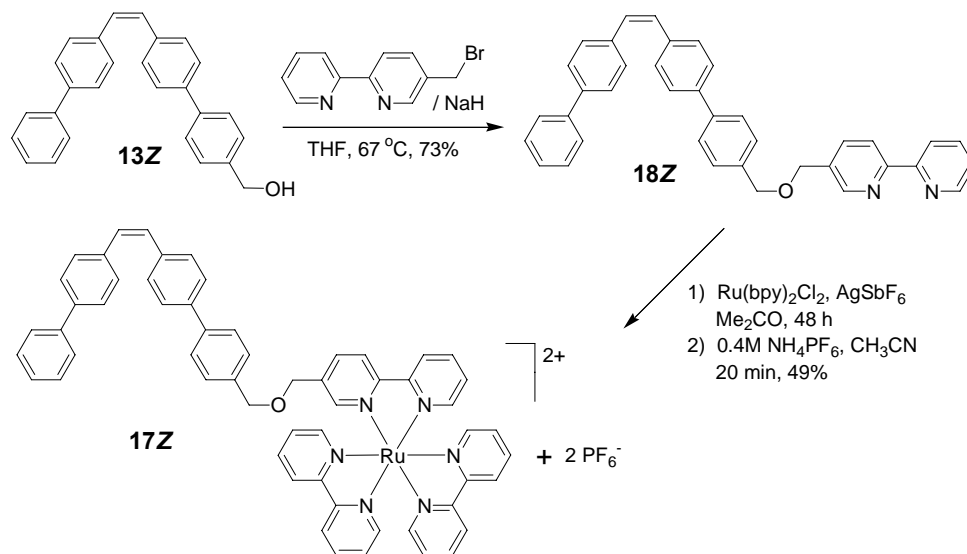


**Figure 19.** Precipitons covalently linked and unlinked to a  $\text{Ru}(\text{bpy})_3^{2+}$  unit.

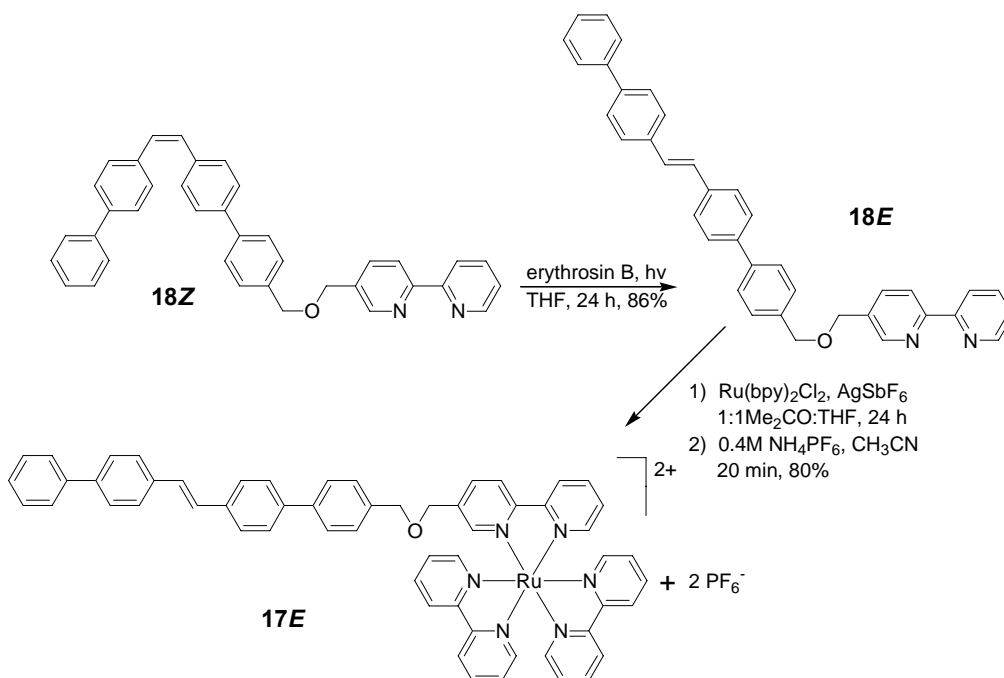
To begin the preparation of complex **17Z**, (Scheme 10) alkylation of the 1,2-bis(biphenyl)ethene alcohol (**13Z**)<sup>42d</sup> with 5-bromomethyl-2,2'-bipyridine<sup>43</sup> afforded a 73%

yield of the bipyridine-tagged 1,2-bis(biphenyl)ethene precipiton **18Z**. The ruthenium complex **17Z** was obtained as its bis(hexafluorophosphate) salt in 49% overall yield, after refluxing *cis*-dichlorobis(2,2'-bipyridine)ruthenium(II) with ligand **18Z** in acetone for 48 h and carrying out counterion exchange ( $\text{NH}_4\text{PF}_6/\text{H}_2\text{O}/\text{CH}_3\text{CN}$ ).



**Scheme 10.** Synthesis of ruthenium complex **17Z**.

The synthesis of complex **17E** is outlined in Scheme 11. Sensitized isomerization of bipyridine tagged *Z*-1,2-bis(biphenyl)ethene precipiton **18Z** with erythrosin B in THF afforded (73%) the *E* isomer **18E**. The ruthenium complex **17E** was obtained as its bis(hexafluorophosphate) salt in 49% overall yield, after refluxing *cis*-dichlorobis(2,2'-bipyridine)ruthenium(II) with ligand **18E** in 1:1 acetone:THF followed by counterion exchange ( $\text{NH}_4\text{PF}_6/\text{H}_2\text{O}/\text{CH}_3\text{CN}$ ). It was observed that **17E** and **17Z** quickly interconvert under normal room illumination. Therefore operations with pure isomers were carried out under red light.



**Scheme 11.** Synthesis of ruthenium complex **17E**.

### 2.4.2 Absorption and Emission Spectroscopy

The photophysical data for the compounds are summarized in Table 2. Figure 20 shows the absorption spectra for **16E**, **16Z**, **17Z**, and **17E**, and  $\text{Ru(bpy)}_3\text{Cl}_2$  at room temperature. Compounds **17Z**, **17E**, and  $\text{Ru(bpy)}_3\text{Cl}_2$  were dissolved in neat acetonitrile while **16E** had to be dissolved in neat  $\text{CH}_2\text{Cl}_2$ . Complexes **17E** and **17Z** are essentially composed of 1,2-bis(biphenyl)ethene TBS ether **16Z/E** appended to a  $\text{Ru(bpy)}_3^{2+}$  moiety. The absorption spectra of Figure 20 indicate that absorption results from additive properties of scarcely interacting Ru-based and 1,2-bis(biphenyl)ethene chromophores. This is consistent with the expectation that the ether linkage provides for an electronic separation between the Ru and 1,2-bis(biphenyl)ethene photoactive units. From the absorption properties of **17Z**, **17E** and their components, it seems reasonable that the use of  $\lambda_{\text{exc}} \geq 400 \text{ nm}$  irradiation would result in selective excitation of the

Ru(bpy)<sub>3</sub><sup>2+</sup> chromophore. Conversely, use of  $\lambda_{\text{exc}} \leq 370$  nm irradiation would produce excited states of both Ru and 1,2-bis(biphenyl)ethene components.

**Table 2.** Spectroscopic and photophysical data (CH<sub>3</sub>CN, 298 K).

Compound	Absorption	Emission
	$\lambda_{\text{max}}/ \text{nm} (\epsilon/\text{M}^{-1} \text{cm}^{-1})$	$\lambda_{\text{max}}/\text{nm}$
<b>16E</b>	265 (61 500), 309 (44 300)	
<b>16Z<sup>c</sup></b>	335 (59 300)	
<b>17Z</b>	247 (30 122), 286 (198 400),	612 <sup>a</sup>
	341 (33 100), 450 (18 260)	
<b>17E</b>	245 (66 757), 286 (178 080),	612 <sup>a</sup>
	341 (59 300), 450 (10 755)	
Ru(bpy) <sub>3</sub> <sup>2+</sup>	288 (57 400), 450 (10 500)	613 <sup>a</sup>
<b>13Z</b>	268 (31 000), 331 (31 600)	315 <sup>b</sup>
<b>18Z</b>	274 (34 200), 330 (24 800)	

---

<sup>a</sup>  $\lambda_{\text{exc}} = 450$  nm. <sup>b</sup>  $\lambda_{\text{exc}} = 285$  nm. <sup>c</sup> Measured in CH<sub>2</sub>Cl<sub>2</sub> at 298 K.

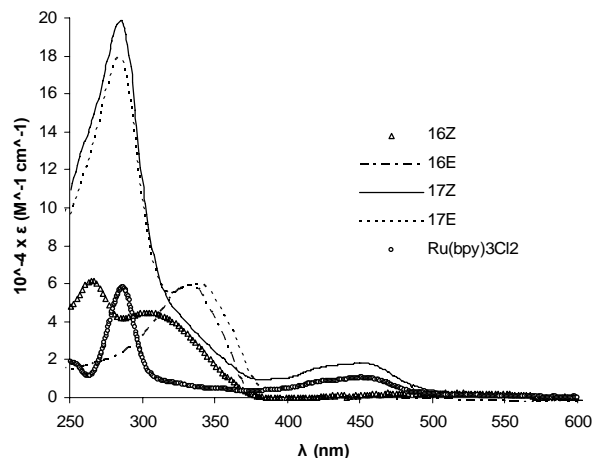


**Figure 20.** The room temperature absorption spectra<sup>a</sup> of **16Z**, **16E**<sup>b</sup>, **17Z**, **17E**, and Ru(bpy)<sub>3</sub><sup>2+</sup>.<sup>a</sup> Degassed 10 μM acetonitrile solutions. <sup>b</sup> Recorded in CH<sub>2</sub>Cl<sub>2</sub>.

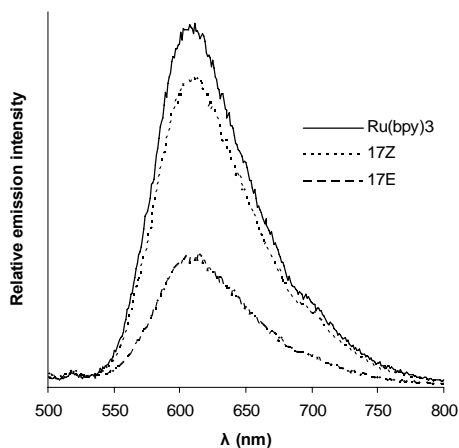


**Figure 21.** The room temperature emission spectra<sup>a</sup> of **17Z**, **17E** and Ru(bpy)<sub>3</sub>Cl<sub>2</sub>.<sup>a</sup> Degassed 10 μM acetonitrile solutions.

Excitation of complexes **17Z** and **17E** at  $\lambda_{\text{exc}} = 450$  nm in acetonitrile at room temperature results in luminescence centered at 570 – 680 nm. The data are summarized in Table 2, and Figure 21 shows the excitation spectra of **17Z**, **17E** and Ru(bpy)<sub>3</sub><sup>2+</sup>. The spectra

exhibit overlapping profiles, with the band maxima peaking at 612 nm. The emission intensity for the *Z* isomer is shown to be approximately 2.5 times more intense than that of the *E* isomer and it is slightly red-shifted, by 3 nm. It was stated earlier that the triplet-state energy for the *Z* stilbene (63 kcal/mol) is higher than that for *E*-stilbene (49 kcal/mol).<sup>44</sup> In the case of **17E**, it is likely that the triplet energy from the <sup>3</sup>MLCT excited state of Ru(bpy)<sub>3</sub><sup>2+</sup> (49 kcal/mol) is favorably intramolecularly transferred to the *E*-alkene moiety as a deactivation pathway. For the *Z* isomer **17Z**, on the other hand, such an intramolecular process is disfavored due to the higher triplet-state energy of the *Z* isomer.<sup>36d</sup>

### 2.4.3 Photoisomerization Reactivity.

#### 2.4.3.1 Electronic Absorption Studies.

For compounds **16Z/E** and **17Z/E**, direct visible light excitation at  $\lambda \geq 400$  nm gave  $Z \rightleftharpoons E$  isomerization as the only observed photoreaction event. To determine if **17Z/E** isomerizes under these conditions primarily due to an intramolecular interaction with the bound Ru(bpy)<sub>3</sub><sup>2+</sup> sensitizer, the concentration was varied and the photoreactivity of analog **16Z/E** with Ru(bpy)<sub>3</sub><sup>2+</sup> was studied for comparison. At dilute concentrations ( $\leq 10$   $\mu$ M), intermolecular quenching processes between donor and acceptor can be reduced so that the observed quenching is primarily due to intercomponent interactions.<sup>45</sup>

A 10  $\mu$ M degassed solution of **16Z/E** in 7:3 THF:CH<sub>3</sub>CN was irradiated in a darkened room using a 25 W incandescent lamp equipped with a 400 nm cutoff filter. UV-Vis spectral changes with a clean and well defined isosbestic point were observed. The isomerizations were

slow (by experimental design), requiring over 9 h to give no further UV-Vis spectroscopic changes. For **16E**, an isosbestic point at 304 nm was observed (Figure 22).

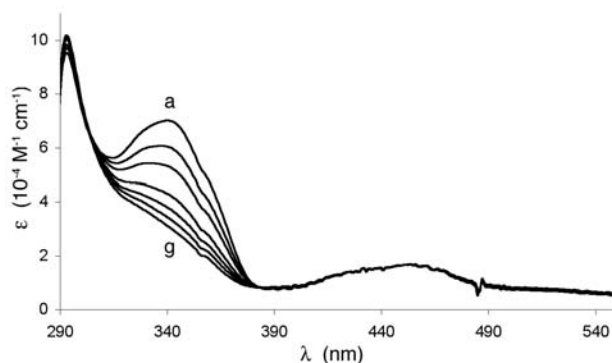


**Figure 22.** The UV-Vis spectral changes observed with complex **16E** upon irradiation at  $\lambda \geq 400$  nm at 0, 50, 100, 210, 300, 410, and 565 min (a-g, respectively) in 10  $\mu$ M 7:3 THF:CH<sub>3</sub>CN.

From initial photoisomerization experiments with **17Z/E**, it was found that the reaction rate was too rapid for direct observation under the conditions used for **16Z/E**. To slow the reaction rate, the light intensity was reduced by 51% through equipping the lamp with a neutral density filter. Upon irradiation of a degassed acetonitrile solution of **17Z** (8.2  $\mu$ M) or **17E** (7.4  $\mu$ M), UV-Vis spectral changes with a clean and well defined isosbestic point were observed. Complex **17Z** showed an increase in absorption intensity at 341 nm as well as an isosbestic point at 305 nm (Figure 23). Complex **17E** showed a decrease in absorption intensity at 341 nm as well as an isosbestic point at 303 nm (Figure 24). The photostationary state was reached within 45 min. The isomers **17Z/E** are distinguishable by <sup>1</sup>H NMR spectroscopy due to the chemical shift differences of the alkene and methylene protons. For instance, the chemical shifts of alkene protons H<sup>G</sup> and H<sup>G'</sup> are downfield in **17E** (7.38 ppm) relative to that of **17Z** (6.74 ppm) (Scheme 12). The methylene protons H<sup>E</sup> and H<sup>E'</sup> of **17Z**, which neighbor the chiral Ru(bpy)<sub>3</sub><sup>2+</sup> unit,

produce an AB quartet and are distinguishable from an AB quartet in **17E**. Observation of the changes in NMR chemical shift and peak intensity of **17Z/E** during photoisomerization confirmed that the UV-Vis spectroscopic changes are associated with the isomerization of the carbon-carbon double bond.

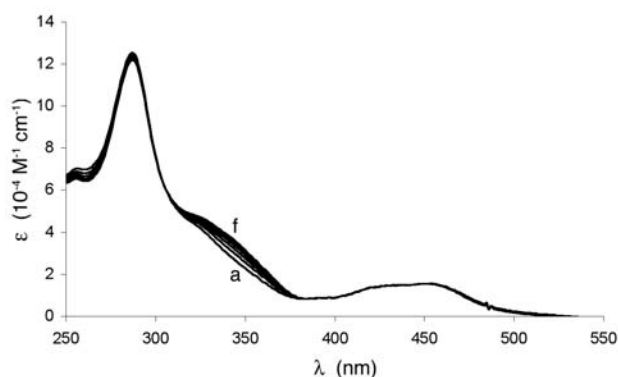


**Figure 23.** The UV-Vis spectral changes observed with complex **17Z** (8.2  $\mu\text{M}$  in degassed acetonitrile) upon irradiation at  $\lambda \geq 400$  nm at 0, 20, 40, 60, 80 and 100 min (a-f, respectively).

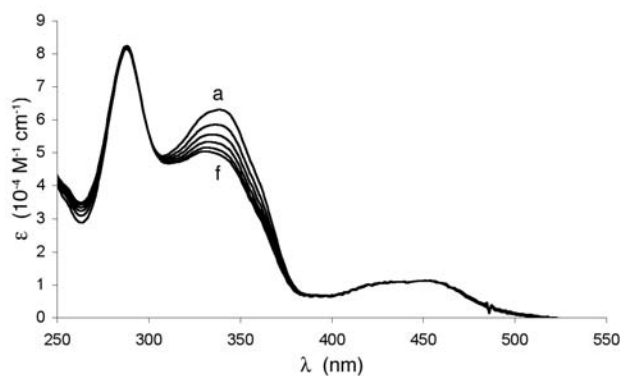
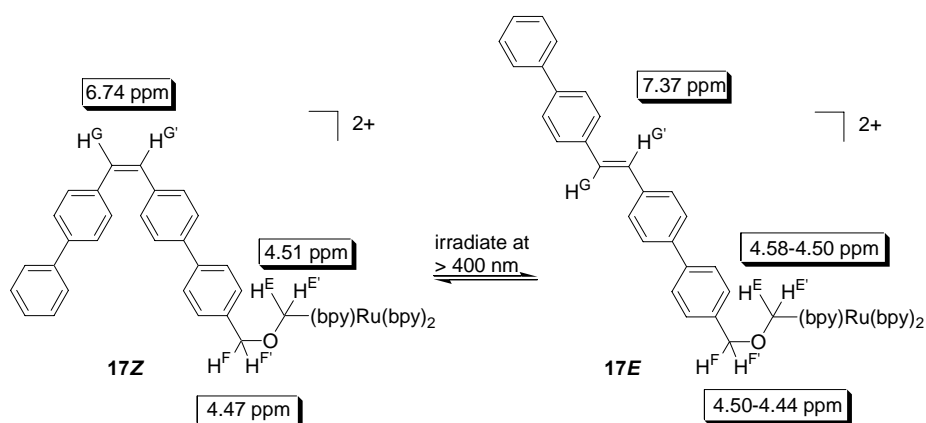


**Figure 24.** The UV-Vis spectral changes observed with complex **17E** (7.4  $\mu\text{M}$  in degassed acetonitrile) upon irradiation at  $\lambda \geq 400$  nm at 0, 20, 40, 60, 80, and 100 min (a-f, respectively).



**Scheme 12.**  $^1\text{H}$  NMR spectroscopic changes of **17Z** and **17E** in  $\text{CD}_3\text{CN}$  at 298 K.

#### 2.4.4 Kinetics.

To further investigate the process occurring in complexes **17Z/E** and compounds **16Z/E**, quantitative rate studies were undertaken. Solutions of pure **16Z** and **16E** ( $10\ \mu\text{M}$ , 70:30 THF: $\text{CH}_3\text{CN}$ ) were irradiated at  $\lambda \geq 400\ \text{nm}$  in the presence of  $10\ \mu\text{M}$   $\text{Ru}(\text{bpy})_3^{2+}$  sensitizer and monitored by UV-Vis at 350 nm. The concentration of *Z* and *E* precipiton present is plotted as a function of irradiation time in Figure 25. After 9.4 h of irradiation, solutions containing each pure isomer came to a final *Z/E* photostationary state, the average ratio of which was determined to be 93/7. The plots fit well to a reversible first-order rate curve (see Figure 25), and the rate constants were determined to be  $k_{Z \rightarrow E} = 0.80 \times 10^{-5}\ \text{s}^{-1}$  and  $k_{E \rightarrow Z} = 11.0 \times 10^{-5}\ \text{s}^{-1}$  (Table 3).

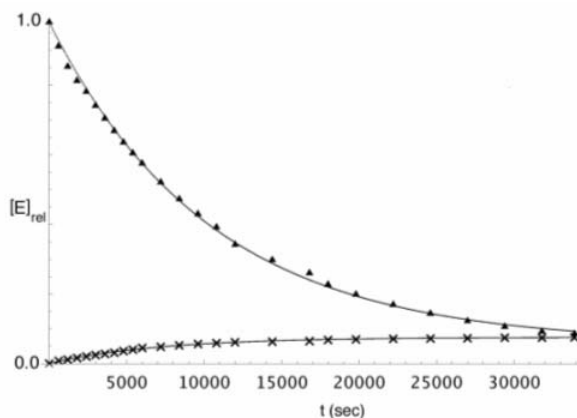
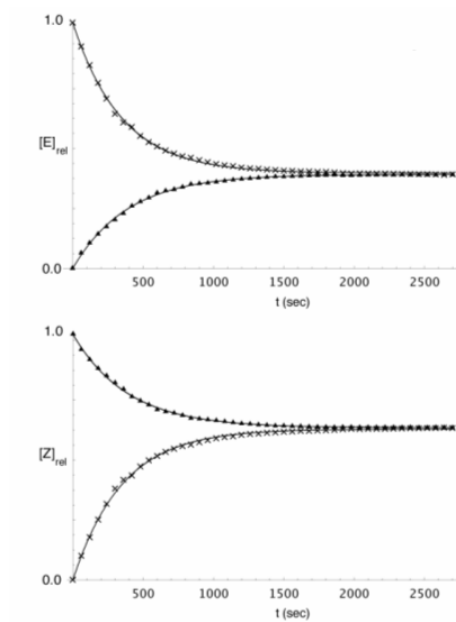


**Figure 25.** Photochemical production of photostationary state concentrations upon irradiation at  $\lambda \geq 400$  nm of **16Z/E** starting from pure **16Z** ( $\blacktriangle$ ) and **16E** ( $\times$ ).

Solutions of **17Z** and **17E** ( $\text{CH}_3\text{CN}$ ) were irradiated under the same conditions<sup>46</sup> as **16Z/E** and came to a final *Z/E* photostationary state, the average ratio of which was determined to be 62/38. Figure 26 plots the relative concentration of **17Z/E** formed or depleted in each reaction as a function of time.<sup>47</sup> The plots fit well to a reversible first order rate curve and the rate constants were determined to be  $k_{Z \rightarrow E} = 1.0 \times 10^{-3} \text{ s}^{-1}$  and  $k_{E \rightarrow Z} = 1.6 \times 10^{-3} \text{ s}^{-1}$ . When factoring the light reduction due to the 51% neutral density filter, the rate constant for  $Z \rightarrow E$  isomerization for **17Z** is 250 times faster than **16Z**, and the  $E \rightarrow Z$  isomerization for **17E** is 29 times faster than **16E**.



<sup>a</sup>[Z] vs time starting with 8.2  $\mu\text{M}$  **17Z**. <sup>b</sup>[E] vs time starting with 7.2  $\mu\text{M}$  **17E**.

**Figure 26.** Photochemical production of photostationary state concentrations upon irradiation at  $\lambda \geq 400$  nm of **17Z** ( $\blacktriangle$ ) and **17E** ( $\times$ ): (top) [**17E**] vs time; (bottom) [**17Z**] vs time.

**Table 3.** Isomerization rate constants and photostationary state ratios for the photoisomerization process of **16Z/E** and **17Z/E** upon irradiation at  $\lambda \geq 400$  nm.

Reaction	$k$ ( $\text{ms}^{-1}$ )	Z/E average ratio
<b>16E</b> $\rightarrow$ <b>16Z</b>	0.0080	
<b>16Z</b> $\rightarrow$ <b>16E</b>	0.11	93/7
<b>17Z</b> $\rightarrow$ <b>17E</b>	1.0	
<b>17E</b> $\rightarrow$ <b>17Z</b>	1.6	62/38

A control experiment to correct for the presence of any background  $Z \leftrightarrow E$  isomerization occurring from simple exposure to direct irradiation was performed on the untethered precipiton **13Z**. A 20 mM solution of **13Z** in acetonitrile was prepared and irradiated at  $\lambda \geq 400$  nm for 1 h. Only 3% had isomerized by  $^1\text{H}$  NMR spectroscopy analysis and produced a small amount of white precipitate. Formation of the *E*-isomer, however, was not observable by NMR due to its high insolubility.

## 2.5 CONCLUSION: RUTHENIUM TETHERED PRECIPITONS AS A MODEL SYSTEM FOR METAL SEQUESTRATION

The ruthenium tethered precipitons discussed in this chapter represent the first intramolecularly activated precipitons. The isomerization process is induced by intramolecular triplet energy transfer from a covalently attached metal complex. The intramolecular sensitization leads to a more rapid isomerization than can be achieved by intermolecular sensitization at accessible concentrations. Upon irradiating with visible light ( $\lambda \geq 400$  nm), **17Z/E** and **16Z/E** obeyed reversible first order rate kinetics. The intramolecularly sensitized precipiton **17Z** isomerized 250 times faster than the intermolecular case **16E**. Each isomer came to a final *Z/E* photostationary state, the average ratio of which was determined to be 31/19 for **17Z**  $\rightarrow$  **17E** and 93/7 for **16E**  $\rightarrow$  **16Z**.

The impetus for this study was to begin to evaluate the possibility of using metal binding precipitons that would precipitate only upon metal-to-precipiton binding and would be inert to visible light in the absence of metals. This investigation demonstrated a significant isomerization rate enhancement for precipitons containing a bound metal sensitizer compared to

their unbound analogs. This is a significant step forward in the development of precipitons as energy-driven metal scavengers.

## 2.6 ADDITIONAL PRECIPITONS FOR METAL SCAVENGING

In addition to the  $\text{Ru}(\text{bpy})_3^{2+}$  bound precipitons, other precipitons were investigated as potential metal sequestering agents.

### 2.6.1 Tetraethyldiethylenetriamine (TEDETA) Functionalized Precipitons

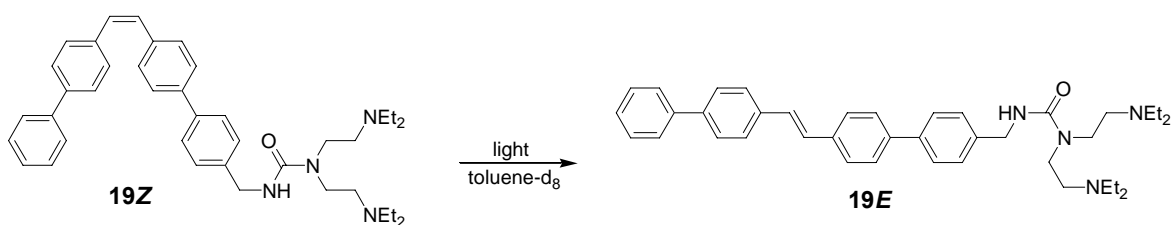
Tetraethyldiethylenetriamine functionalized precipitons were reported by Brittain et al. as successful scavengers of CuBr catalyst from ATRP reactions. However, the precipiton scavenging mechanism was not determined. Was this an example of isomerization “triggered” by metal sequestration? To answer this question, 1,2-bis(biphenyl)ethene TEDETA precipiton **19Z** was resynthesized and isomerized under various reaction conditions (Table 4).

In each reaction, a 20 mM solution of **19Z**, internal standard, and 50  $\mu\text{M}$  sensitizer (where appropriate) was prepared in air-equilibrated toluene- $\text{D}_8$ . The reaction mixture was irradiated at the specified wavelength and the  $^1\text{H}$  NMR spectroscopic changes of **19Z** were observed. The results indicated no significant outcome difference with and without the presence of CuBr.

Brittain’s group employed a high intensity xenon arc lamp to irradiate the precipiton containing polymer mixture. It is likely that the precipiton isomerization proceeded through a singlet excited state pathway. From the present experiments it can be seen that a special relationship between the binding metal and its ligands must exist in order to allow for triplet

energy excitation. For example, some very effective inorganic triplet energy sensitizers are polypyridyl complexes containing low spin  $d^6$  transition metals. This combination allows electronic transitions such as metal-to-ligand charge transfer (MLCT).<sup>48</sup> Some polypyridyl transition metal complexes known to have triplet character include Ru(II), Re(I), Cu(I) and Os (II).

**Table 4.** The results of photochemical isomerizations of **19Z**.



Reaction	Light (nm)	Catalyst (eq)	Time (h)	Product
1	> 400	----	8.5	15% <i>E</i>
2	> 400	CuBr (1.5)	6.5	17% <i>E</i>
3	> 400	Erythrosine B (0.05)	5	96% <i>E</i>
4	> 400	CuBr (1.0), erythrosine B (0.05)	9	44%
5	350	----	0.6	18% <i>E</i> , 70% cyclobutane <b>39</b> + <b>40</b>
6	350	CuBr (1.0)	3	15% <i>E</i> , 80% cyclobutane <b>39</b> + <b>40</b>

## 2.6.2 Bipyridine Functionalized Precipiton with a Rigid Phenylene

A main purpose for the development of metal binding precipitons is the sequestration of metal contaminants from solution. The  $\text{Ru}(\text{bpy})_3^{2+}$  bound precipitons previously described provided a model system toward this goal. However, in order for precipitons to be useful as scavengers, they need to bind with metals while in solution. The possibility of capturing ruthenium using precipiton **20Z** (Figure 27) was therefore examined.

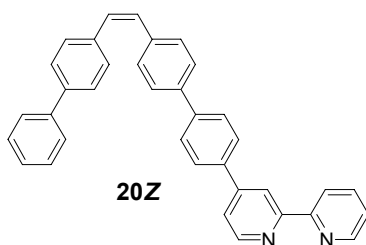
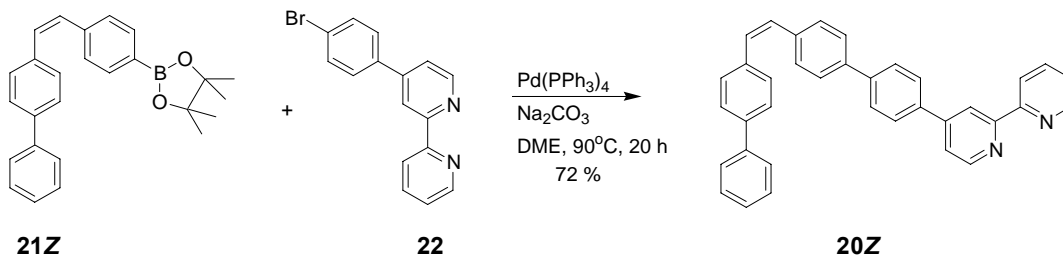


**Figure 27.** Dexter-type precipiton **20Z**.

The preparation of **20Z** was achieved through a Suzuki cross-coupling reaction between 4-(4-bromophenyl)-[2,2']bipyridine **22** and pinacolboronic ester **21Z** in 72 % yield (Scheme 13).



**Scheme 13.** Synthesis of precipiton **20Z**.

To test the possibility of a change in the isomerization rate of **20Z** due to metal binding, the isomerization rates of **20Z** and **13Z** were compared in 11 different conditions (Figure 28, 29). In each experiment, a 1 mM solution of precipiton, internal standard, and 50  $\mu\text{M}$  sensitizer (where appropriate) was prepared in air-equilibrated 1/1  $\text{CD}_2\text{Cl}_2/\text{CD}_3\text{CN}$  and transferred via syringe into an NMR tube. The reaction mixture was irradiated at  $\lambda_{\text{exc}} \geq 400 \text{ nm}$  and the  $^1\text{H}$  NMR spectroscopic changes of the precipiton were observed by Method A. Table 5 summarizes the isomerization rates for **20Z** and **13Z**.

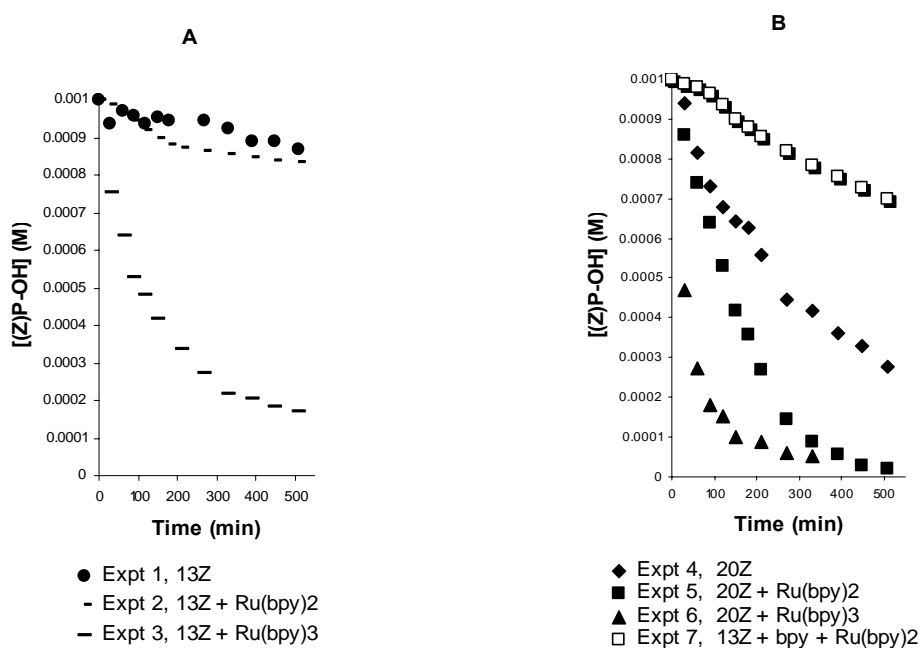


**Figure 28.** Plot of photoisomerization reactions 1-7 ( $[\mathbf{13Z}]$ ,  $[\mathbf{20Z}] = 1 \text{ mM}$ ;  $[\text{Ru}(\text{bpy})_3^{2+}]$ ,  $[\text{Ru}(\text{bpy})_2^{2+}] = 50 \mu\text{M}$ , solvent = 1/1  $\text{CD}_2\text{Cl}_2/\text{CD}_3\text{CN}$ ).

**Table 5.** Summary of isomerization rates after 30 min of irradiation.

Expt	Slope ( $\times 10^{-8}$ )	k ( $\times 10^{-5}$ )( $\text{sec}^{-1}$ )	pseudo 1 <sup>st</sup> -order rxn rate ( $\times 10^{-8}$ ) ( $\text{sec}^{-1}$ )	% conversion (510 min)
1	3.6	3.6	3.6	13
2	0.56	5.6	0.56	16
3	12.9	12.9	12.9	83
4	3.3	3.4	3.3	72
5	7.7	7.8	7.7	98
6	29.4	29.4	29.4	100
7	0.56	5.6	0.56	30
8	6.9	6.9	6.69	92
9	2.0	2.0	2.01	73
10	28.1	28.1	28.1	90
11	15.0	15.0	15.0	82

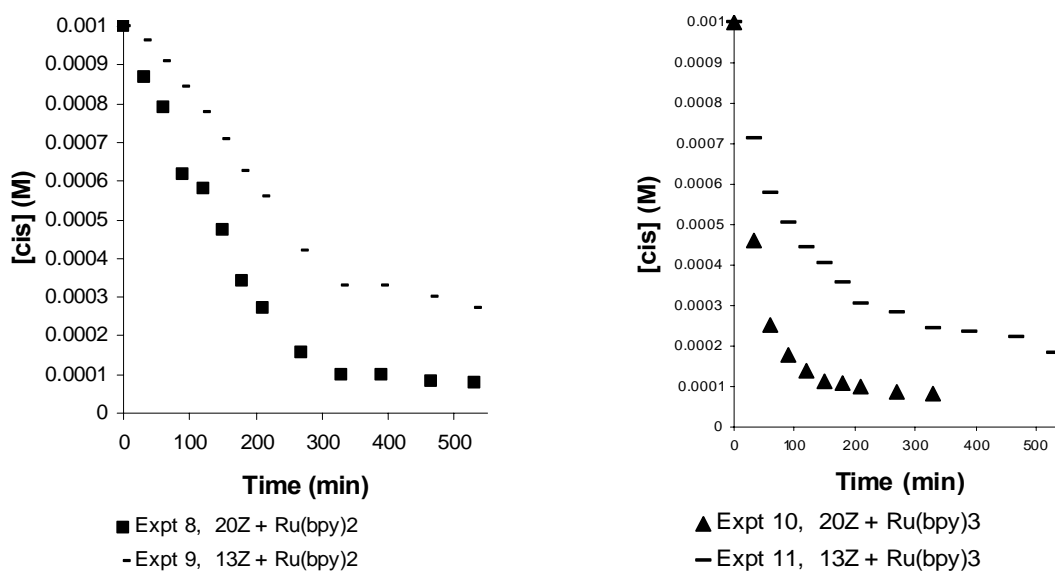


**Figure 29.** Plot of photoisomerization reactions 8-11. Reactions 8 and 9 were performed in one NMR tube and reactions 10 and 11 were performed in one NMR tube.

Several conclusions may be based on the data in Figure 28, 29, and Table 5. First,  $\text{Ru}(\text{bpy})_3^{2+}$  is a more effective sensitizer than  $\text{Ru}(\text{bpy})_2^{2+}$ , based on the % conversions of **13Z** and **20Z**. Second, direct irradiation of **13Z** and **20Z** at  $\lambda_{\text{exc}} \geq 400$  nm showed that **20Z** is a better chromophore for isomerization. Third, the initially slow isomerization rate of **13Z** in experiment 7 showed that 2,2'-bipyridine binding to  $\text{Ru}(\text{bpy})_2^{2+}$  is slow if occurring at all. Although the initial isomerization rate of **13Z** in experiment 9 is 4 times faster than experiment 2, consistent with **20Z**: $\text{Ru}(\text{bpy})_2^{2+}$  binding, the isomerization rate of **20Z** (experiment 8) did not show a characteristic increase.

Four complications with precipiton **20Z** prevented further conclusions. They were : 1) the lack of quantitative knowledge of ligand exchange rates, 2) the significant background isomerization rate of **20Z**, 3) the heterogeneous nature of the reaction mixtures, and 4) the photodissociation of  $\text{Ru}(\text{bpy})_3^{2+}$  in specific solvents.

It was assumed that  $\text{Ru}(\text{bpy})_2^{2+}$  binding to **20Z** is facile. However, the precipiton studies showed no evidence of 2,2'-bipyridine binding to  $\text{Ru}(\text{bpy})_2^{2+}$ . Attempts at determining a binding constant (Figure 30) revealed little or no binding between 2,2'-bipyridine and  $\text{Ru}(\text{bpy})_2^{2+}$ .

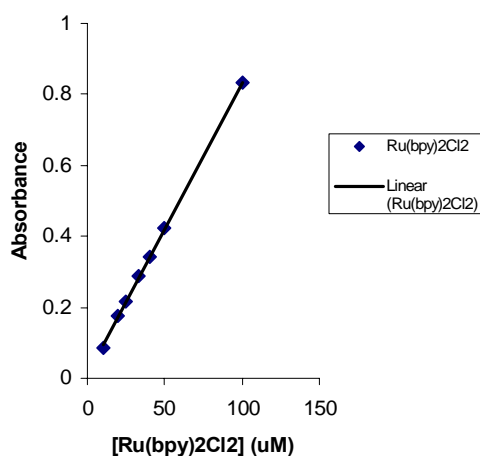


**Figure 30.** Absorbance spectra of the dilution of a 1/1 2,2'-bipyridine/ $\text{Ru}(\text{bpy})_2^{2+}$ .

The design of rigid, conjugated linkers such as that in **20Z** can be problematic due to an accompanying bathochromic shift in absorbance (Figure 31). Any observable isomerization rate enhancement due to ruthenium binding may be made irrelevant by the background direct irradiation pathway.

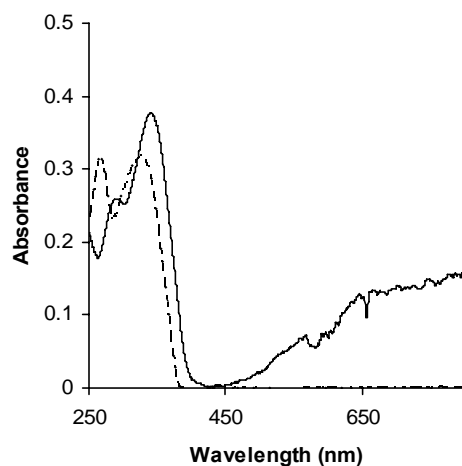
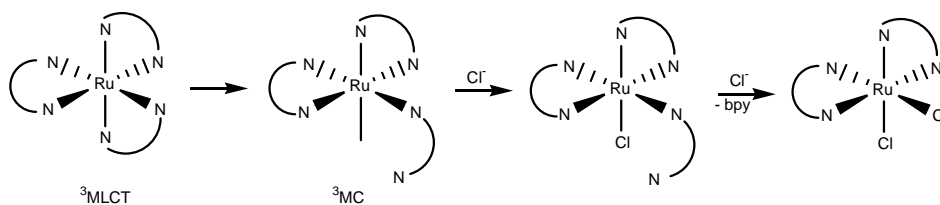


**Figure 31.** A comparison of room-temperature absorption spectra of **13Z** (---) and **20Z** (—) (10  $\mu$ M, air-equilibrated  $\text{CH}_3\text{CN}$ ).

Irradiation of **20Z** +  $\text{Ru}(\text{bpy})_2^{2+}$  /  $\text{Ru}(\text{bpy})_3^{2+}$  (Figure 28, Experiment 5, 6) results in precipitation and a color change of the solution from red to colorless. This observation could be interpreted as evidence of  $\text{Ru}:\mathbf{20Z}$  binding and precipitation. A more reasonable explanation is the known photodissociation and photosubstitution of the Ru complexes (Scheme 14).<sup>49</sup>



**Scheme 14.** Modes of ring opening that can result in the formation of photosubstitution.

### **3.0 BENZIL TETHERED PRECIPITONS FOR CONTROLLING SOLUBILITY**

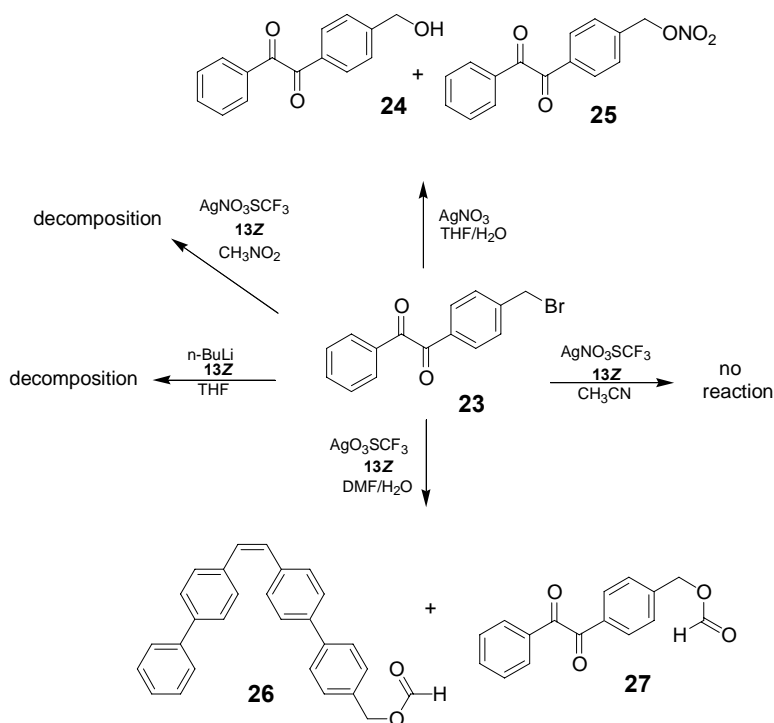
### 3.1 INTRODUCTION

The Wilcox lab is interested in developing precipitons as solubility-based photoswitchable materials. Methods traditionally employed to alter morphology include changing the temperature or pressure of a material's environment. However, an additional strategy for accomplishing this is the incorporation of a photo-responsive component into the molecular structure, which could allow a controlled structural change to occur. Precipitons may be useful for this because the solubilities of their two isomeric forms (*Z* and *E*) can differ by factors greater than 2000. Precipiton  $Z \rightarrow E$  photoisomerization and precipitation has been well established by the Wilcox group. However, the reverse  $E \rightarrow Z$  isomerization to cause resolubilization of the *Z* precipitate has not been optimized and there are interesting questions regarding that process. For example, what is the rate determining step? Is the  $E \rightarrow Z$  isomerization the slow step or is the dissolution of starting *E* precipiton the slow step? Studies of precipiton isomerization activated by a covalently attached organic sensitizer for the purpose of optimizing  $E \rightarrow Z$  isomerization are important to answering these questions.

### 3.2 PRECIPITON DESIGN

It is expected that controlled  $E \rightarrow Z$  photoisomerization can be accomplished by chemical attachment of a sensitizer to the precipiton that contains the appropriate triplet energy. The data compiled by Hammond et al. (Figure 4) shows that triplet energy sensitizers in the range of 48-

52 kcal/mol produce the highest levels of *Z*-stilbene at the photostationary state. A search for the commercial availability of functionalized variations of those sensitizers revealed that benzil (53 kcal/mol) can be purchased as its benzil bromide analog. It planned to be couple to 1,2-bis(biphenyl)ethene alcohol **13Z** through an ether linkage. However, 4-(bromomethyl)benzil was not stable under base treatment and attempts at coupling 4-(bromomethyl)benzil to precipiton **13Z** using halide abstractor  $\text{AgO}_3\text{SCF}_3$  resulted in either decomposition (in  $\text{CH}_3\text{NO}_2$  solvent), no reaction (in  $\text{CH}_3\text{CN}$  solvent), or formation of formate ester products **26** and **27** (in DMF solvent) (Scheme 15).



**Scheme 15.** Reactions of 4-(bromomethyl)benzil **23**.

Treatment of 4-(bromomethyl)benzil **23** with aqueous AgNO<sub>3</sub> in THF afforded the benzyl alcohol **24** and nitrate ester **25**. Coupling was therefore pursued based on an ester linkage. The commercial availability of precipiton synthetic precursors allowed the flexibility to design precipiton analogs that attach benzil at differing positions relative to the precipiton (*para* **28Z/E** vs *meta* **29Z/E**) (Figure 32). It was suspected that the benzil-precipiton orientation may affect the photoisomerization kinetics and photostationary state ratios.

In this chapter, the synthesis, photophysical properties, and photoisomerization kinetics of precipitons that are covalently linked and unlinked to a benzil unit<sup>50</sup> are discussed. The photoisomerization kinetics and photostationary state ratios of the benzil-linked precipitons **28Z/E** and **29Z/E** at low concentration (10 μM) were compared to those of unlinked examples **16Z/E**. Compounds **28Z/E** and **29Z/E** differ in regard to the position of the benzil sensitizer relative to the precipiton (*para* vs *meta*). The differences in photoisomerization kinetics and photostationary state ratios will be discussed and a mechanism for the isomerization will be proposed.

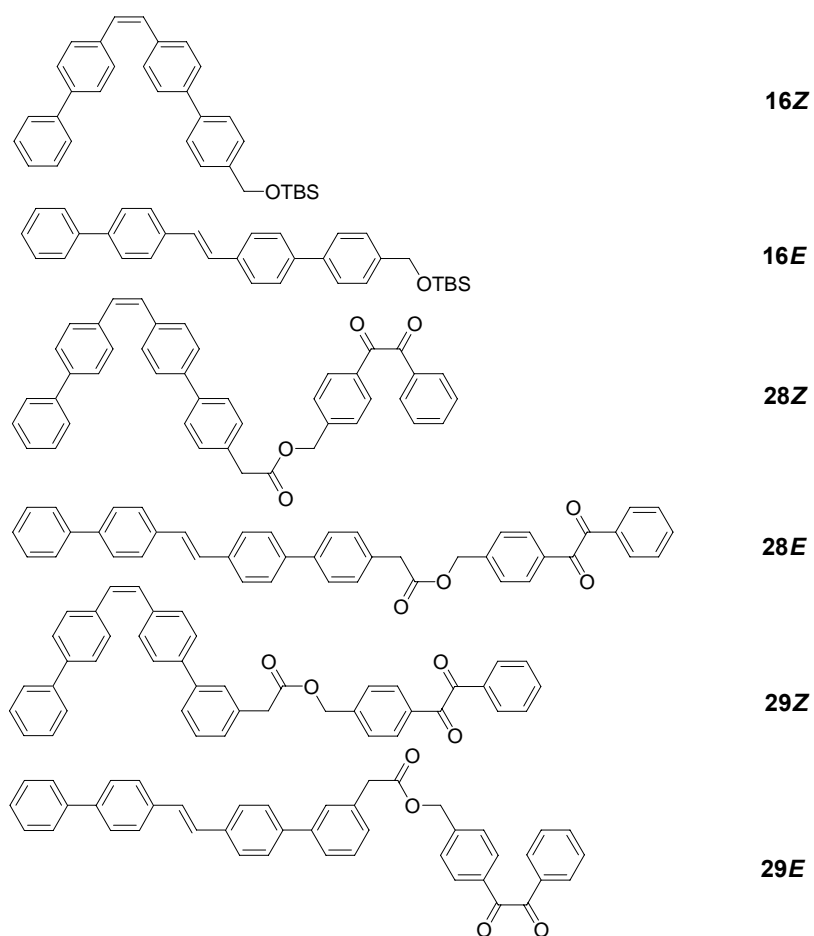


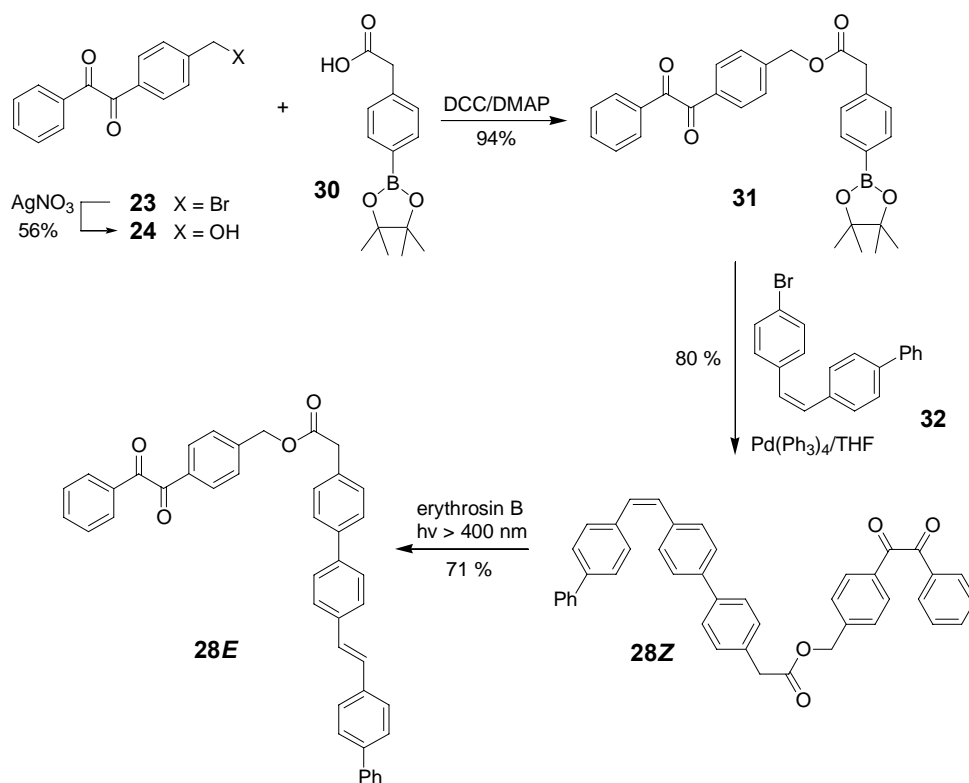
**Figure 32.** *Para* and *meta* benzil precipiton esters and their unbound analogs.

### 3.3 RESULTS AND DISCUSSION

#### 3.3.1 Synthesis

Esterification of alcohol **24** (Scheme 16) with the *para*-substituted phenylboronate ester **30** afforded a 94% yield of the benzil-tagged boronic ester **31**. Suzuki coupling between **31** and 1-[2-(4-bromophenyl)]biphenyl ethene **32** afforded the benzil modified 1,2-bis(biphenyl)ethene

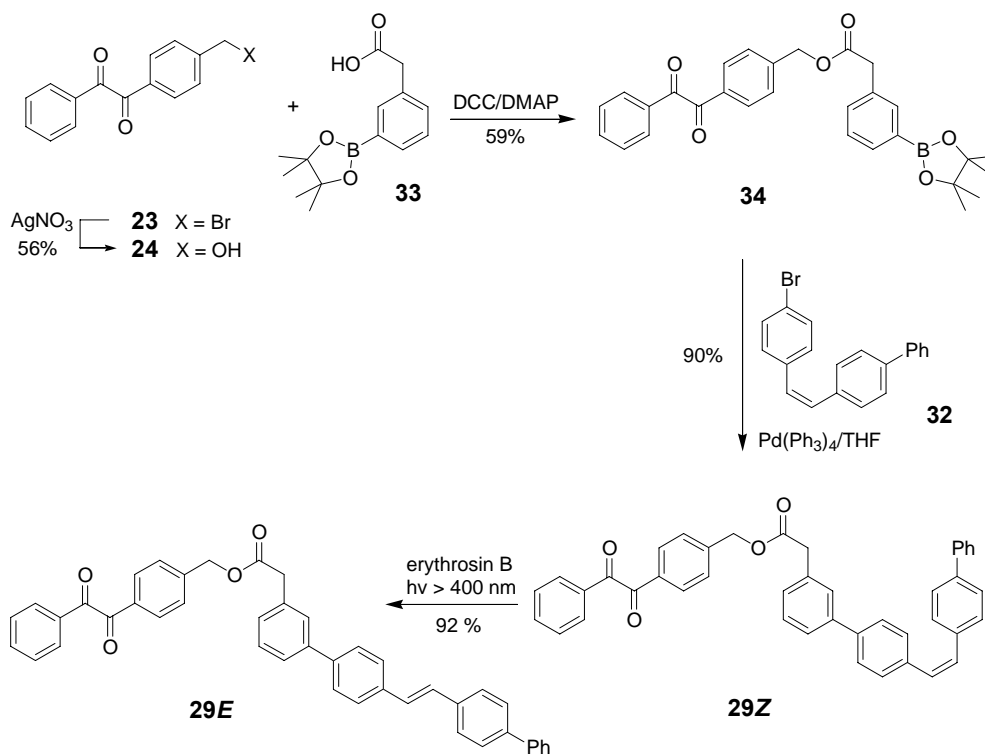
analog **28Z** in 80% yield. Sensitized photoisomerization of **28Z** using erythrosin B in THF afforded *E* isomer **28E** in 71% yield.



**Scheme 16.** Synthesis of **28Z** and **28E**.

Synthesis of the *meta*-linked isomers **29Z** and **29E** followed a similar pathway (Scheme 17). Esterification of alcohol **24** with the *meta*-substituted phenylboronate ester **33** afforded a 59% yield of the benzil-tagged boronic ester **34**. Suzuki coupling between **34** and 1-[2-(4-bromophenyl)]biphenyl ethene **32** afforded the benzil modified 1,2-bis(biphenyl)ethene analog

**29Z** in 90% yield. Sensitized photoisomerization of **29Z** using erythrosin B in THF afforded *E* isomer **29E** in 92% yield.



**Scheme 17.** Synthesis of **29Z** and **29E**.

### 3.3.2 Absorption and Emission Spectroscopy

The photophysical data for the compounds are summarized in Table 6. Figure 33 shows the absorption spectra for each compound in neat THF at room temperature. As expected, the ethylene absorption in this region is more intense for the *E* isomers compared to the *Z* isomers.

The most intense absorptions are seen for the *para*-substituted precipiton **28E** and the untethered precipiton **28Z**. The *meta*-substituted precipiton **29E** is the weakest absorbing *E* isomer. This sequence of absorbance intensity is repeated for the *Z* isomers.

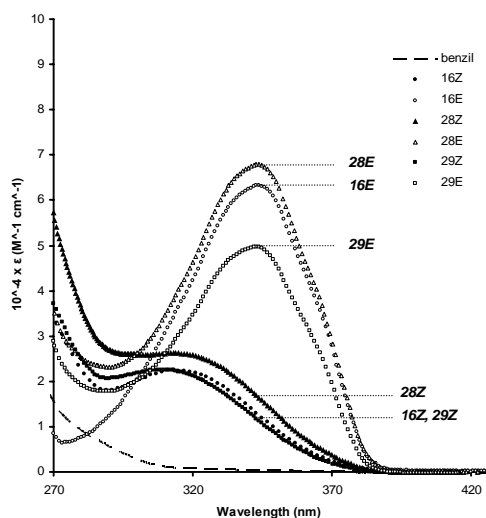


**Figure 33.** Room-temperature absorption spectra for degassed 10  $\mu$ M THF solutions of **16Z**, **16E**, **28Z**, **28E**, **29Z**, **29E**, and benzil.

Benzil exhibits only very weak absorption in the UV range above 300 nm and has insignificant absorption above 340 nm. In the studies of the  $\text{Ru(II)(bpy)}_3^{2+}$  intramolecularly sensitized isomerization of these stilbenes, light of wavelengths greater than 400 nm was used. The interest here, for practical reasons, was in the behavior of these molecules under the influence of inexpensive visible light sources. Therefore, the isomerization studies were conducted with irradiation from an incandescent source without filtering. For the lamp used, the power output in the 300-320 nm wavelength range is less than 1% of the power output in the 320-400 nm range. It should be noted before further discussion that the absorbance of the

precipiton moiety is far larger than that of the benzil moiety in the region of highest output from this light source.

**Table 6.** Spectroscopic data in THF at 298 K.

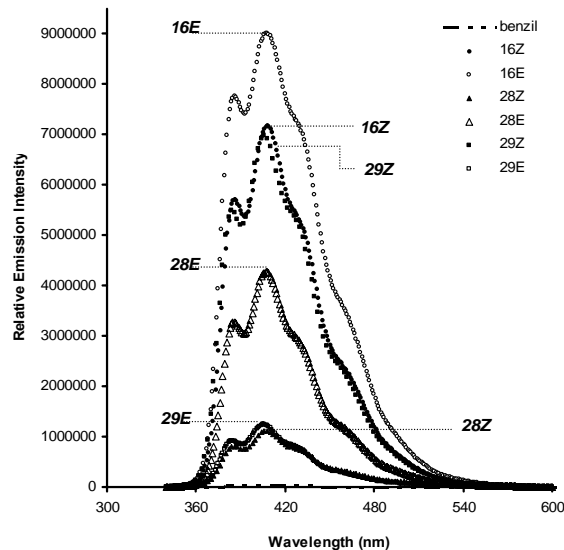
<b>Compound</b>	<b>Absorption</b> $\lambda_{\max}/\text{nm}$ ( $\epsilon/\text{M}^{-1} \text{cm}^{-1}$ )	<b>Emission</b> $\lambda_{\max}/\text{nm}$ <sup>a</sup>
<b>16Z</b>	313 (22 610)	387, 409, 432, 465
<b>16E</b>	344 (63 267)	384, 409, 433, 464
<b>Benzil</b>	249 (39 103), 255 (43 193), 261 (35 851), 282 (8 303)	413
<b>28Z</b>	249 (12 394), 255 (13 902), 261 (11 862), 319 (25 931)	386, 408, 431
<b>28E</b>	249 (11 761), 255 (12 771), 261 (99 979), 341 (67 480)	386, 408, 431, 464
<b>29Z</b>	249 (59 937), 255 (60 602), 261 (53 967), 306 (23 272)	385, 407, 428, 461
<b>29E</b>	249 (97 959), 255 (109 682), 261 (85 832), 340 (49 315)	385, 407, 432

---

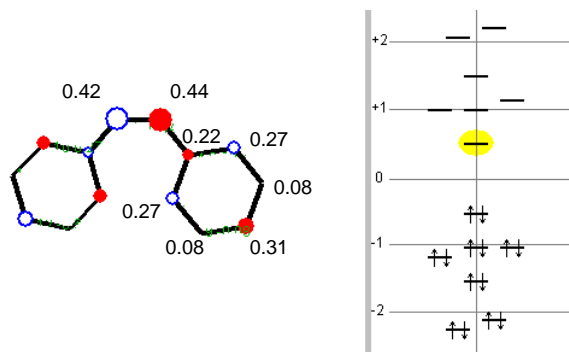
<sup>a</sup>  $\lambda_{\text{exc}} = 320\text{nm}$ .

Figure 34 illustrates the fluorescence of the investigated compounds upon excitation at 320 nm. Viewing **16E** as the control, these results indicate that the observed precipiton luminescence is quenched when the precipiton is covalently linked to the benzil moiety. The

luminescence of **16E** is two times more intense than the luminescence of **28E** and seven times more intense than that of **29E**. The emission positions and vibronic progressions for each precipiton remained unchanged. The same quenching effect is observed for **28Z** compared to the untethered **16E**. The luminescence of **29Z** is interesting in that it is identical with that of **16Z**. The origin of this effect is not clear, but is probably not due to the movement of the non-conjugating substituent to the *meta* position for **29Z**. It has been observed that methyl substitution in different positions on the phenyl rings in *E*-stilbene has an insignificant effect on absorption and fluorescence spectra.<sup>51</sup> Figure 35 shows the LUMO coefficient approximations for the carbon atoms of *Z* and *E*-stilbene.<sup>52</sup> The *meta* carbons have smaller coefficients than the *para* carbons, thus contributing less to the overall molecular orbital.



**Figure 34.** Emission spectra for degassed 10  $\mu\text{M}$  THF solutions of **16Z**, **16E**, **28Z**, **28E**, **29Z**, **29E** at 25  $^{\circ}\text{C}$ .



**Figure 35.** The approximate coefficients for the LUMO state of *Z*-stilbene.

### 3.3.3 Photoisomerization Kinetics

To test whether isomerization of the tethered precipiton is influenced by an intramolecular interaction with the nearby benzil chromophore, quantitative rate studies were undertaken. Separate degassed solutions of pure **16Z** and **16E** (10  $\mu\text{M}$ , THF) were irradiated with a 25 W incandescent lamp in the presence of 10  $\mu\text{M}$  benzil sensitizer and changes in absorbance were monitored at 345 nm. The concentration of **16Z** and **16E** present is plotted as a function of irradiation time in Figure 36. After 7 h of irradiation, solutions containing each pure isomer came to a final *Z/E* photostationary state, the average ratio of which was determined to be 22/78. The plots analyzed according to a reversible first-order rate curve and the sum of the forward and reverse rate constants for each reaction were averaged and determined to be  $k_1 + k_{-1} = 2.1 \times 10^{-4} \text{ s}^{-1}$  (Table 7). There are small deviations from first order behavior here and with **29Z/E** (Figure 37b) but not in **28Z/E** (Figure 37a). The extent of deviation correlates with the extent of singlet participation in the process (see discussion below), and is probably caused by minor side reactions from the singlet excited states.

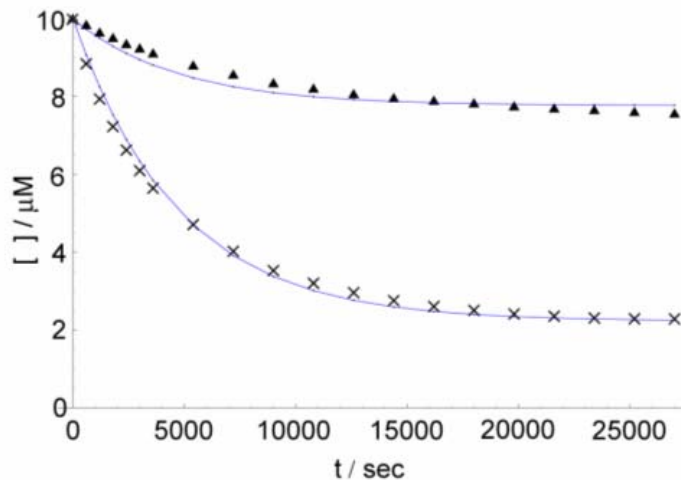


**Figure 36.** Reaction progress upon irradiation of 10  $\mu\text{M}$  THF solutions of **16Z** (x) and **16E** (▲) in the presence of one equivalent of benzil.

Separate solutions of each isomer **28Z/E** and **29Z/E** were irradiated under the same conditions as used in the isomerization of **16Z/E**. For all four isomers, the photostationary state was reached within 70 minutes. The average ratio of the photostationary state was determined to be 90/10 for **28Z/E** and 76/24 for **29Z/E** (Table 7). The concentration of **E** and **Z** precipiton present is plotted as a function of irradiation time and fits well to a reversible first-order rate curve (Figure 37). The sum of the forward and reverse rate constants for each reaction were averaged and determined to be  $k_1 + k_{-1} = 9.5 \times 10^{-4} \text{ s}^{-1}$  for the *para* tethered benzil isomers **28Z/E**, and  $k_1 + k_{-1} = 6.7 \times 10^{-4} \text{ s}^{-1}$  for the *meta* tethered benzil isomers **29Z/E**.

**Table 7.** Isomerization rate constants, half-lives, and photostationary state ratios for the photoisomerization process of **16Z**, **16E**, **28Z**, **28E**, **29Z**, and **29E** upon irradiation at 10  $\mu\text{M}$ .

<b>Reaction</b>	<b>k (s<sup>-1</sup>) x 10<sup>4</sup></b>	<b>t<sub>1/2</sub> (sec)</b>	<b>Z/E ratio</b>
<b>16Z</b> $\rightarrow$ <b>16E</b> <sup>a</sup>	1.7	4077	19/81
<b>16E</b> $\rightarrow$ <b>16Z</b> <sup>a</sup>			
<b>16Z</b> $\rightarrow$ <b>16E</b> <sup>b</sup>	2.1	3300	22/78
<b>16E</b> $\rightarrow$ <b>16Z</b> <sup>b</sup>			
<b>28Z</b> $\rightarrow$ <b>28E</b>	9.5	730	90/10
<b>28E</b> $\rightarrow$ <b>28Z</b>			
<b>29Z</b> $\rightarrow$ <b>29E</b>	6.7	1034	76/24
<b>29E</b> $\rightarrow$ <b>29Z</b>			

<sup>a</sup>Reaction observed only for the first half-life. All others were observed for the first five half-lives. <sup>b</sup>Reaction carried out in the presence of benzil (10  $\mu\text{M}$ ).

A control experiment was performed to evaluate the intermolecular effect of benzil (Table 7). Separate solutions of 10  $\mu\text{M}$  **16Z** and **16E** were prepared in degassed THF and irradiated using the same experimental conditions as described above. After 7.5 h of irradiation, solutions containing each pure isomer came to a final Z/E photostationary state, the average ratio of which was determined to be 19/81. The sum of the forward and reverse rate constants for each reaction were averaged and determined to be  $k_1 + k_{-1} = 1.7 \times 10^4 \text{ s}^{-1}$ .

The effect of covalent attachment of benzil to the precipiton can be observed in the resulting isomerization kinetic data and final photostationary state ratios (Table 7). The first half-life for the direct irradiation of **16Z/E** (no benzil) was weakly affected (1.2 times longer)

upon addition of benzil. It can be concluded that under these experimental conditions singlet excitation of the precipiton *via* direct irradiation plays a major role in the isomerization process,<sup>53</sup> and that benzil contributes only to a minor extent as an intermolecular agent at 10  $\mu\text{M}$ . This is not unexpected upon consideration of the low light absorption of benzil compared to precipiton in this wavelength range. The final photostationary state ratios were changed only very slightly (toward the *Z* isomer) by the presence of benzil.

In contrast, when the benzil moiety is covalently attached and thus restricted in distance and orientation relative to the precipiton, the final photostationary states for the isomerizations are significantly shifted in favor of the *Z* isomers. This effect is most pronounced for the *para* substituted benzil tethered isomers **28Z/E**. Here the final equilibrium consisted of 90% *Z*-isomer, whereas the intermolecular benzil effect led to only 20% *Z*-isomer. The half-lives for isomerization also decreased significantly for the benzil-tethered precipitons. The first half-life for *para* substituted **28Z/E** was completed 4.5 times faster than that for **16Z/E** + benzil, and *meta* substituted **29Z/E** was completed 3 times faster than than that for **16Z/E** + benzil.

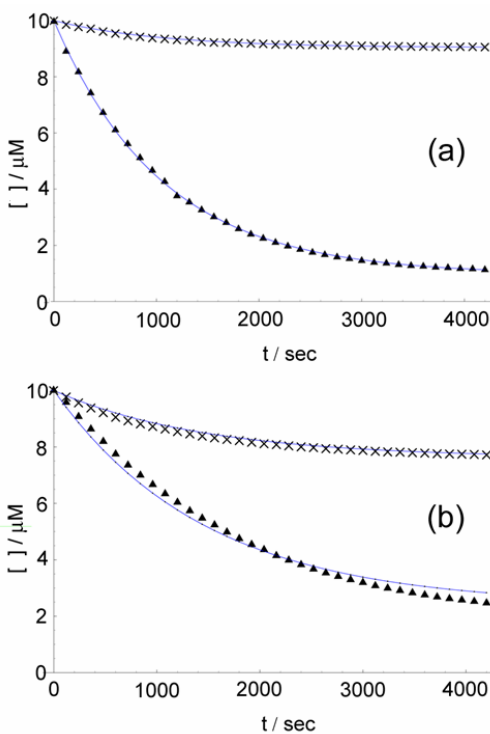


**Figure 37.** (a) Reaction progress upon irradiation of 10  $\mu\text{M}$  THF solutions of **28Z** ( $\times$ ) and **28E** ( $\blacktriangle$ ). (b) Reaction progress upon irradiation of 10  $\mu\text{M}$  THF solutions of **29Z** ( $\times$ ) and **29E** ( $\blacktriangle$ ).

### 3.4 INVESTIGATION OF THE ENERGY TRANSFER PATHWAY

An interesting observation from the data was that benzil had the most significant effect on the precipiton photostationary states and the rates of isomerization only when it was chemically attached, yet benzil barely absorbs light energy. It was expected that photoisomerization for these precipitons begins with the singlet excited state of the precipiton. The absorbance of this chromophore is dominant within the range of available wavelengths. It is known that isomerization of stilbene upon direct photoexcitation proceeds via a singlet excited state and not

a triplet excited state (unless a substituent that promotes intersystem crossing is present).<sup>54</sup> Therefore isomerization of **16Z/E** (Table 7) under direct irradiation is expected to follow a singlet pathway. There was no effect on rate of isomerization of **16Z/E** when an equal concentration of benzil sensitizer was added. This is good evidence against any intermolecular triplet sensitization in the isomerizations of **28Z/E** and **29Z/E**. To test whether benzil at the investigated concentrations (10  $\mu\text{M}$  benzil:10  $\mu\text{M}$  precipiton) quenches the singlet state of the precipiton, fluorescence spectra of **16Z/E** were compared to **16Z/E** + benzil (Figure 38). The fluorescence intensity from **16Z** was slightly quenched, and **16Z** was essentially unchanged when benzil was added to the solution (this is consistent with Figure 34 which also shows *Z* being less quenched than *E*). This reveals that intermolecular quenching is very slight at these concentrations (10  $\mu\text{M}$ ).

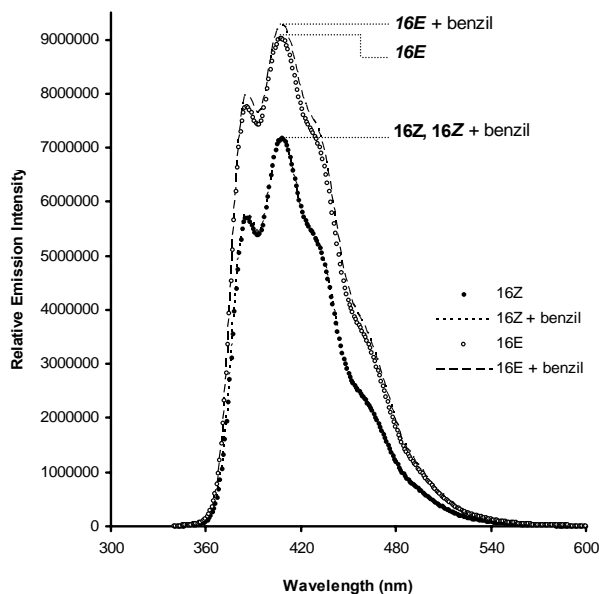


**Figure 38.** Fluorescence emission spectra of 10  $\mu\text{M}$  **16Z** and **16E** compared to a solution of **16Z/E** + benzil at the same concentration in THF;  $\lambda_{\text{exc}} = 320\text{nm}$ .

### 3.4.1 Proposal of a Round-Trip Energy Transfer Pathway

The isomerization kinetics are significantly faster for the benzil-tethered precipitons **28Z/E** and **29Z/E**. As shown in Figure 34, the normal stilbene-derived fluorescence caused by singlet excitation for **16E** and **16Z** is considerably quenched for **28Z/E** and **29E**. The explanation for the proposed rate enhancement is that the singlet-singlet energy transfer to the benzil moiety is followed by efficient intersystem crossing to the triplet state of benzil. Benzil has a very low singlet emission quantum yield ( $\sim 0$ ) and a very high intersystem crossing quantum yield (0.9).<sup>55</sup> Following singlet energy transfer to benzil and intersystem crossing, back transfer of excitation energy to the precipiton will yield the precipiton triplet excited state. The isomerization rate enhancement for the tethered precipitons compared to their intermolecularly sensitized unbound analogs is consistent with this triplet energy transfer back to the precipiton, which allows the precipiton to enter upon the triplet energy surface and partake of the usual triplet isomerization pathway. Because benzil fluorescence overlaps only to a minor extent with precipiton absorption, FRET is not likely to contribute significantly to the operative mechanism and that a Dexter-type pathway is more dominant.<sup>56</sup> The FRET affect may be less present in the *Z* isomers than the *E* isomers since *E* fluorescence is quenched more by the attached benzil.

The proposed precipiton-benzil “round-trip” energy transfer is presented graphically in Figure 39 and illustrated schematically in Figure 40. The proposal is that excitation of the precipiton affords a singlet excited state localized on the precipiton, and that this excitation energy is transferred to the benzil. (The evidence for this lies in the fluorescence quenching observed in the benzil-tethered precipiton isomers.) Rapid ISC affords the benzil-localized triplet, and back-transfer to the precipiton results in the precipiton triplet state and allows efficient isomerization. Both the forward singlet excitation from the precipiton to benzil, and the

back triplet energy transfer from the benzil to the precipiton maybe influenced by the relative geometries of each of the chromophoric partners and how well their excited state energies complement each other.

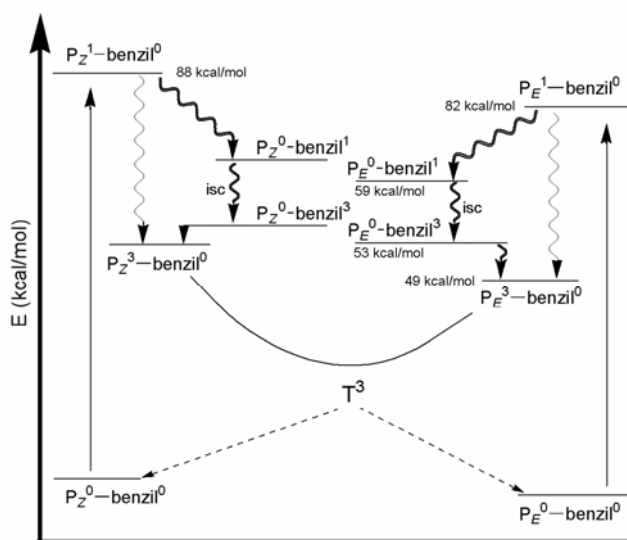


**Figure 39.** Energy diagram illustrating the “round-trip” precipiton/benzil energy transfer pathway. Radiationless transitions are represented by wavy arrows.  $P_E^0$ -benzil<sup>0</sup> and  $P_Z^0$ -benzil<sup>0</sup> represent the ground states of the precipiton-benzil bichromophore. Changes in superscripts identify changes in localized electronic excited states (1 = singlet, 3 = triplet).  $T^3$  represents the minimum energy conformer of the precipiton triplet.

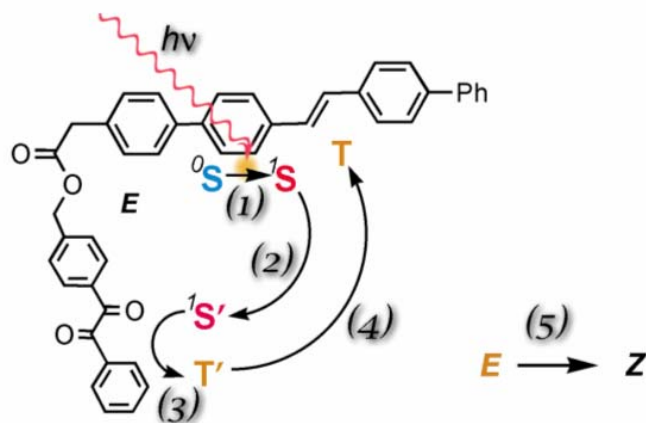


**Figure 40.** A step-wise depiction of the “round-trip” precipiton/benzil energy transfer pathway: 1) formation of the precipiton singlet state, 2) singlet excitation transfer from the precipiton unit to the benzil, 3) benzil centered intersystem crossing to the localized benzil triplet state, 4) triplet energy transfer from the benzil moiety back to the precipiton, and 5) isomerization.

Although the ‘round-trip’ energy transfer pathway proposed is still speculative, supportive evidence in the literature exists. It is consistent with studies in the Rothe labs, wherein they describe benzil acting as an effective “singlet-triplet converter” for polyfluorene sensitization. Bergamini, et al. recently reported a similar forward and backward energy transfer in a dendrimer with peripheral naphthalene units and a benzophenone core.<sup>57</sup> The basic scheme for round-trip energy transfer was proposed by Hammond in 1965 to explain enhanced naphthalene phosphorescence in a benzophenone-naphthalene bichromophoric system (Figure 41). The singlet and triplet levels of benzophenone lie between the singlet and triplet levels of naphthalene. In these compounds, selective singlet excitation of naphthalene results in intramolecular singlet excitation transfer to benzophenone. Very efficient intersystem crossing operates in the benzophenone moiety, and triplet excitation is transferred to the naphthalene group with high efficiency. In that case, in the Rothe work with benzil, and in the recent work

by Bergamini, et al. with benzophenone, the round-trip concluded with enhanced triplet state emission from a readily excited chromophore that was inefficient in intersystem crossing. In those studies, as in the present studies, the enhancement occurred due to the effect of a nearby partner, and the evidence for the round trip was based on total emission measurements. The precipiton-benzil systems investigated here are the first examples of a round trip energy pathway leading to a chemical event (isomerization). Isomerization provides the evidence of the round trip energy pathway. Ketonic steroids have also been shown to serve as singlet-triplet switches for intramolecular olefin sensitization, although not through a round-trip pathway (Figure 14).

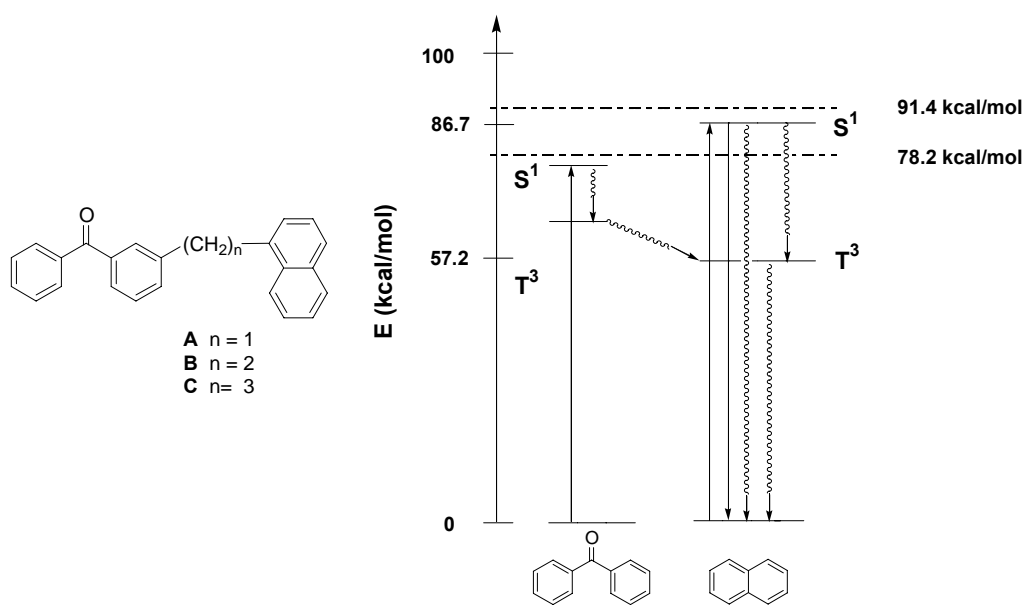


**Figure 41.** The excitation energies of the relevant excited levels (excited singlet (S), excited triplet (T)) of benzophenone and naphthalene. Radiationless transitions are represented by wavy arrows, possible radiative transitions by straight arrows. Changes in superscripts identify changes in localized electronic excited states (1 = singlet, 3 = triplet).

### 3.4.2 Effect of the Attached Benzil on the Precipiton Photostationary States

The photostationary state ratios for the photoisomerization process of **16Z**, **16E**, **28Z**, **28E**, **29Z**, and **29E** upon irradiation at 10  $\mu\text{M}$  are shown in Table 7. The observed difference among **16Z/E**, **28Z/E**, and **29Z/E** can be explained as occurring from a competition between direct singlet state isomerization (in which benzil plays no part) and the round-trip pathway. Introduction of benzil into the solution of **16Z/E** induces a small change in rate and a small change in the photostationary state toward the *Z* isomer. The close proximity of the benzil chromophore in **28Z/E** and **29Z/E** increases the efficiency of singlet energy transfer to the benzil chromophore, and through back transfer increases the effect of the triplet energy isomerization pathway. The round-trip pathway competes most effectively with the direct pathway in the case of **28Z/E**, where both isomers, on excitation, lead to the formation of the benzil triplet state. In the case of **29Z/E**, only one isomer (**29E**) is quenched by the tethered benzil. The failure of **29Z** to carry singlet energy to the benzil chromophore results in a reduced rate of precipiton triplet state formation, and the photostationary state is more influenced by the direct singlet pathway.

## 3.5 CONCLUSION

The benzil tethered precipitons discussed in this chapter represent the first studies of precipiton isomerization activated by a covalently attached organic sensitizer. Isomerization of these stilbene analogs is little affected by the presence of benzil in solution, but the intramolecular benzil effect is to increase the rate of isomerization and to significantly change the photostationary state. One interesting aspect of these observations is that the precipiton is the

primary chromophore in this bichromophoric system, yet the neighboring benzil has a significant effect on the rate and the photostationary state. The effect of unattached benzil on the rate was small – about a 24% increase in rate as compared with 4-6 fold changes for an attached benzil. It can be speculated that the isomerization process occurs by a “round-trip” energy transfer pathway. Initial excitation of the precipiton chromophore initiates a sequence that includes 1) formation of the precipiton singlet state, 2) singlet excitation transfer from the precipiton unit to the benzil, 3) benzil centered intersystem crossing to the localized benzil triplet state, 4) triplet energy transfer from the benzil moiety back to the precipiton, and 5) isomerization.

A major goal of this investigation was to identify a precipiton derivative that would efficiently isomerize the insoluble *E* form of our precipitons to the soluble *Z* form for the purpose of developing solubility-switchable materials. Therefore, precipitons rich in the *Z* isomer at the photostationary state are desirable. Benzil modified precipiton **29E/Z** meets this need. The molecule will be applied in further investigations of the mechanism of solubilization-isomerization and solubility-based photoswitchable materials.

## **4.0 THE PRECIPITATION EVENT**

## 4.1 INTRODUCTION

The observations of the precipitation event of precipitons have stimulated interest in the area of nanoparticles. Nanoparticles, particles in the range of about 1-100 nm in dimension, are interesting because they have special properties that lie between those of molecules and bulk material.<sup>58</sup> In addition, they have wide ranging implications in everyday life. They take the form of many cellular components such as viruses and protein complexes. They have industrial roles as adhesives, pigments, and in the production of catalysts. They are important to the pharmaceutical industry as drug forms as they are delivered to active sites in the body, and as quantum dots for electronic applications. While much has been written about inorganic nanoparticles, much less has been discussed about particle formation in organic systems. Because precipitons, including purely organic precipitons, can be precipitated in a controlled fashion using light, it is possible that they can be used to further the understanding of organic nanocrystal formation.

The theory of nucleation, as described by V. LaMer and R. Dinegar for the formation of monodispersed sulfur hydrosols, is described as occurring in three stages (Figure 42).<sup>59</sup> If this nucleation process is treated as analogous to the precipitons, solution phase  $Z \rightarrow E$  precipiton isomerization is not an event that instantly leads to precipitation. The crystallization process begins with the concentration buildup of  $E$  precipiton in solution until a critical concentration is reached (Stage I). Upon reaching this concentration, the system becomes heterogeneous by a process of self-nucleation. The appearance of nuclei (Stage II) relieves the supersaturation concentration enough so that the rate of nucleation falls to essentially zero. In Stage III, the

system is still supersaturated and the growth of nuclei proceeds by the diffusion of dissolved molecules to the nuclei. The concentration of dissolved molecules in Stage III is controlled by a balance between the rate of formation of those molecules (in this present case,  $Z \rightarrow E$  precipiton) and their removal by diffusion to the nuclei.

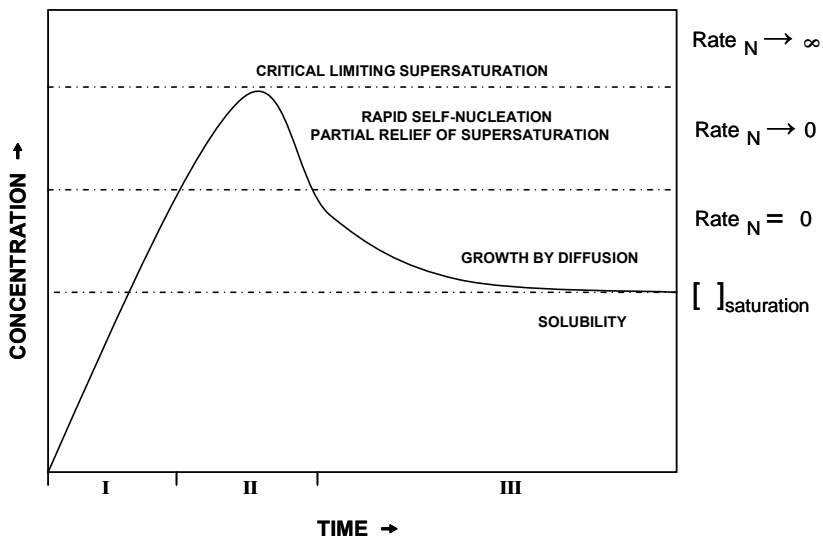
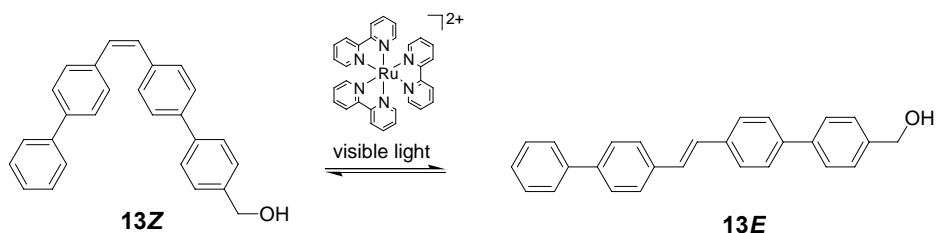


**Figure 42.** Schematic representation of the concentration of molecularly dissolved sulfur before and after nucleation as a function of time. Based on a figure presented by Lamer and Dinegar in reference 59.

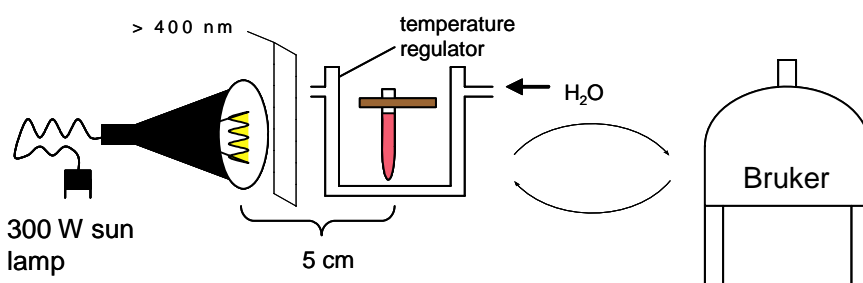
## 4.2 RESULTS AND DISCUSSION

The present investigation focused on the intermolecular triplet sensitization of 1,2-bis-(biphenyl)ethene alcohol precipiton **13Z** using  $\text{Ru}(\text{bpy})_3\text{Cl}_2$  sensitizer (Scheme 18).



**Scheme 18.** Intermolecular sensitization of precipiton **13Z** by  $\text{Ru}(\text{bpy})_3^{2+}$ .

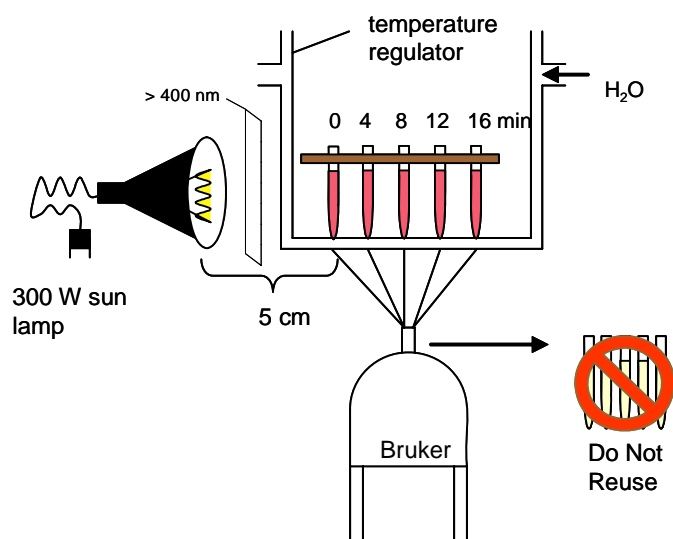
Two basic methods were developed for observing the isomerization process, designated “A” and “B”. In Method A (Scheme 19), a solution of **13Z** (20 mM),  $\text{Ru}(\text{bpy})_3^{2+}$  (50  $\mu\text{M}$ ), and an internal standard (20 mM) was added to a single NMR tube. The tube was placed in front of a light source and irradiated for a specific time interval. After that time interval, the tube was removed from the light and a  $^1\text{H}$  NMR measurement was taken. After recording the measurement, the tube was placed in front of the light source again, and the procedure was repeated until the reaction was complete.



**Scheme 19.** Method A for kinetic data collection.

In Method B (Scheme 20), data were acquired from parallel experiments. A reaction mixture was divided among ten or more individual NMR tubes. Each tube was designated to

represent a specific time period of irradiation. The tubes were gathered together and irradiated simultaneously. When an irradiation time period had expired, the designated NMR tube was removed from the light source and a  $^1\text{H}$  NMR measurement was taken. The tube was not irradiated again. This process was performed with each NMR tube until the reaction was complete.



**Scheme 20.** Method B for kinetic data collection.

It was anticipated that  $\text{Ru}(\text{bpy})_3^{2+}$  sensitized isomerization of **13Z** would obey first-order kinetics, and thus a plot of the reaction progress versus time would be a simple exponential curve. To test this, a solution of 20 mM **13Z**, 50  $\mu\text{M}$   $\text{Ru}(\text{bpy})_3^{2+}$ , and an internal standard (20 mM) was prepared in air-equilibrated 1/1  $\text{CD}_3\text{CN}/\text{CD}_2\text{Cl}_2$  and syringed into 11 NMR tubes. The solution was irradiated at  $\lambda_{\text{exc}} \geq 400$  nm and the  $^1\text{H}$  NMR spectroscopic changes of **13Z** were

observed by Method B. A plot for the reaction (Figure 43A) was not linear and had a distinct sigmoidal shape during the first 10 min. One possible explanation considered is autocatalysis. If the *cis*  $\rightarrow$  *trans* isomerization is first-order in **13Z**, but the reaction is catalyzed by **13E**, as **13E** is formed the reaction rate will increase. The first-order plot will deviate from linearity as the plot slope increases. To test this, **13E** (~ 3mg) was added to a solution of 20 mM **13Z**, 50  $\mu$ M Ru(bpy)<sub>3</sub><sup>2+</sup>, and an internal standard (20 mM) in air-equilibrated 1/1 CD<sub>3</sub>CN/CD<sub>2</sub>Cl<sub>2</sub> and syringed into 11 NMR tubes. The solution was irradiated at  $\lambda_{\text{exc}} \geq 400$  nm and the <sup>1</sup>H NMR spectroscopic changes of **13Z** were observed by Method B. In the presence of **13E** seed crystals, the sigmoidal shape was significantly diminished (Figure 43B) and the initial reaction rate (as judged by the amount of isomerization observed by NMR after 4 min) was faster than without **13E** seed crystals.

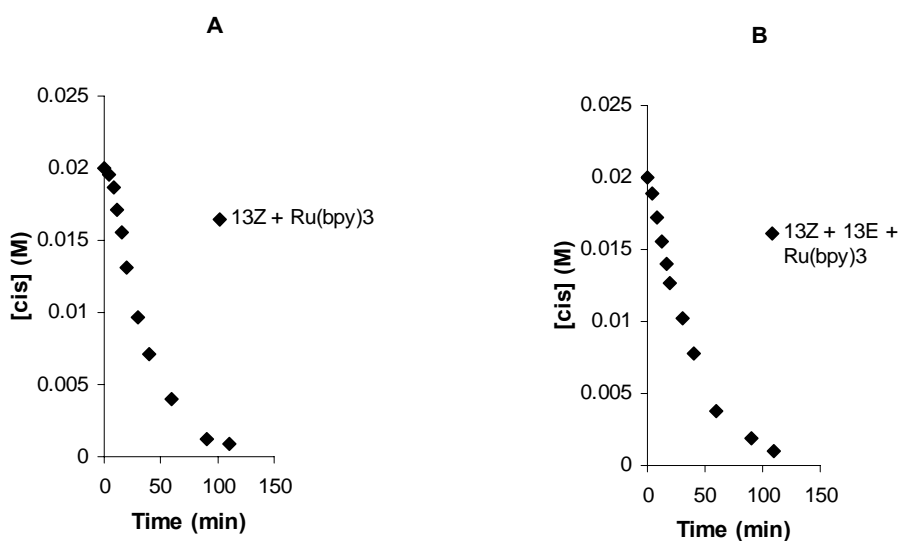


**Figure 43.** Reaction progress of **13Z**  $\rightarrow$  **13E** isomerization with/out **13E** ([**13Z**] = 20 mM, [**13E**] = saturated; [Ru(bpy)<sub>3</sub><sup>2+</sup>] = 50  $\mu$ M, solvent = 1/1 CD<sub>3</sub>CN/CD<sub>2</sub>Cl<sub>2</sub>).

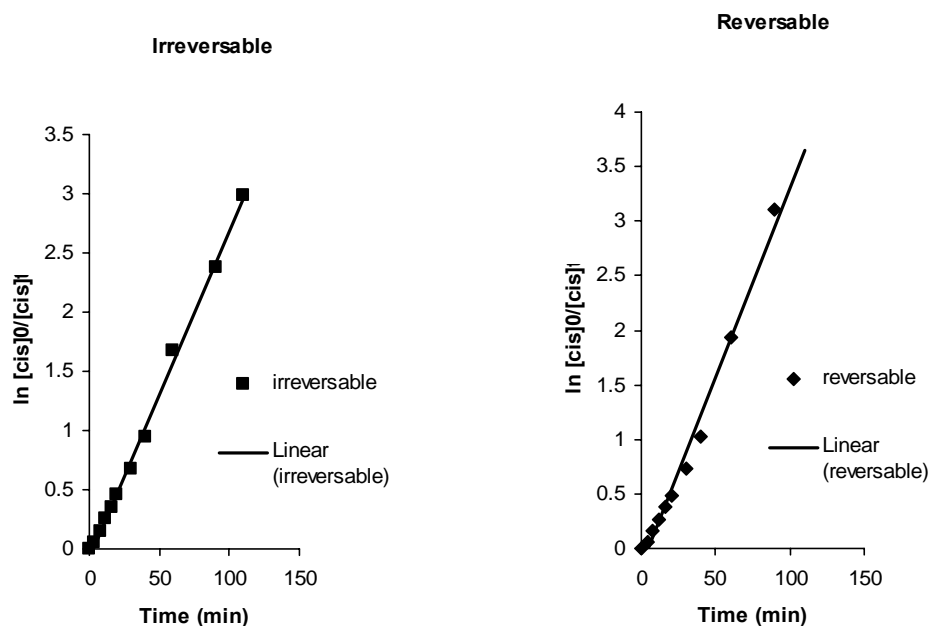


**Figure 44.** Reaction progress of **13Z** + **13E** ( $[\mathbf{13Z}] = 20 \text{ mM}$ ,  $[\mathbf{13E}] = \text{saturated}$ ;  $[\text{Ru}(\text{bpy})_3^{2+}] = 50 \text{ }\mu\text{M}$ , solvent = 1/1  $\text{CD}_3\text{CN}/\text{CD}_2\text{Cl}_2$ ) plotted according to an irreversible first-order rate law ( $k_{\text{obs}} = 0.028 \text{ s}^{-1}$ ) and a reversible first-order rate law ( $k_{\text{obs}} = 0.035 \text{ s}^{-1}$ ).

Data from the reaction containing **13E** seed crystals gave a reasonable fit to first order kinetics ( $R^2 = 0.997$ )(Figure 44). However, there may be some small systematic deviation. A possible explanation is Ostwald ripening of the precipitate, which may interfere with the reaction kinetics. A plot fitted to reversible first-order kinetics did not fit a reversible first-order rate law as well ( $R^2 = 0.986$ )(Figure 44).

If **13E** was acting as a catalyst for **13Z** isomerization, a similar rate enhancement should be observed upon irradiation without sensitizer  $\text{Ru}(\text{bpy})_3^{2+}$ . To test this, a 20 mM solution of **13Z**, and internal standard was prepared in air-equilibrated 99/1  $\text{CD}_3\text{CN}/\text{D}_2\text{O}$  and transferred via syringe into an NMR tube. In reaction 2 a small amount of **13E** ( $\sim 3 \text{ mg}$ ) was then added to the

tube, and the reaction mixture was sonicated for 2 min to insure saturation of **13E**. The reaction mixtures were irradiated at  $\lambda_{\text{exc}} \geq 400$  nm and the  $^1\text{H}$  NMR spectroscopic changes of **13Z** were observed by the Method B. A plot for each reaction is given in Figure 45. No rate enhancement was observed when **13E** seed crystals were initially present.

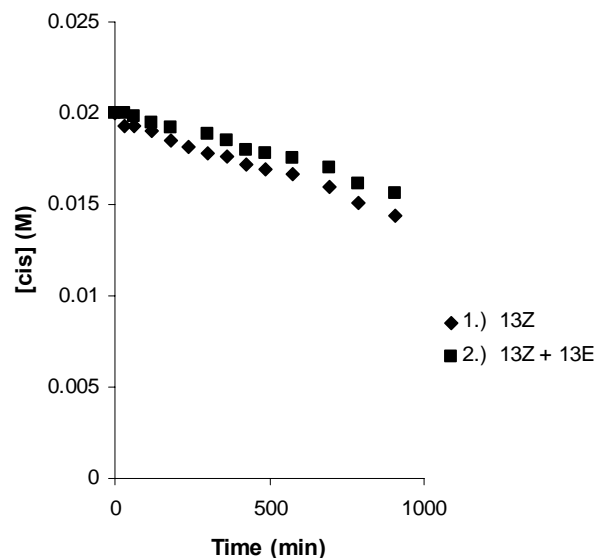


**Figure 45.** Reaction progress of **13Z**  $\rightarrow$  **13E** isomerization with/out **13E** and  $\text{Ru}(\text{bpy})_3^{2+}$  ( $[\mathbf{13Z}] = 20$  mM,  $[\mathbf{13E}] = \text{saturated}$ ; solvent = 99/1  $\text{CD}_3\text{CN}/\text{D}_2\text{O}$ ).

A second explanation that was considered focused on the large amount of precipitate that quickly forms early in the reaction. It was hypothesized that the precipitate may impede light from penetrating the NMR tube, and thus distort the isomerization rates. To test this hypothesis, a solution of 20 mM **13Z**, 50  $\mu\text{M}$   $\text{Ru}(\text{bpy})_3^{2+}$ , and an internal standard was prepared in air-equilibrated 1/1  $\text{CD}_3\text{CN}/\text{CD}_2\text{Cl}_2$  and transferred by syringe into 12 NMR tubes. The reaction mixtures were irradiated at  $\lambda_{\text{exc}} \geq 400$  nm and the  $^1\text{H}$  NMR spectroscopic changes of **13Z** were

observed. Reaction 1 was monitored by Method B and reaction 2 was monitored by Method A. A plot for each reaction is given in Figure 46. If the precipitate was responsible for retarding the isomerization rate, then the “disturbed” method should reduce this effect by aggregating the precipitate and accelerating precipitation. Indeed, when the “disturbed” method is employed, the sigmoidal shape at the beginning of the reaction was diminished.

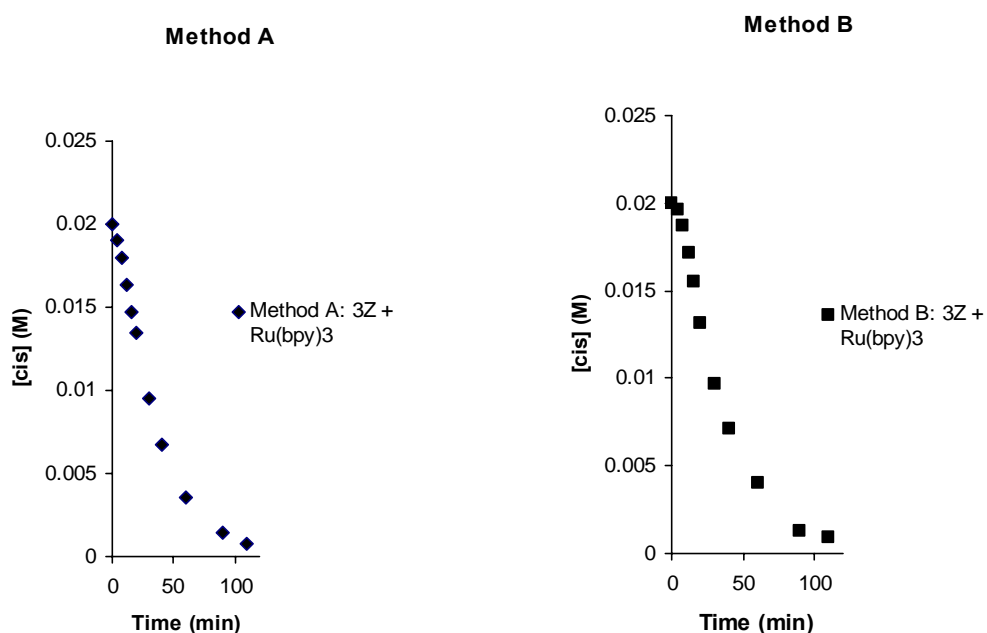


**Figure 46.** Reaction progress of **13Z**  $\rightarrow$  **13E** isomerization using Method A and Method B ( $[13Z] = 20 \text{ mM}$ ,  $[\text{Ru}(\text{bpy})_3^{2+}] = 50 \text{ }\mu\text{M}$ , solvent = 1/1  $\text{CD}_3\text{CN}/\text{CD}_2\text{Cl}_2$ ).

It is proposed that a critical distinction between Method A and Method B is the degree in which the reaction mixture is disturbed. The effect of disturbance becomes significant in kinetic studies whenever precipitation occurs. In the case of 20 mM **13Z**, **13E** product reaches

saturation early in the reaction (within 2 min), which results in a large amount of precipitate. If the semi-opaque material (which is formed first) is undisturbed as in Method B, it will hinder light from penetrating the NMR tube, and thus retard the isomerization rate. If the semi-opaque material is aggregated by disturbance as in Method A, the resulting precipitate “agglomerations” permit additional light to penetrate the tube, allowing reaction kinetics to be less impeded.

In the  $\text{Ru}(\text{bpy})_3^{2+}$  sensitized isomerizations described above, the initially clear and homogeneous reactions mixtures were transformed into a uniform semi-opaque material within 4 min of irradiation regardless of whether Method A or B was used. It is suspected this suspension contains micro- or nanocrystals because no actual precipitation particles could be seen with the naked eye, and no precipitate settling was observed. In general, crystal development begins with molecules meeting and coalescing to form small embryos as they randomly diffuse through solution.<sup>60</sup> The embryos grow to a critical size above which they transform into crystals. Ostwald ripening can occur, where small crystals transform into large crystals.<sup>61,58</sup> It was observed that if the semi-opaque material formed during isomerization is disturbed by physically handling the NMR tube (which occurs in Method A), aggregation occurs and visible precipitate particles appear. In contrast, if the semi-opaque suspension is not handled (thus “undisturbed”) during isomerization or at any time before the NMR (which occurs in Method B), aggregation resulting in visible precipitate particles is delayed and the optical properties of the solution are changed. This change affects the light penetration and the progress of the isomerization. Table 8 summarizes the isomerization rates in each of the discussed conditions.

**Table 8.** Summary of **13Z** → **13E** isomerization rates after 4 min ([**13Z**] = 20 mM, [Ru(bpy)<sub>3</sub><sup>2+</sup>] = 50 μM, [**3E**] = saturated, solvent = 1/1 CD<sub>3</sub>CN/CD<sub>2</sub>Cl<sub>2</sub>).

$\text{substrate(s)} \xrightarrow[\text{conditions}]{\text{Ru(bpy)}_3^{2+}, h\nu > 400 \text{ nm}} \text{product}$					
Substrates	Conditions	Slope (x 10 <sup>-4</sup> )	k <sup>a</sup> (min <sup>-1</sup> )	Pseudo 1 <sup>st</sup> -order rxn rate (x 10 <sup>-4</sup> )	% <b>13E</b> (110 min)
<b>13Z</b>	Disturbed	2.46	0.012	2.46	96
<b>13Z</b>	Undisturbed	1.03	0.005	1.03	95
<b>13Z + 13E</b>	Disturbed	3.76	0.019	3.76	95
<b>13Z + 13E</b>	Undisturbed	2.73	0.014	2.73	95

<sup>a</sup> The rates were calculated using the amount of isomerization observed by NMR after 4 min.

### 4.3 CONCLUSION

The conclusion drawn from the above experiments are that the large amount of precipitate generated during the isomerization of **13Z** → **13E** is responsible for diverting the apparent reaction kinetic data from obeying irreversible first-order rate theory. Using Method A, in which the NMR tubes were not disturbed, micro- and nanocrystal formation impeded light from penetrating the reaction vessel thus decreased the reaction rate. When the solution was agitated, particles agglomerated to form precipitate aggregates, allowing more light to penetrate the

reaction vessel. The precipitation process is expedited by adding **13E** “seed crystals” to the reaction mixture before irradiation.

## **5.0 SUMMARY AND FUTURE DIRECTIONS**

A limitation to the usefulness of precipitons is the requirement of ultraviolet light irradiation and the addition of a triplet sensitizer to the solution in order to facilitate precipitation. A possible solution to this problem is the chemical attachment of a triplet sensitizer to the precipiton moiety. Isomerization may then occur by using mild visible light conditions without sensitizer additives.

My doctoral research involved the development of the first intramolecularly activated precipitons. The isomerization process is induced by intramolecular triplet energy transfer from a covalently attached sensitizer. This approach was utilized to evaluate the possibility of using metal-binding precipitons for the purpose of metal sequestration. In a model study, a Ru(bpy)<sub>3</sub><sup>2+</sup> sensitizer was covalently linked to a precipiton moiety by an ether tether **17Z/E**. A comparison of the photoisomerization kinetics of **17Z/E** with those of untethered analogues **16Z/E** + Ru(bpy)<sub>3</sub><sup>2+</sup> showed that **17Z/E** isomerized 250 times faster. This is a significant step forward in the development of precipitons as energy-driven metal scavengers.

In my second project, the photoisomerization kinetics of precipitons containing tethered benzil units at varying positions (*para* **28Z/E** vs *meta* **29Z/E**) were studied for the purpose of demonstrating controlled soluble/insoluble phase switching. The intramolecular sensitization leads to a more rapid isomerization (4.5 times faster) than could be achieved by **16Z/E** + benzil. Investigations into the photo spectroscopy of these systems led us to propose a new “round-trip” mechanistic model for the precipiton ↔ benzil energy transfer process.

These results have left many exciting frontiers to explore. It was observed that the precipitation of **13Z** begins with the formation of microscopic seed crystals. A promising direction to investigate is the possibility of “isolating” a suspension of **13E** seed crystals as

they form in a highly viscous medium. Controlled precipitation may also allow observation of the agglomeration process and the size of the crystals formed.

Another stimulating observation is that the intramolecular benzil effect is geometrically selective. The round-trip mechanism opens access to the precipiton triplet state, but does so to different extents for the *Z* and *E* isomers and for the *meta* and *para* linked chromophores. This is surely because the geometry of the molecules and their conformational microstates influence the efficiency of intramolecular singlet energy transfer and also affect the back transfer of triplet excitation energy. Which effect is most important, if either, is unknown. It may be productive to contemplate potential uses of this stereoselectivity in energy transfer for any investigator interested in new separation strategies and new chemoselective processes.

## **6.0 EXPERIMENTAL**

## 6.1 GENERAL

$^1\text{H}$  NMR and  $^1\text{H}$ - $^1\text{H}$  COSY spectra were recorded on a Bruker Avance 300 at 300 MHz.  $^{13}\text{C}$  NMR spectra were recorded on a Bruker Avance 300 at 75 MHz or a Bruker Avance 600 at 150 MHz. The chemical shifts are given in parts per million (ppm) on the delta scale ( $\delta$ ), and the coupling constant values ( $J$ ) are in hertz. The solvent peak was used as the reference value. For  $^1\text{H}$  NMR:  $\text{CDCl}_3 = 7.27$  ppm;  $\text{CD}_2\text{Cl}_2 = 5.32$ ;  $\text{CD}_3\text{CN} = 1.94$ . For  $^{13}\text{C}$  NMR:  $\text{CDCl}_3 = 77.23$  ppm;  $\text{CD}_2\text{Cl}_2 = 54.00$ ;  $\text{CD}_3\text{CN} = 1.39$ . Abbreviations for NMR data: s = singlet; d = doublet; t = triplet; q = quartet; dd = doublet of doublets; dt = doublet of triplets; dq = doublet of quartets; tt = triplet of triplets; m = multiplet; br = broad; app = apparent, ABq = AB quartet.

High resolution and low resolution mass spectra were recorded on a VG 7070 spectrometer. Infrared (IR) spectra were collected on an Avatar 380 Nicolet FT-IR spectrometer. Samples for IR were prepared either as a thin film on a NaCl plate by dissolving the sample in  $\text{CH}_2\text{Cl}_2$  and then evaporating the  $\text{CH}_2\text{Cl}_2$  or as a KBr pellet. Melting points were determined using a Thomas Hoover capillary melting point apparatus and are uncorrected. UV-Vis spectra were obtained in air-equilibrated or degassed solvent solution at 23 °C using an Ocean Optics S2000-TR fiber-optic spectrometer with a Mikropack deuterium/halogen light source. Emission spectra were recorded in air-equilibrated solvent solution at 23 °C with a Cary Eclipse fluorescence spectrometer equipped with Varian software.

Thin layer chromatography (TLC) was performed using E. Merck silica gel 60F-254 (0.25 mm) analytical glass plates. Light absorption by compounds was observed using ultraviolet light (254 nm or 365 nm). Silica gel columns for flash chromatography, according to the method of Still, were prepared with E. Merck silica gel 60 (230-240 mesh ASTM).

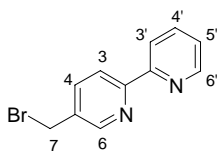
Dry solvents were distilled shortly before use from an appropriate drying agent under nitrogen atmosphere. Tetrahydrofuran (THF), diethyl ether (Et<sub>2</sub>O), and toluene were distilled from sodium and benzophenone. Dry methanol was distilled from magnesium turnings and stored under nitrogen or was purchased as anhydrous and used as obtained. Ethyl acetate was dried over 4 Å molecular sieves for at least 24 h prior to use. *n,n*-Dimethylformamide (DMF) was dried over MgSO<sub>4</sub>, distilled *in vacuo*, and stored over 4 Å molecular sieves. Pyridine was distilled from calcium hydride and stored over 4 Å molecular sieves. Hexane refers to the mixed hydrocarbon fraction (bp 68-70 °C), principally *n*-hexane, and was purified as follows: the commercial solvent was stirred over concentrated H<sub>2</sub>SO<sub>4</sub> for at least 24 h, decanted, stirred over anhydrous NaHCO<sub>3</sub> for at least 6 h, decanted, and distilled. Benzene, methylene chloride (CH<sub>2</sub>Cl<sub>2</sub>) and triethylamine (TEA) were distilled from CaH<sub>2</sub>. Anhydrous dimethylsulfoxide (DMSO) and acetonitrile (CH<sub>3</sub>CN) were purchased from Acros and used as is. Other commercially available reagents and solvents were reagent grade and were used without further purification.

Reactions performed under a nitrogen atmosphere were arranged with a mercury bubbler so that the system could be alternately evacuated and filled with nitrogen and left under positive pressure. Syringes and reaction flasks were dried in an oven at 120 °C and cooled in a desiccator over calcium sulfate prior to use. Reactions at “room temperature” were conducted under ambient laboratory conditions T = 20-27 °C, p = 720-770 mmHg. References to “removal of volatile components *in vacuo*” refer to rotary evaporation of the sample at 25-65 °C *in vacuo* (18-25 mmHg), followed by removal of residual volatile materials under vacuum (0.05-0.5 mmHg) at room temperature.

## 6.2 EXPERIMENTAL PROCEDURES

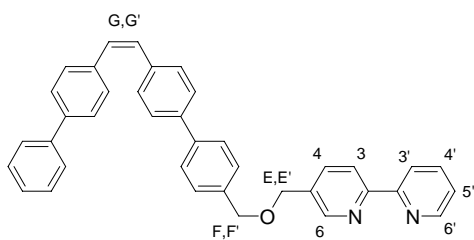
### 6.2.1 Synthesis and Characterization

Assignments of the  $^1\text{H}$  NMR signals of the bipyridine containing compounds were determined by examining and comparing their  $^1\text{H}$ - $^1\text{H}$  COSY spectra and coupling constants.



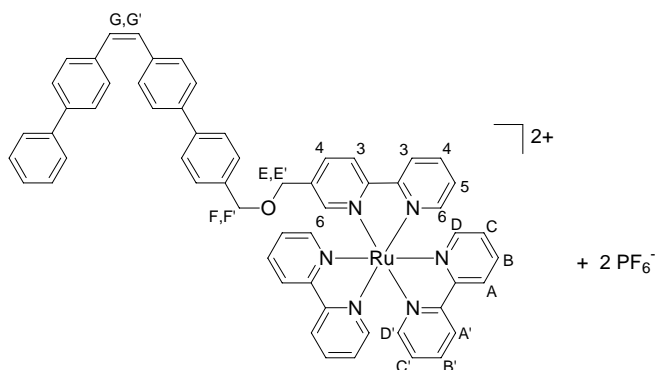
**5-Bromomethyl-2,2'-bipyridine.** 5-Methyl-2,2'-bipyridine (1.99 g, 11.8 mmol), *N*-bromosuccinimide (2.09 g, 11.8 mmol), and azobis(iso-butyronitrile) (483 mg, 2.94 mmol) were dissolved in  $\text{CCl}_4$  (179 mL) under  $\text{N}_2$  and the mixture was stirred at an internal temperature of  $43\text{ }^\circ\text{C}$  for 23 h. Reaction progress was monitored by  $^1\text{H}$  NMR to observe the consumption of NBS and the formation of product. After 23 h, an additional 0.5 eq of NBS was added and the mixture was stirred at  $43\text{ }^\circ\text{C}$  for 2 additional h. The mixture was cooled to  $23\text{ }^\circ\text{C}$ , filtered, and the volatile components of the filtrate were removed *in vacuo* to afford a crude solid that was purified by flash chromatography ( $\text{SiO}_2$ , 5:1 Hex:EtOAc, column was pretreated with 19:1 Hex: $\text{NEt}_3$  then washed with 5:1 Hex:EtOAc) to afford the bipyridine as a white solid (1.35 g, 46%):  $R_f$  0.15 (5:1 Hex:EtOAc, pretreated with 19:1 Hex: $\text{NEt}_3$ ); mp  $74\text{-}76\text{ }^\circ\text{C}$ ; IR (KBr) 3050, 2998, 2967, 1596, 1556, 1461, 1434, 1392, 1252, 1203, 1127, 1088, 1039, 834, 797, 749, 730, 650; The  $^1\text{H}$  and  $^{13}\text{C}$  NMR data matches the data described by Ballardini and coworkers:  $^1\text{H}$  NMR (300 MHz,  $\text{CDCl}_3$ )  $\delta$  8.70 (app d,  $J = 2\text{ Hz}$ , 2 H,  $\text{H}^6+\text{H}^6'$ ), 8.43 (dd,  $J = 6, 2\text{ Hz}$ , 2 H,  $\text{H}^3+\text{H}^3'$ ), 7.89-7.81 (m, 2 H,  $\text{H}^4+\text{H}^4'$ ), 7.34 (ddd,  $J = 7, 5, 1\text{ Hz}$ , 1 H,  $\text{H}^5$ ), 4.55 (s, 2 H,  $\text{H}^7$ );  $^{13}\text{C}$

NMR (75 MHz, CD<sub>3</sub>CN)  $\delta$  156.3, 155.8, 149.6, 149.5, 137.8, 137.2, 133.9, 124.2, 121.5, 121.3, 29.9.



**(Z)-5-[4'-(2-Biphenyl-4-ylvinyl)-biphenyl-4-ylmethoxymethyl]-[2,2']bipyridine (18Z)**. A cooled solution (0 °C) of benzyl alcohol **13Z** (500 mg, 1.38 mmol) in THF (138 mL) was treated with dry NaH (66.2 mg, 2.76 mmol). The solution was warmed to 23 °C and stirred for 2 h. 5-Bromomethyl-2,2'-bipyridine (354 mg, 1.42 mmol) was then added, stirred for 2 h at 23 °C, then heated at reflux for 17.5 h. The solution was cooled to 23 °C and volatile components of the reaction mixture were removed *in vacuo*. The crude solid was combined with H<sub>2</sub>O (300 mL) and the solution was extracted with CH<sub>2</sub>Cl<sub>2</sub> (3 x 20 mL). The combined organic phases were washed with brine (360 mL), dried with MgSO<sub>4</sub>, and filtered. Volatile components in the filtrate were removed *in vacuo* to afford a crude solid that was purified by flash chromatography (SiO<sub>2</sub>, CH<sub>2</sub>Cl<sub>2</sub> then 99:1 CH<sub>2</sub>Cl<sub>2</sub>:MeOH) to afford **18Z** as a pale green solid (537 mg, 73%): *R<sub>f</sub>* 0.31 (CH<sub>2</sub>Cl<sub>2</sub>); mp 113-115 °C; IR (KBr) 3030, 3003, 2857, 1598, 1588, 1557, 1460, 1395, 1353, 1088, 881, 815; UV-Vis (CH<sub>3</sub>CN, 10 μM)  $\lambda_{\max}$  274 nm,  $\epsilon$  34200 M<sup>-1</sup>cm<sup>-1</sup>, 290 nm,  $\epsilon$  33200 M<sup>-1</sup>cm<sup>-1</sup>, 330 nm,  $\epsilon$  24800 M<sup>-1</sup>cm<sup>-1</sup>; <sup>1</sup>H NMR (300 MHz, CD<sub>3</sub>CN)  $\delta$  8.69-8.66 (m, 2 H, H<sup>6</sup>+H<sup>6'</sup>), 8.43-8.41 (app d, *J* = 8 Hz, 2 H, H<sup>3</sup>+H<sup>3'</sup>), 7.95-7.90 (m, 2 H, H<sup>4</sup>+H<sup>4'</sup>), 7.72-7.63 (m, 5 H, phenyl), 7.56 (app d, *J* = 7 Hz, 4 H, phenyl), 7.46 (app d, *J* = 8.5 Hz, 4 H, phenyl), 7.42 (app s, 1 H, H<sup>5'</sup>), 7.34 (app d, *J* = 8 Hz, 4 H, phenyl), 6.72 (s, 2 H, H<sup>G</sup>+H<sup>G'</sup>), 4.67 (s, 2 H, H<sup>E</sup>+H<sup>E'</sup>), 4.65 (s, 2 H, H<sup>F</sup>+H<sup>F'</sup>); <sup>13</sup>C NMR (75 MHz, CD<sub>3</sub>CN)  $\delta$  156.1, 156.8, 149.3, 148.8, 140.8, 140.4, 140.0, 139.6, 137.0, 136.6, 136.5, 136.4, 130.2, 130.1, 129.6,

129.5, 129.8, 128.4, 127.4, 127.1, 127.0, 126.9, 124.0, 121.2, 121.0, 72.3, 69.6; HRMS(EI)  $m/z$  calcd for  $C_{38}H_{30}N_2O$  530.2358, found 530.2383.



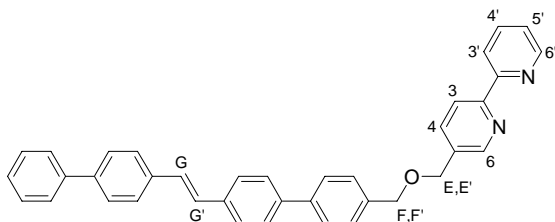
**(Z)-[5-(4'-(2-Biphenyl-4-yl-vinyl)-**

**biphenyl-4-ylmethoxymethyl]-[2,2']bipyridine]-bis(2,2'-bipyridine)ruthenium(II)-**

**bis(hexafluorophosphate) (17Z).**

A solution of *cis*-dichlorobis(2,2'-bipyridine)ruthenium(II)dihydrate (90.8 mg, 0.188 mmol) and silver hexafluoroantimonate(V) (132 mg, 0.376 mmol) in acetone (12.5 mL) under  $N_2$  was heated at reflux for 48 h, followed by filtration of AgCl. Bipyridine **18Z** (99.8 mg, 0.188 mmol) was added to the filtrate and the mixture was heated at reflux for 24 h. Volatile components of the reaction mixture were removed *in vacuo* to afford a crude red solid that was purified by flash chromatography ( $SiO_2$ , 19:1  $CH_3CN$ :0.4 M  $KNO_3$ (aq)). The desired fractions were combined and volatile components were reduced in volume to 25 mL. The solution was combined with 0.25 M  $NH_4PF_6$  (10 mL), and then stirred at 23 °C for 20 min, and then extracted with  $CHCl_3$  (3 x 100 mL). The organic extract was washed with  $H_2O$  (2 x 200 mL). Volatile components of the organic layer were removed *in vacuo* to afford complex **17Z** as a red solid (114 mg, 49%):  $R_f$  0.16 (19:1  $CH_3CN$ :0.4 M  $KNO_3$ (aq) on pretreated silica); mp 164-166 °C; IR (KBr) 3027, 2919, 2853, 1603, 1464, 1446, 1093, 838, 761, 730, 699; UV-Vis ( $CH_3CN$ , 10  $\mu M$ )  $\lambda_{max}$  290 nm,  $\epsilon$  91800  $M^{-1}cm^{-1}$ , 340 nm,  $\epsilon$  22900  $M^{-1}cm^{-1}$ , 450 nm,  $\epsilon$  13700  $M^{-1}cm^{-1}$ ;  $^1H$  NMR (300 MHz,  $CD_3CN$ )  $\delta$

8.49-8.46 (m, 4 H, H<sup>A</sup>+H<sup>A'</sup>), 8.44-8.39 (m, 2 H, H<sup>3</sup>+H<sup>3'</sup>), 8.06-8.01 (app t,  $J = 15, 8$  Hz, 4 H, H<sup>B</sup>+H<sup>B'</sup>), 7.97 (dd,  $J = 5, 2$  Hz, 1 H, H<sup>4</sup> or H<sup>4'</sup>), 7.92 (dd,  $J = 8, 1$  Hz, 1 H, H<sup>4</sup> or H<sup>4'</sup>), 7.73-7.69 (m, 5 H, H<sup>D</sup>+H<sup>D'</sup> + phenyl), 7.65-7.60 (m, 6 H, H<sup>S</sup>+phenyl), 7.58-7.55 (m, 3 H, phenyl), 7.47-7.45 (m, 2 H, phenyl), 7.42-7.34 (m, 9 H, H<sup>C</sup>+H<sup>C'</sup>+phenyl), 7.33-7.27 (m, 1 H, phenyl), 7.23 (app d,  $J = 8, 2$  Hz, 2 H, H<sup>6</sup>+H<sup>6'</sup>), 6.74 (s, 2 H, H<sup>G</sup>+H<sup>G'</sup>), 4.51 (ABq,  $J = 14$  Hz, 2 H, H<sup>E</sup>+H<sup>E'</sup>), 4.47 (s, 2 H, H<sup>F</sup>+H<sup>F'</sup>); <sup>13</sup>C NMR (75 MHz, CD<sub>3</sub>CN)  $\delta$  158.5, 158.4, 158.3, 157.4, 153.1, 153.0, 150.9, 141.7, 141.2, 141.0, 140.8, 140.6, 139.3, 139.2, 138.7, 138.1, 138.0, 137.7, 131.5, 131.4, 130.9, 130.8, 130.3, 129.8, 129.7, 129.6, 129.04, 129.01, 128.97, 128.94, 128.90, 128.90, 128.2, 128.1, 125.7, 125.6, 125.5, 125.3, 73.6, 69.6; HRMS(ES)  $m/z$  calcd for C<sub>58</sub>H<sub>46</sub>F<sub>6</sub>N<sub>6</sub>OPRu [M – PF<sub>6</sub>]<sup>+</sup> 1089.2418, found 1089.2452, 944.14 [M – 2PF<sub>6</sub>]<sup>+</sup>.

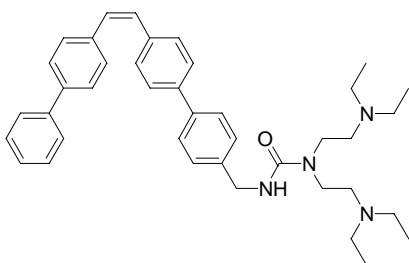


**(E)-5-[4'-(2-Biphenyl-4-yl-vinyl)-biphenyl-**

**4-ylmethoxymethyl]-[2,2']bipyridine (18E).** A solution of bipyridine **18Z** (153 mg, 0.289 mmol) and diphenyl diselenide (9.1 mg, 0.029 mmol) in THF (1.18 mL) was heated at reflux for 23 h. The solution was cooled to 23 °C and volatile components of the reaction mixture were removed *in vacuo*. The crude solid was triturated with Et<sub>2</sub>O (3 x 5 mL), filtered, and the volatile components of the filtrate were removed *in vacuo* to afford ligand **18E** as a yellow solid (45.5 mg, 84%): mp 300-310 °C; IR (KBr) 3048, 3030, 2855, 1911, 1589, 1557, 1496, 1461, 1436, 1397, 1357, 1081, 970, 832, 807, 795, 763, 752, 742, 731, 691; <sup>1</sup>H NMR (300 MHz, CDCl<sub>3</sub>)  $\delta$  8.75-8.69 (m, 2 H, H<sup>6</sup>+H<sup>6'</sup>), 8.46 (app d,  $J = 8$  Hz, 2 H, H<sup>3</sup>+H<sup>3'</sup>), 7.90 (dd,  $J = 8, 2$  Hz, 1 H, H<sup>4</sup> or H<sup>4'</sup>), 7.85 (dd,  $J = 8, 2$  Hz, 1 H, H<sup>4</sup> or H<sup>4'</sup>), 7.66-7.62 (m, 12 H, phenyl), 7.50 (app d,  $J = 9$  Hz, 3



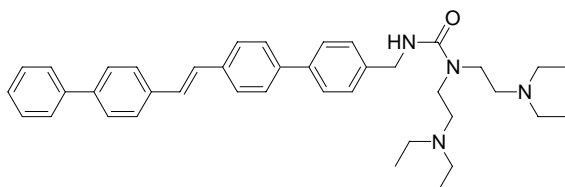
1 H, phenyl), 7.54-7.44 (m, 2 H, phenyl), 7.44-7.30 (m, 9H, H<sup>C</sup>+H<sup>C'</sup>+H<sup>G</sup>+H<sup>G'</sup>+phenyl), 7.26 (d,  $J = 8$  Hz, 2 H, H<sup>6</sup> +H<sup>6'</sup>), 4.58-4.50 (m, 2 H, H<sup>E</sup>+ H<sup>E'</sup>), 4.50-4.44 (m, 2 H, H<sup>F</sup>+H<sup>F'</sup>); <sup>13</sup>C NMR (151 MHz, CD<sub>3</sub>CN)  $\delta$  157.97, 157.94, 157.90, 156.9, 152.72, 152.66, 152.63, 150.4, 141.26, 141.12, 140.82, 140.49, 140.31, 138.80, 138.79, 138.17, 137.85, 137.59, 137.17, 129.95, 129.28, 129.22, 129.04, 128.60, 128.56, 128.49, 128.42, 128.25, 128.22, 128.09, 128.04, 127.70, 125.25, 125.13, 124.85, 73.09, 69.12; HRMS(ES)  $m/z$  calcd for C<sub>58</sub>H<sub>46</sub>F<sub>6</sub>N<sub>6</sub>OPRu [M – PF<sub>6</sub>]<sup>+</sup> 1089.2418, found 1089.2368.



**(Z)-(3-[4'-2-Biphenyl-4-ylvinyl]-biphenyl-3-ylmethyl)-1,1-bis-(2-diethylaminoethyl)urea (19Z).**

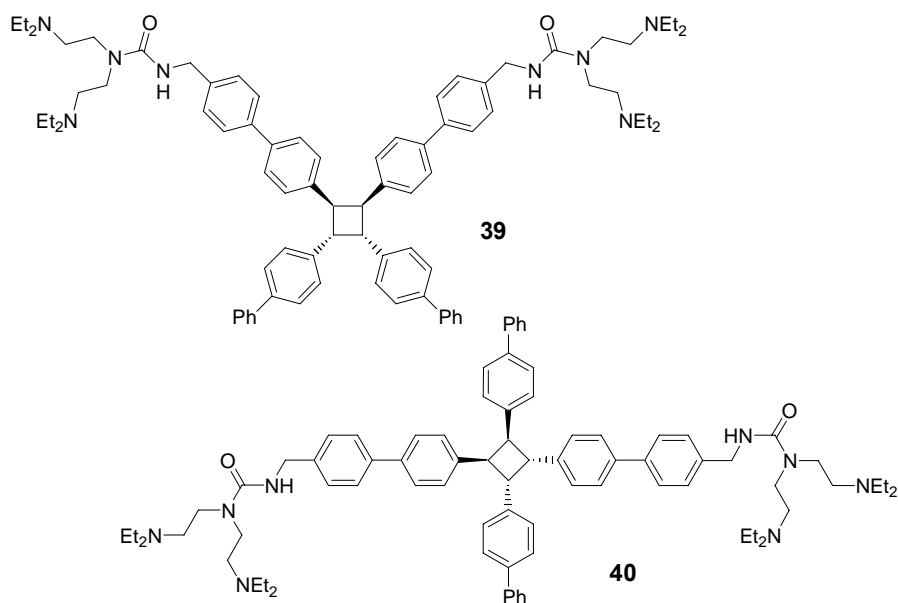
A solution of isocyanate (635 mg, 1.64 mmol) and TEDETA (389 mg, 1.80 mmol) in THF (4.5 mL) under N<sub>2</sub> was stirred at 23 °C for 24 h. Volatile components of the reaction mixture were removed *in vacuo* to afford a yellow oil that was diluted with EtOAc (100 mL), washed with 25% aq NaHCO<sub>3</sub> (3 x 150 mL), dried with MgSO<sub>4</sub>, and filtered. Volatile components of the filtrate were removed *in vacuo* to afford a yellow oil which was purified by flash chromatography (SiO<sub>2</sub>, 9:1 EtOAc:MeOH, then 10:1:1 EtOAc:MeOH:NEt<sub>3</sub>) to afford ligand **19Z** as a yellow oil (711 mg, 72%):  $R_f$  0.56 (10:1:1 EtOAc:MeOH:NEt<sub>3</sub>); IR (neat) 3231, 3025, 2968, 2932, 2872, 2813, 1649, 1540, 1469, 1468, 1402, 1385, 1254, 1198, 1154, 1119, 1066, 1006, 884 cm<sup>-1</sup>; <sup>1</sup>H NMR (300 MHz, CDCl<sub>3</sub>)  $\delta$  8.45 (br t,  $J = 7$  Hz, 1 H), 7.62-7.31 (m, 17 H), 6.65 (s, 2 H), 4.37 (d,  $J = 5$  Hz, 2 H), 3.37 (t,  $J = 6$  Hz, 4 H), 2.61 (t,  $J = 6$  Hz, 4H), 2.51 (q,  $J = 7$  Hz, 8 H), 0.96 (t,  $J = 7$  Hz, 12 H); <sup>13</sup>C NMR (75

MHz, CDCl<sub>3</sub>)  $\delta$  160.6, 140.9, 140.0, 139.9, 139.8, 139.4, 136.6, 136.4, 130.2, 130.1, 129.5, 128.9, 128.5, 127.4, 127.1, 127.0, 126.9, 53.6, 48.1, 47.7, 44.5, 11.7; HRMS(ES)  $m/z$  calcd for C<sub>40</sub>H<sub>51</sub>N<sub>4</sub>O [M + H]<sup>+</sup> 603.4057, found 603.4082.



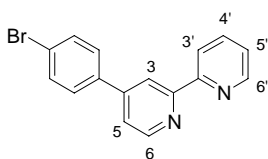
**(E)-(3-[4'-2-Biphenyl-4-ylvinyl]biphenyl-**

**3-ylmethyl]-1,1-bis-(2-diethylaminoethyl)urea (19E).** A solution of TEDETA ligand **19Z** (60.6 mg, 0.101 mmol) and diphenyl diselenide (31.9 mg, 0.101 mmol) in THF (0.42 mL) was heated at reflux for 23 h. The solution was cooled to 23 °C and volatile components of the reaction mixture were removed *in vacuo*. The crude solid was triturated with cold hexanes (3 x 3 mL) and filtered to afford TEDETA ligand **19E** as a tan solid (49.2 mg, 81%); mp 204 °C, IR (KBr) 3356, 3028, 2968, 1651, 1538, 1495, 1449, 1402, 1257, 1115, 968, 833, 804, 763, 729, 690; <sup>1</sup>H NMR (300 MHz, CDCl<sub>3</sub>)  $\delta$  8.48 (br s, 1 H), 7.65-7.34 (m, 17 H), 7.20 (s, 2 H), 4.37 (d,  $J$  = 4 Hz, 2 H), 3.37 (t,  $J$  = 6 Hz, 4 H), 2.59 (t,  $J$  = 6 Hz, 4H), 2.51 (q,  $J$  = 7 Hz, 8 H), 0.96 (t,  $J$  = 7 Hz, 12 H); <sup>13</sup>C NMR, too insoluble to obtain. HRMS(ES)  $m/z$  calcd for C<sub>40</sub>H<sub>51</sub>N<sub>4</sub>O [M + H]<sup>+</sup> 603.4063, found 603.4063.



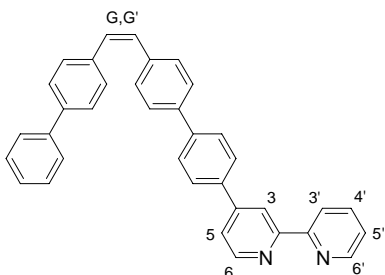
**Irradiation of 19Z at 350 nm.** A solution of **19Z** (102 mg, 0.169 mmol) in toluene (9.47 mL) was irradiated at 350 nm for 14 h. Volatile components of the reaction mixture were removed *in vacuo* to afford a crude solid that was purified by flash chromatography (SiO<sub>2</sub>, 10:0.75 EtOAc:NEt<sub>3</sub>, then 100:10:1 CHCl<sub>3</sub>:MeOH:NH<sub>4</sub>OH) to afford **39** (56.7 mg, 56%) and **40** (15.6 mg, 15%) as yellow oils. **Syn H-T cyclobutane 39:** *R<sub>f</sub>* 0.13 (10:0.75 EtOAc:NEt<sub>3</sub>); IR (neat) 3229, 3052, 2972, 2933, 2820, 2304, 1643, 1561, 1487, 1467, 1402, 1265, 1198, 1119, 1065, 1040, 1006, 909, 833 cm<sup>-1</sup>; <sup>1</sup>H NMR (300 MHz, CD<sub>3</sub>CN) δ 8.50 (br t, *J* = 6 Hz, 2 H), 7.70-7.29 (m, 34 H), 4.68 (s, 4 H), 4.26 (d, *J* = 5 Hz, 4 H), 3.32 (t, *J* = 5 Hz, 8 H), 2.59 (t, *J* = 5 Hz, 8H), 2.52 (q, *J* = 7 Hz, 16 H), 0.92 (t, *J* = 7 Hz, 24 H); <sup>13</sup>C NMR (75 MHz, CDCl<sub>3</sub>) δ 157.3, 141.0, 140.52, 140.0, 139.8, 139.0, 138.6, 128.9, 128.87, 128.81, 128.4, 127.2, 127.1, 126.9, 126.8, 126.6, 58.8, 47.8, 47.6, 47.5, 22.9, 22.8, 14.3, 11.1; HRMS(ES) *m/z* calcd for C<sub>80</sub>H<sub>101</sub>N<sub>8</sub>O<sub>2</sub> [M + H]<sup>+</sup> 1205.8048, found 1205.8087. **Syn H-H cyclobutane 40:** *R<sub>f</sub>* 0.15 (100:10:1 CHCl<sub>3</sub>:MeOH:NH<sub>4</sub>OH); IR (neat) 3054, 2986, 2928, 2854, 2305, 1711, 1648, 1421, 1265, 895, 738 cm<sup>-1</sup>; <sup>1</sup>H NMR (300 MHz, CD<sub>3</sub>CN) δ 8.45 (br t, *J* = 6 Hz, 2 H), 7.66-7.30 (m, 34

H), 4.68 (s, 4 H), 4.26 (d,  $J = 5$  Hz, 4 H), 3.31 (t,  $J = 5$  Hz, 8 H), 2.57 (t,  $J = 5$  Hz, 8H), 2.52 (q,  $J = 7$  Hz, 16 H), 0.93 (t,  $J = 7$  Hz, 24 H);  $^{13}\text{C}$  NMR (75 MHz,  $\text{CDCl}_3$ )  $\delta$  160.6, 141.0, 140.15, 140.03, 140.0, 139.9, 139.6, 139.4, 138.9, 138.8, 128.9, 128.8, 128.7, 128.5, 128.4, 128.3, 127.7, 127.5, 127.4, 127.3, 127.2, 127.1, 127.08, 127.02, 126.9, 126.8, 53.53, 53.52, 53.51, 51.79, 51.78, 51.77, 47.91, 47.77, 44.53, 29.89, 11.62, 11.50; HRMS(ES)  $m/z$  calcd for  $\text{C}_{80}\text{H}_{101}\text{N}_8\text{O}_2$  [M + H] 1205.8048, found 1205.8049.



**4-(4-Bromophenyl)-[2,2']bipyridine (22).**<sup>62</sup> To a solution of dihydropyran<sup>63</sup> (503 mg, 1.40 mmol) in acetonitrile (9.3 mL) was added  $\text{H}_2\text{NOH}\cdot\text{HCl}$  (973 mg, 14.0 mmol). The solution was heated at reflux for 6 h then cooled to 23 °C. Volatile components of the reaction mixture were removed *in vacuo* to give a brownish-green solid. A solution of 10:1 brine: $\text{NH}_4\text{OH}$  (20 mL) and  $\text{CH}_2\text{Cl}_2$  (20 mL) were added to the solid and the mixture was stirred vigorously until all the solid dissolved. The organic layer was extracted with  $\text{CH}_2\text{Cl}_2$  (4 x 20 mL), dried with  $\text{Na}_2\text{SO}_4$ , and evaporated *in vacuo* to give a brown solid. The solid was extracted with warm ether (4 x 20 mL) and volatile components were removed *in vacuo* to give a yellow solid. The solid was recrystallized from hot methanol to yield white microcrystals (208 mg, 48%): mp 94-98 °C; IR (KBr) 3054, 1597, 1583, 1564, 1538, 1457, 1380, 1257, 1080, 1008, 990, 909, 817, 793, 739, 748, 661, 651; The  $^1\text{H}$  and  $^{13}\text{C}$  NMR data matches the data described by Bergman and coworkers:<sup>64</sup>  $^1\text{H}$  NMR (300 MHz,  $\text{CDCl}_3$ )  $\delta$  8.74 (d,  $J = 5$  Hz, 1 H,  $\text{H}^6$ ), 8.73-8.71 (m, 1 H,  $\text{H}^{6'}$ ), 8.65 (d,  $J = 2$  Hz, 1 H,  $\text{H}^3$ ), 8.46 (app d,  $J = 7$  Hz, 1H,  $\text{H}^3$ ), 7.86 (dt,  $J = 7,7,2$  Hz, 1 H,  $\text{H}^4$ ), 7.69-7.60 (m, 4 H, phenyl), 7.51 (dd,  $J = 5,2$  Hz, 1 H,

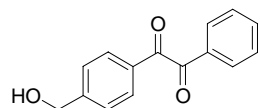
H<sup>5</sup>), 7.35 (ddd,  $J = 7,5,1$  Hz, 1H, H<sup>5</sup>); <sup>13</sup>C NMR (75 MHz, CDCl<sub>3</sub>)  $\delta$  157.2, 156.3, 150.0, 149.5, 148.4, 137.5, 137.2, 132.5, 128.9, 124.2, 123.8, 121.6, 121.5, 119.0.



**(Z)-4-[4'-(2-Biphenyl-4-ylvinyl)biphenyl-4-yl]-**

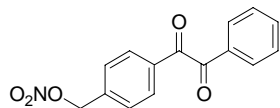
**[2,2']bipyridine (20Z).** A solution of 4-(4-bromo-phenyl)-[2,2']bipyridine **22** (100 mg, 0.321 mmol) and boronic ester **21Z** (135 mg, 0.353 mmol) in DME (2 mL) was deoxygenated by freeze-pump-thaw cycles (3 x) and kept under N<sub>2</sub>. Sodium carbonate (102 mg, 0.963 mmol) was dissolved in a minimal amount of H<sub>2</sub>O and degassed similarly. To the first flask was added tetrakis-(triphenylphosphine)palladium(0) (16 mg, 0.014 mmol) followed immediately by the sodium carbonate solution, transferred by cannula. The solution was stirred for 1 h at 23 °C, and then heated to 85 °C for 20 h. The solution was cooled to 23 °C and volatile components of the reaction mixture were removed *in vacuo*. The crude solid was combined with H<sub>2</sub>O (40 mL) and extracted with CH<sub>2</sub>Cl<sub>2</sub> (3 x 20 mL). The combined organic layers were then washed with 10% NH<sub>4</sub><sup>+</sup>OH(aq) (3 x 30 mL), dried with K<sub>2</sub>CO<sub>3</sub>, and filtered. Volatile components of the filtrate were removed *in vacuo* to afford a crude solid that was purified by flash chromatography (SiO<sub>2</sub>, CH<sub>2</sub>Cl<sub>2</sub> then 99:1 CH<sub>2</sub>Cl<sub>2</sub>:MeOH, column pretreated with 19:1 CH<sub>2</sub>Cl<sub>2</sub>:NEt<sub>3</sub> then washed with CH<sub>2</sub>Cl<sub>2</sub>) to afford **20Z** as a pale yellow solid (112.7 mg, 72%):  $R_f$  0.24 (99:1 CH<sub>2</sub>Cl<sub>2</sub>:MeOH, pretreated with 19:1 CH<sub>2</sub>Cl<sub>2</sub>:NEt<sub>3</sub>); mp 116-118 °C; IR (KBr) 3053, 3028, 1583, 1598, 1565, 1497, 1485, 1457, 1387, 910, 821; UV-Vis (CH<sub>2</sub>Cl<sub>2</sub>, 8.3  $\mu$ M)  $\lambda_{max}$  345 nm,  $\epsilon$  4465 M<sup>-1</sup>cm<sup>-1</sup>, 293 nm,  $\epsilon$  3109 M<sup>-1</sup>cm<sup>-1</sup>, 569 nm,  $\epsilon$  792 M<sup>-1</sup>cm<sup>-1</sup>, 687 nm,  $\epsilon$  1560 M<sup>-1</sup>cm<sup>-1</sup>; <sup>1</sup>H NMR (300 MHz,

CDCl<sub>3</sub>) δ 8.80 (br d, *J* = 7 Hz, 1 H, H<sup>6</sup>), 8.77-8.75 (m, 2 H, H<sup>6</sup>+H<sup>3</sup>), 8.58 (br d, *J* = 7 Hz, 1 H, H<sup>3</sup>), 7.94-7.88 (m, 1 H, H<sup>4</sup>), 7.88 (app d, *J* = 8 Hz, 2 H, phenyl), 7.76 (app d, *J* = 8 Hz, 2 H, phenyl), 7.67 (br d, *J* = 7 Hz, 1 H, H<sup>5</sup>), 7.63-7.51 (m, 8 H, phenyl), 7.47-7.36 (m, 7 H, phenyl), 7.36-7.31 (m, 1 H, H<sup>5</sup>), 6.68 (s, 2 H, G+G'); <sup>13</sup>C NMR (75 MHz, CD<sub>3</sub>CN) δ 156.9, 156.4, 149.9, 149.4, 149.0, 141.6, 140.9, 140.1, 139.1, 137.2, 137.1, 137.0, 136.5, 130.4, 130.0, 127.7, 129.6, 128.9, 127.7, 127.6, 127.5, 127.1, 127.0, 124.0, 121.5, 119.0; HRMS(EI) *m/z* calcd for C<sub>36</sub>H<sub>26</sub>N<sub>2</sub> 486.2095, found 486.2090.



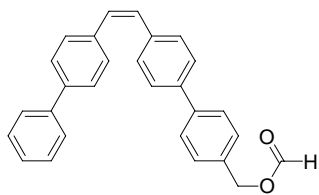
**4-(Hydroxymethyl)benzil (24).** To a solution of 4-(bromomethyl)benzil

(100 mg, 0.33 mmol) in 33 mL of THF was added a solution of AgNO<sub>3</sub> (653 mg, 0.38 mmol) in 11 mL of water. The resulting mixture was heated at reflux for 3.5 h. After the mixture was cooled, the AgBr was removed by filtration using acetone for rinsing. Volatile components of the filtrate were removed in vacuo and the resulting mixture was extracted with CH<sub>2</sub>Cl<sub>2</sub> (3 x 50 mL). The CH<sub>2</sub>Cl<sub>2</sub> extracts were combined, washed with brine (150 mL), dried with MgSO<sub>4</sub>, and filtered. Volatile components of the filtrate were removed in vacuo, and the residue was purified by flash chromatography (SiO<sub>2</sub>, 1% EtOAc in CH<sub>2</sub>Cl<sub>2</sub>) to afford **6** as a light yellow wax (25.9 mg, 56%): *R<sub>f</sub>* 0.21 (2% EtOAc in CH<sub>2</sub>Cl<sub>2</sub>); IR (thin film) 3419, 3062, 2923, 1674, 1605, 1579 cm<sup>-1</sup>; <sup>1</sup>H NMR (300 MHz, CDCl<sub>3</sub>) δ 7.98 (app d, *J* = 8 Hz, 4H), 7.68 (dddd, *J* = 8, 8, 2, 2 Hz, 1 H), 7.53 (m, 4 H), 4.82 (s, 2 H); <sup>13</sup>C NMR (75 MHz, CH<sub>2</sub>Cl<sub>2</sub>) δ 194.6, 194.2, 148.4, 134.9, 133.0, 132.2, 130.3, 129.9, 129.0, 126.9, 64.4; HRMS (EI) *m/z* calcd for C<sub>15</sub>H<sub>12</sub>O<sub>3</sub> 240.0786, found 240.0776.



**4-(Nitrateestermethyl)benzil (25).**

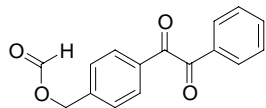
**25** was obtained as a byproduct of the reaction described for the synthesis of **24**. The ratio of **24** to **25** obtained was 18/25. Flash chromatography (SiO<sub>2</sub>, 1% EtOAc in CH<sub>2</sub>Cl<sub>2</sub>) to afforded **7** as a yellow oil (42.8 mg): *R<sub>f</sub>* 0.79 (1% EtOAc in CH<sub>2</sub>Cl<sub>2</sub>); IR (thin film) 2924, 1672, 1626, 1607, 1596, 1580, 1450, 1279, 1211, 1173 cm<sup>-1</sup>; <sup>1</sup>H NMR (300 MHz, CDCl<sub>3</sub>) δ 8.04-7.97 (m, 4 H), 7.69 (dddd, *J* = 8, 8, 1, 1 Hz, 1 H), 7.54 (app d, *J* = 6 Hz, 3 H), 7.51 (m, 1 H), 5.50 (s, 1 H); <sup>13</sup>C NMR (75 MHz, CH<sub>2</sub>Cl<sub>2</sub>) δ 194.0, 193.6, 139.4, 135.0, 133.6, 132.8, 130.3, 129.9, 129.1, 128.8, 73.3; HRMS (EI) *m/e* calcd for C<sub>15</sub>H<sub>11</sub>NO<sub>3</sub> 285.063723, found 285.063638.



**Formic acid 4'-(2-biphenyl-4-ylvinyl)biphenyl-4-ylmethyl ester (26).**

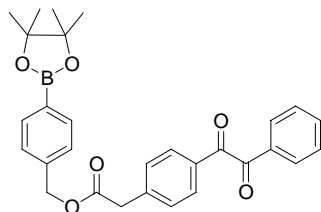
A solution of 4-(bromomethyl)benzil **23** (83.7 mg, 0.276 mmol) in dry DMF (2.8 mL) was syringed into a flask containing AgO<sub>3</sub>SCF<sub>3</sub> (70.9 mg, 0.276 mmol) and **13Z** (100 mg, 0.276 mmol) under a nitrogen atmosphere. The mixture was stirred for 24 h then diluted with CH<sub>2</sub>Cl<sub>2</sub> (30 mL) and water (30 mL) and extracted with CH<sub>2</sub>Cl<sub>2</sub> (3 x 30 mL). The CH<sub>2</sub>Cl<sub>2</sub> extracts were combined, washed with brine (150 mL), dried with MgSO<sub>4</sub>, and filtered. Volatile components in the filtrate were removed in vacuo, and the residue was purified by flash chromatography (SiO<sub>2</sub>, toluene) to afford **26** as a yellow solid (20.1 mg): *R<sub>f</sub>* 0.40 (toluene); mp: decomposition at 100-110 °C; IR (KBr) 3031, 3002, 1918, 1726, 1704, 1496, 1486, 1399, 1368, 1177, 819 cm<sup>-1</sup>; <sup>1</sup>H NMR (300 MHz, CDCl<sub>3</sub>) δ 8.18 (s, 1 H), 7.63-7.60 (m, 4 H), 7.53-7.38 (m, 13 H), 6.66 (s, 2 H), 5.25 (s, 2 H); <sup>13</sup>C NMR (75 MHz, CH<sub>2</sub>Cl<sub>2</sub>) δ 160.9, 141.2, 140.9, 140.1, 139.3, 136.8, 136.4,

134.4, 130.3, 130.0, 129.6, 129.5, 129.0, 128.9, 127.5, 127.3, 127.1, 65.6; HRMS (EI)  $m/z$  calcd for  $C_{28}H_{22}O_2$  390.161980, found 390.163471.



**Formic acid 4-(2-oxo-2-phenylacetyl)-benzyl ester (27).** **27** was

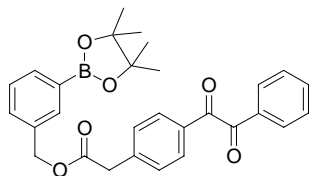
obtained as a byproduct of the reaction described for the synthesis of **26**. The ratio of **26** to **27** obtained was 13/40. Flash chromatography ( $SiO_2$ , toluene) to afforded **27** as a yellow oil (42.8 mg):  $R_f$  0.15 (toluene); IR (thin film) 3653, 3558, 3434, 3330, 3063, 2937, 2256, 1724, 1666, 1609, 1596, 1450, 1417, 1323, 1178  $cm^{-1}$ ;  $^1H$  NMR (300 MHz,  $CDCl_3$ )  $\delta$  8.18 (s, 1 H), 8.01-7.96 (m, 4 H), 7.68 (dddd,  $J = 7, 7, 1, 1$  Hz, 1 H), 7.56-7.51 (m, 4 H), 5.29 (s, 2 H);  $^{13}C$  NMR (75 MHz,  $CH_2Cl_2$ )  $\delta$  194.5, 194.2, 160.6, 142.6, 135.2, 133.23, 133.2, 130.5, 130.2, 129.3, 128.5, 64.9; HRMS (EI)  $m/z$  calcd for  $C_{16}H_{12}NO_4$  268.073559, found 268.073712.



**[4-(2-Oxo-2-phenylacetyl)phenyl]acetic acid 4-(4,4,5,5-tetramethyl-**

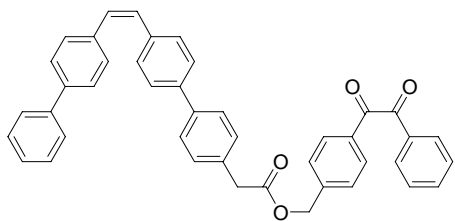
**[1,3,2]dioxaborolan-2-yl)benzyl ester (31).** Under a nitrogen atmosphere, a flask containing anhydrous  $CH_2Cl_2$  (40 mL) was sequentially charged with 4-(hydroxymethyl)benzil **24** (968 mg, 4.03 mmol), para-substituted carboxylic acid pinacol ester **30** (1.05 g, 3.99 mmol), and then stirred at 0 °C. The solution was then sequentially treated with 4-(dimethylamino)pyridine (DMAP, 97.4 mg, 0.798 mmol) and dicyclohexylcarbodiimide (DCC, 905 mg, 4.39 mmol). The solution was stirred for 10 min at 0 °C and then warmed to room temperature and stirred for 3 h. The white precipitate that forms was discarded by filtration and the volatile components of the filtrate were removed in vacuo to give a yellow oil. The oil was purified by flash

chromatography (SiO<sub>2</sub>, 1% EtOAc in CH<sub>2</sub>Cl<sub>2</sub>) to afford **31** as a yellow oil (1.81 g, 94%): *R<sub>f</sub>* 0.55 (CH<sub>2</sub>Cl<sub>2</sub>); IR (thin film) 3399, 2978, 1736, 1678, 1608, 1450, 1360, 1322, 1274, 1213, 1174, 1143 cm<sup>-1</sup>; <sup>1</sup>H NMR (300 MHz, CDCl<sub>3</sub>) δ 7.99-7.94 (m, 4H), 7.78 (d, *J* = 8 Hz, 2 H), 7.68 (dddd, *J* = 8, 8, 1, 1 Hz, 1 H), 7.55-7.50 (m, 2 H), 7.42 (d, *J* = 9 Hz, 2 H), 7.30 (d, *J* = 8 Hz, 2 H), 5.19 (s, 2 H), 3.72 (s, 2 H), 1.35 (s, 12 H); <sup>13</sup>C NMR (75 MHz, CH<sub>2</sub>Cl<sub>2</sub>) δ 194.2, 193.9, 170.8, 143.1, 136.6, 135.1, 134.8, 132.9, 132.6, 130.1, 129.9, 129.0, 128.6, 127.9, 83.8, 65.5, 41.5, 24.8; HRMS (ES) *m/z* calcd for C<sub>29</sub>H<sub>29</sub>BO<sub>6</sub>Na 507.1955, found 507.1947.



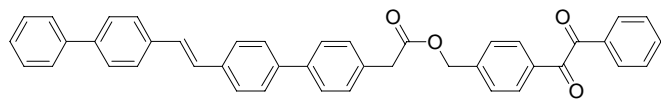
**[4-(2-Oxo-2-phenylacetyl)phenyl]acetic acid 3-(4,4,5,5-tetramethyl-[1,3,2]dioxaborolan-2-yl)benzyl ester (34).** Under a nitrogen atmosphere, a flask containing anhydrous CH<sub>2</sub>Cl<sub>2</sub> (43 mL) was sequentially charged with 4-(hydroxymethyl)benzil **24** (1.02 g, 4.26 mmol), meta-substituted carboxylic acid pinacol ester **33** (1.10 g, 4.21 mmol), and then stirred at 0 °C. The solution was then sequentially treated with 4-(dimethylamino)pyridine (DMAP, 103 mg, 0.843 mmol) and dicyclohexylcarbodiimide (DCC, 957 mg, 4.64 mmol). The solution was stirred for 10 min at 0 °C and then warmed to room temperature and stirred for 2.5 h. The white precipitate that forms was discarded by filtration and the volatile components of the filtrate were removed in vacuo to give a yellow oil. The oil was purified by flash chromatography (SiO<sub>2</sub>, 1% EtOAc in CH<sub>2</sub>Cl<sub>2</sub>) to afford **34** as a yellow oil (1.21 g, 59%): *R<sub>f</sub>* 0.61 (1% EtOAc in CH<sub>2</sub>Cl<sub>2</sub>); IR (thin film) 3057, 2978, 2931, 1740, 1674, 1608, 1430, 1360, 1323, 1213, 1144, 1099, 1000, 709 cm<sup>-1</sup>; <sup>1</sup>H NMR (300 MHz, CDCl<sub>3</sub>) δ 7.95 (app t, *J* = 14, 6 Hz, 4H), 7.74 (m, 2 H), 7.64 (app t, *J* = 14, 7, 1 Hz, 1 H), 7.50 (app t, *J* = 15, 8, 2 H), 7.43-7.31 (m, 4 H), 5.19 (s, 2 H), 3.71 (s, 2 H), 1.34 (s, 12 H); <sup>13</sup>C NMR (75 MHz, CH<sub>2</sub>Cl<sub>2</sub>)

$\delta$  194.2, 193.8, 170.9, 143.1, 135.1, 134.8, 133.6, 132.8, 132.5, 132.0, 130.0, 129.8, 128.9, 128.0, 127.8, 83.4, 65.3, 41.0, 24.8; HRMS (ES)  $m/z$  calcd for  $C_{29}H_{29}BO_6Na$  507.1955, found 507.197.



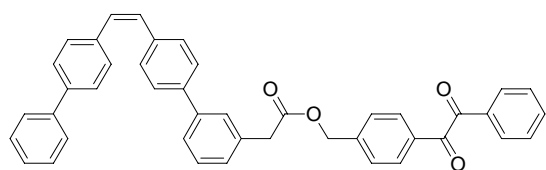
**[4'-(2-Biphenyl-4-ylvinyl)biphenyl-4-yl]acetic acid 4-(2-**

**oxo-2-phenylacetyl)benzyl ester (28Z).** 1-[2-(4-Bromo-phenyl)]-biphenyl ethene **32** (555 mg, 1.66 mmol), pinacol boronic ester **31** (884 mg, 1.82 mmol),  $Pd(PPh_3)_4$  (82.5 mg, 0.071 mmol), and THF (10.3 mL) were placed in a flask and the solution was degassed *via* three freeze-pump-thaw cycles, and then placed under nitrogen. Sodium carbonate (527 mg, 4.97 mmol) was dissolved in a minimum amount of water in a separate flask and degassed similarly, then cannula transferred. The resulting mixture was heated at reflux for 20 h. After the mixture was cooled, volatile components were removed in vacuo, and the crude residue was dissolved in water (100 mL) and extracted with  $CH_2Cl_2$  (3 x 100 mL). The  $CH_2Cl_2$  extracts were combined, washed with brine (300 mL), dried with  $MgSO_4$ , and filtered. Volatile components of the filtrate were removed in vacuo, and the residue was purified by flash chromatography ( $SiO_2$ , 7:3  $CH_2Cl_2$ :Hex) to afford **28Z** as a light yellow wax (81.3 mg, 80%):  $R_f$  0.39 (7:3  $CH_2Cl_2$ :Hex); mp 82-84 °C; IR (thin film) 3028, 1738, 1671, 1608, 1596, 1496, 1486, 1449, 1416, 1213, 1173, 1146, 1006, 883  $cm^{-1}$ ;  $^1H$  NMR (300 MHz,  $CDCl_3$ )  $\delta$  7.98-7.94 (m, 4H), 7.71-7.30 (m, 22 H), 6.66 (s, 2 H), 5.22 (s, 2 H), 3.74 (s, 2 H);  $^{13}C$  NMR (75 MHz,  $CH_2Cl_2$ )  $\delta$  194.2, 193.9, 171.0, 143.1, 140.6, 139.9, 139.7, 139.3, 136.4, 136.3, 134.9, 133.0, 132.7, 132.6, 130.1, 130.0, 129.9, 129.7, 129.4, 129.3, 129.0, 128.7, 128.0, 127.4, 127.3, 127.1, 127.0, 126.9, 126.85, 126.75; HRMS (EI)  $m/z$  calcd for  $C_{43}H_{32}O_4$  612.230060, found 612.232163.



**[4'-(2-Biphenyl-4-ylvinyl)biphenyl-4-yl]-**

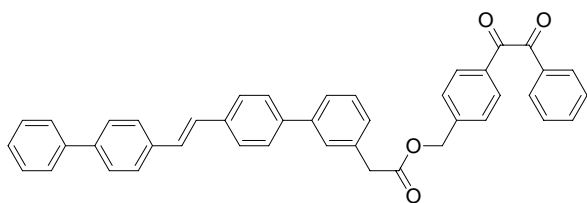
**acetic acid 4-(2-oxo-2-phenylacetyl)benzyl ester (16E).** Precipiton **28Z** (100 mg, 0.163 mmol) and erythrosine B (6.8 mg, 0.008 mmol) in THF (1.63 mL) were placed in a flask and the solution was degassed *via* three freeze-pump-thaw cycles, and then placed under nitrogen. The resulting mixture was stirred and irradiated with a 250-W incandescent lamp for 20 h. The resulting precipitate **28E** (70.8 mg, 71%) was isolated by filtering the reaction mixture through filter paper and washing it with THF until all traces of red dye were removed: mp > 240 °C; IR (KBr) 3030, 1729, 1665, 1608, 1496, 1450, 1409, 1374, 1243, 1162, 1003, 971 cm<sup>-1</sup>; <sup>1</sup>H NMR (300 MHz, CDCl<sub>3</sub>) δ 7.99-7.96 (m, 4H), 7.68-7.34 (m, 22 H), 7.21 (s, 2 H), 5.24 (s, 2 H), 3.76 (s, 2 H); <sup>13</sup>C NMR, too insoluble to obtain; HRMS (EI) *m/z* calcd for C<sub>43</sub>H<sub>32</sub>O<sub>4</sub> 612.230060, found 612.232850.



**[4'-(2-Biphenyl-4-ylvinyl)biphenyl-3-yl]acetic acid**

**4-(2-oxo-2-phenylacetyl)benzyl ester (29Z).** 1-[2-(4-Bromo-phenyl)]-biphenyl ethene **32** (372 mg, 1.11 mmol), pinacol boronic ester **34** (592 mg, 1.22 mmol), Pd(PPh<sub>3</sub>)<sub>4</sub> (55.4 mg, 0.048 mmol), and THF (6.9 mL) were placed in a flask and the solution was degassed *via* three freeze-pump-thaw cycles, and then placed under nitrogen. Sodium carbonate (353 mg, 3.33 mmol) was dissolved in a minimum amount of water in a separate flask and degassed similarly, then cannula transferred. The resulting mixture was heated at reflux for 23 h. After the mixture was cooled, volatile components were removed in vacuo, and the crude residue was dissolved in water (100

mL) and extracted with CH<sub>2</sub>Cl<sub>2</sub> (3 x 100 mL). The CH<sub>2</sub>Cl<sub>2</sub> extracts were combined, washed with brine (300 mL), dried with MgSO<sub>4</sub>, and filtered. Volatile components of the filtrate were removed in vacuo, and the residue was purified by flash chromatography (SiO<sub>2</sub>, 8:2 Hex:CH<sub>2</sub>Cl<sub>2</sub>) to afford **29Z** as a light yellow wax (608 mg, 90%): R<sub>f</sub> 0.16 (5:5 Hex:CH<sub>2</sub>Cl<sub>2</sub>); mp 44-46 °C; IR (thin film) 3056, 3029, 1739, 1672, 1607, 1579, 1485, 1449, 1417, 1241, 1212, 1174, 1147, 883 cm<sup>-1</sup>; <sup>1</sup>H NMR (300 MHz, CDCl<sub>3</sub>) δ 8.03 (app t, 4H), 7.68-7.28 (m, 22 H), 6.73 (s, 2 H), 5.25 (s, 2 H), 3.81 (s, 2 H); <sup>13</sup>C NMR (75 MHz, CH<sub>2</sub>Cl<sub>2</sub>) δ 194.0, 193.7, 170.7, 142.9, 140.8, 140.3, 139.6, 139.1, 136.3, 136.0, 134.7, 133.9, 132.7, 132.4, 129.9, 129.7, 129.6, 129.2, 128.9, 128.8, 128.5, 128.0, 127.8, 127.6, 127.1, 126.8, 126.6, 125.6, 65.3, 40.1; HRMS (ES) *m/z* calcd for C<sub>43</sub>H<sub>32</sub>O<sub>4</sub>Na 635.2218, found 635.2198.



**[4'-(2-Biphenyl-4-ylvinyl)biphenyl-3-yl]acetic**

**acid 4-(2-oxo-2-phenylacetyl)benzyl ester (29E).** Precipiton **29Z** (66.8 mg, 0.109 mmol) and erythrosine B (4.6 mg, 0.006 mmol) in THF (1.09 mL) were placed in a flask and the solution was degassed *via* three freeze-pump-thaw cycles, and then placed under nitrogen. The resulting mixture was stirred and irradiated with a 250-W incandescent lamp equipped with a  $\lambda \leq 400$  nm cutoff filter for 4 h. The resulting homogeneous solution was then purified by flash chromatography (SiO<sub>2</sub>, 8:2 Hex:CH<sub>2</sub>Cl<sub>2</sub>) to afford **29E** as a light yellow solid (61.4 mg, 92%): mp 181-183 °C; IR (KBr) 3434, 3030, 1736, 1670, 1607, 1596, 1579, 1486, 1449, 1408, 1375, 1213, 1174, 1146, 1004, 970 cm<sup>-1</sup>; <sup>1</sup>H NMR (300 MHz, CDCl<sub>3</sub>) δ 7.99-7.95 (m, 4H), 7.69-7.30 (m, 22 H), 7.21 (s, 2 H), 5.24 (s, 2 H), 3.79 (s, 2 H); <sup>13</sup>C NMR, too insoluble to obtain; HRMS (EI) *m/z* calcd for C<sub>43</sub>H<sub>32</sub>O<sub>4</sub> 612.230060, found 612.230060.

## 6.2.2 $^1\text{H}$ NMR Spectra, $^1\text{H}$ - $^1\text{H}$ COSY, and $^{13}\text{C}$ NMR Spectra

Figure 47.  $^1\text{H}$  NMR spectra of compound 13Z.

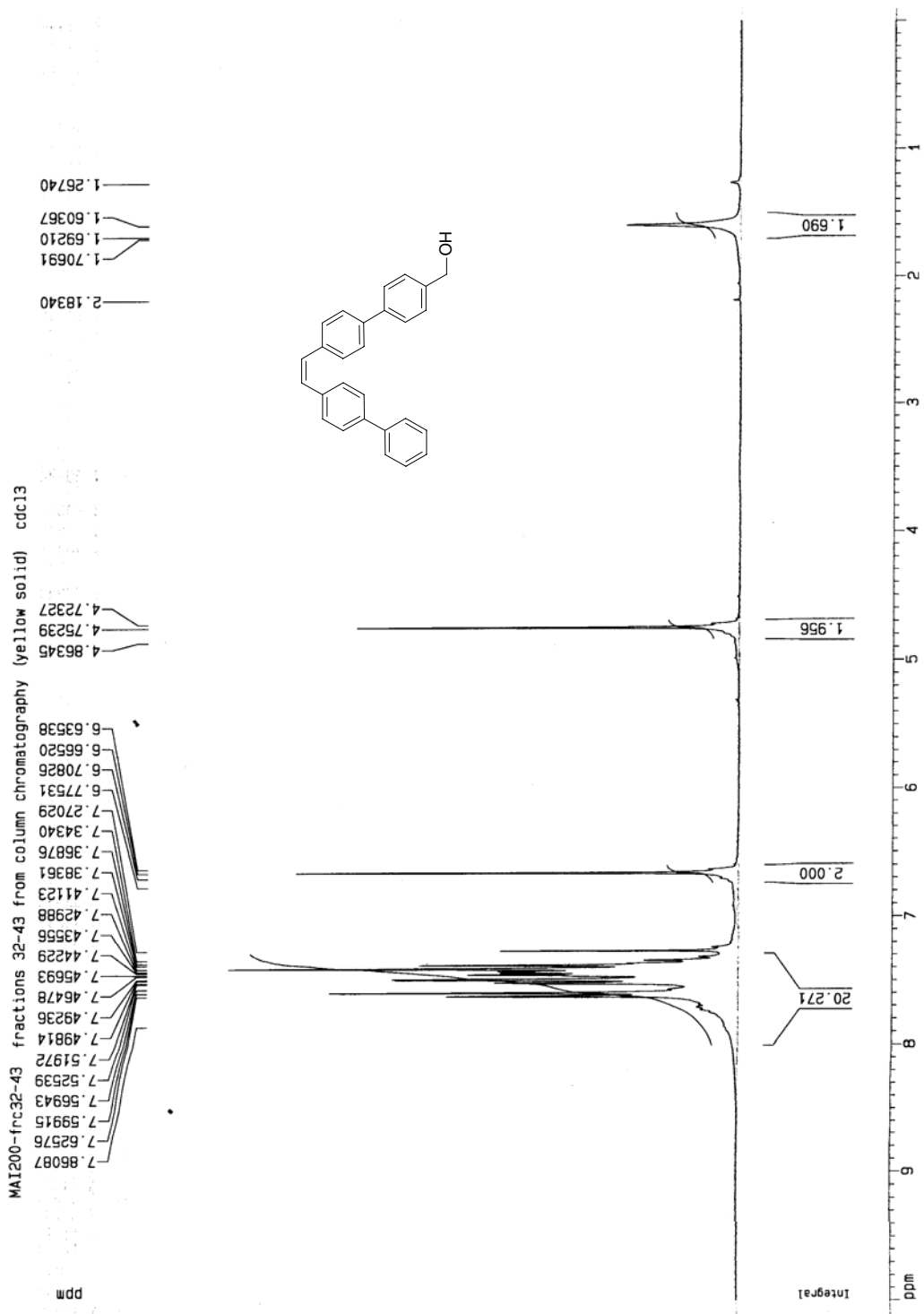


Figure 48.  $^1\text{H}$  NMR spectra of compound 16Z.

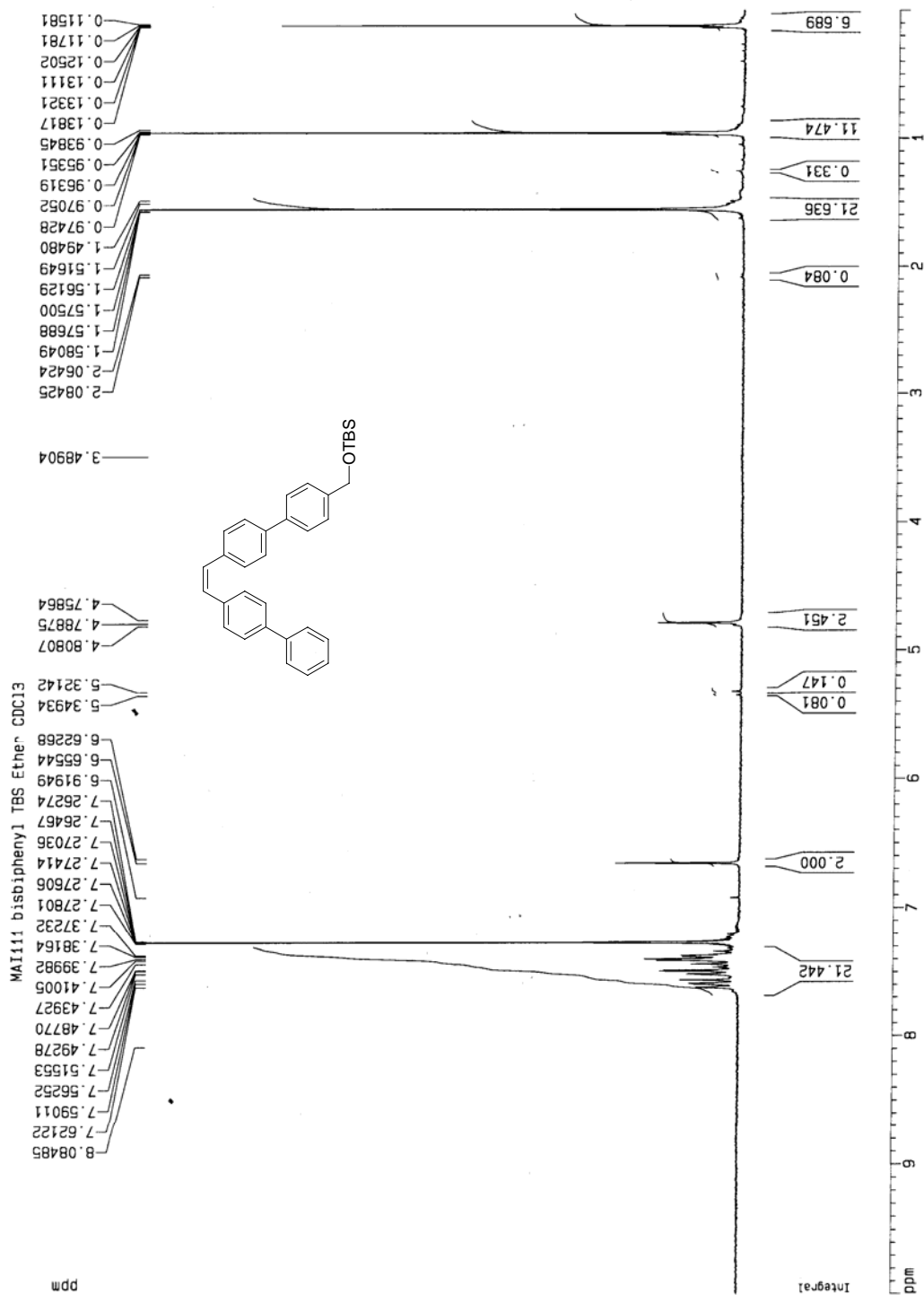


Figure 49.  $^{13}\text{C}$  NMR spectra of compound 16Z.

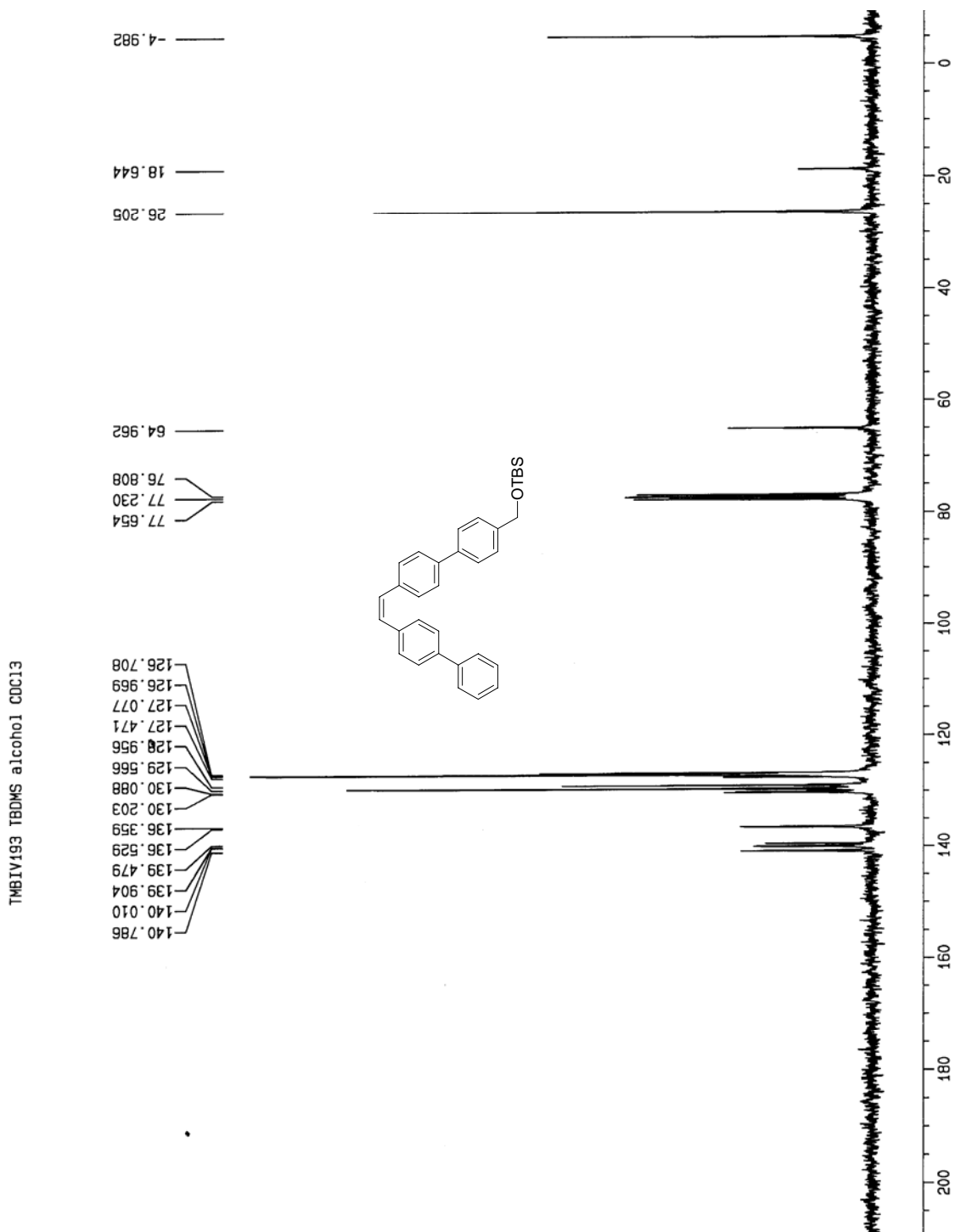


Figure 50.  $^1\text{H}$  NMR spectra of compound **16E**.

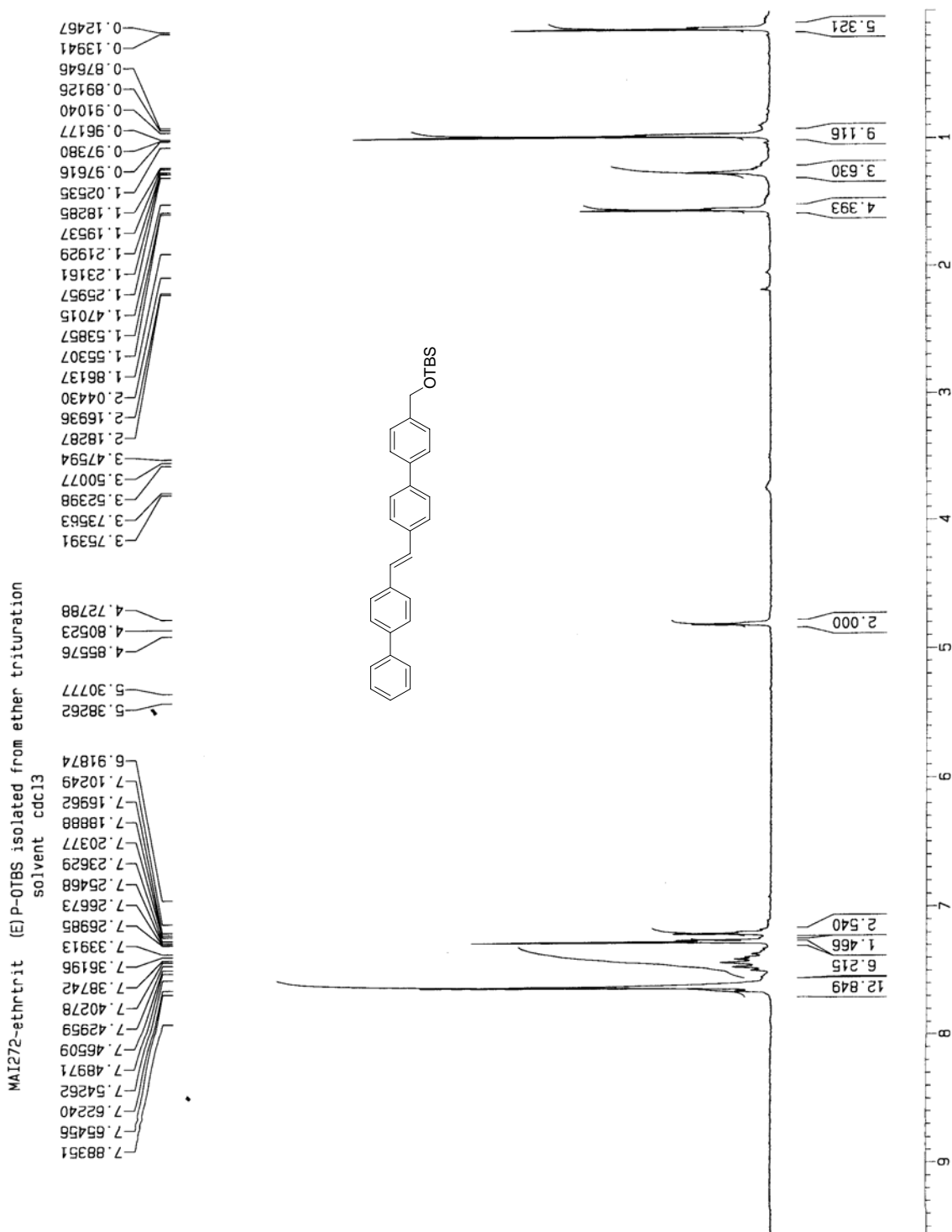


Figure 51.  $^1\text{H}$ - $^1\text{H}$  COSY of 5-bromomethyl-2,2'-bipyridine.

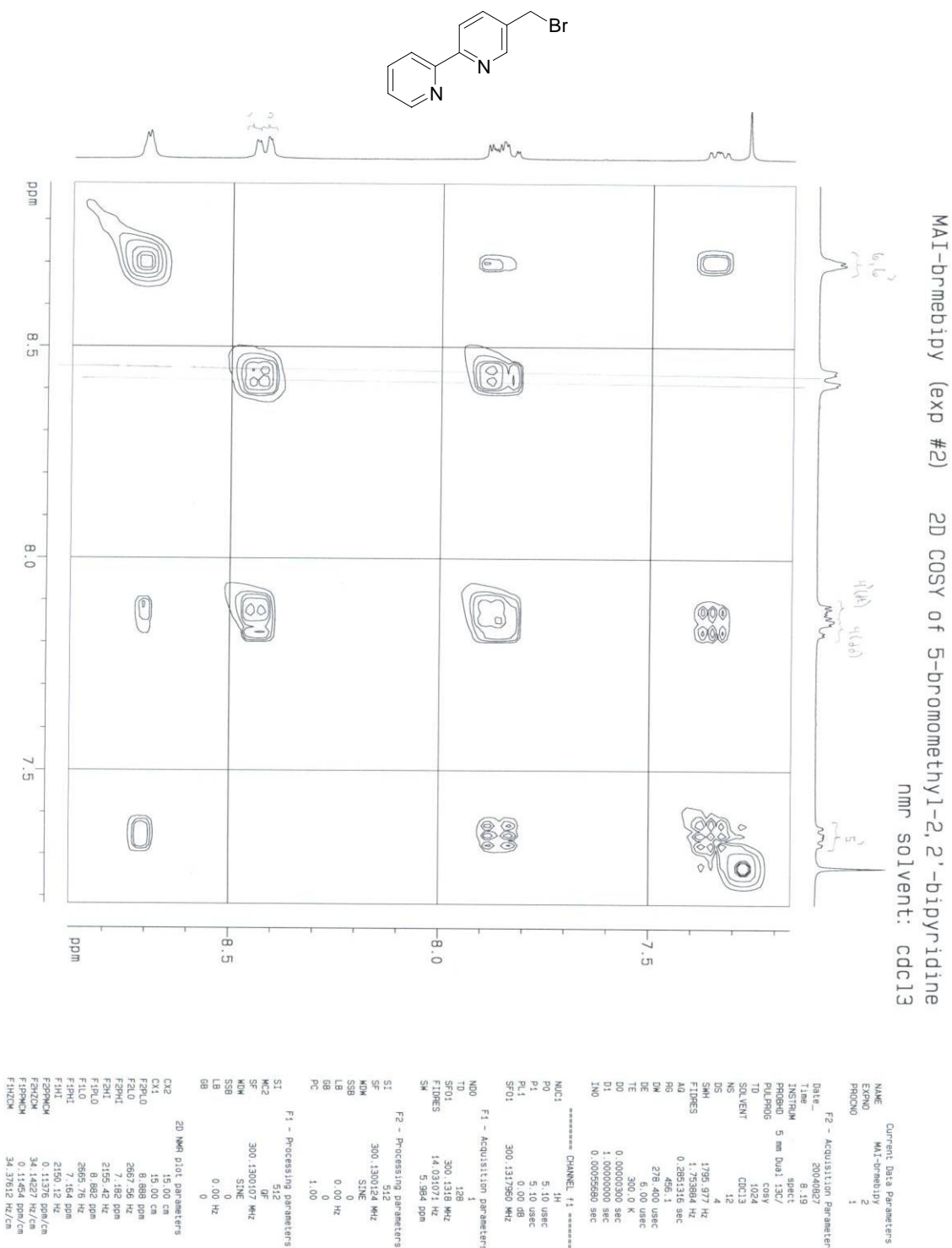


Figure 52.  $^1\text{H}$  NMR spectra of compound 17Z.

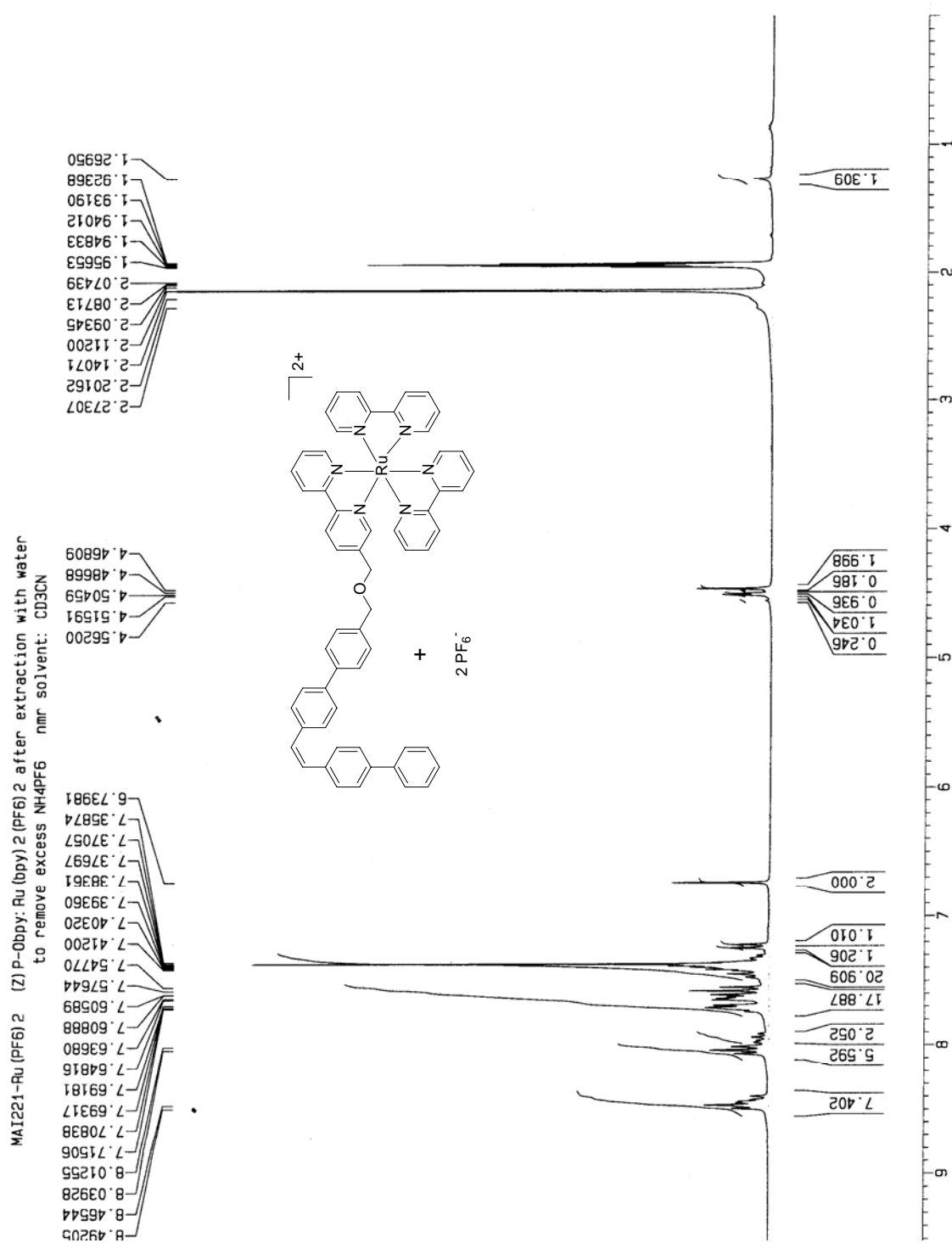




Figure 54.  $^{13}\text{C}$  NMR spectra of compound 17Z.

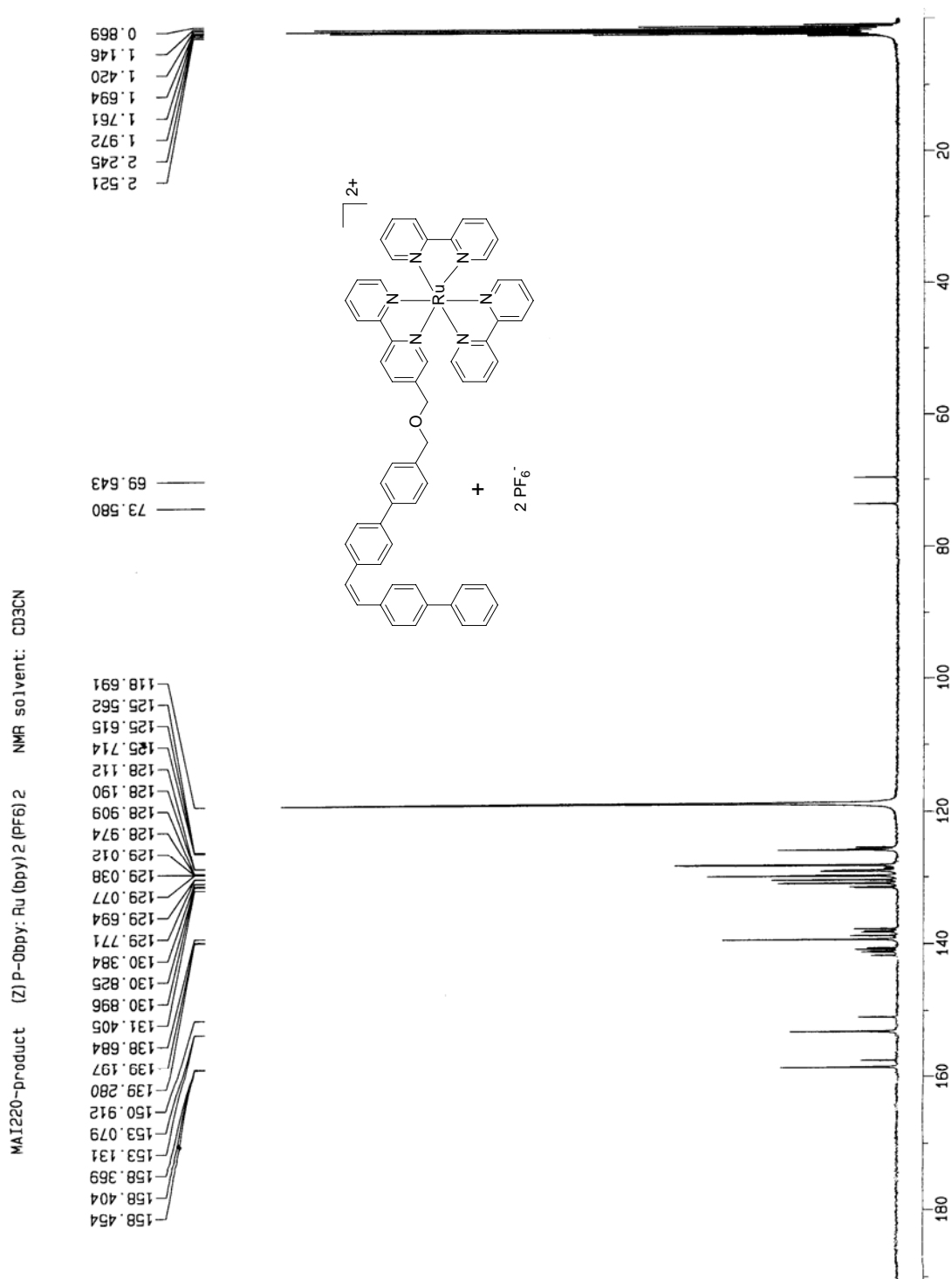


Figure 55.  $^1\text{H}$  NMR spectra of compound **17E**.

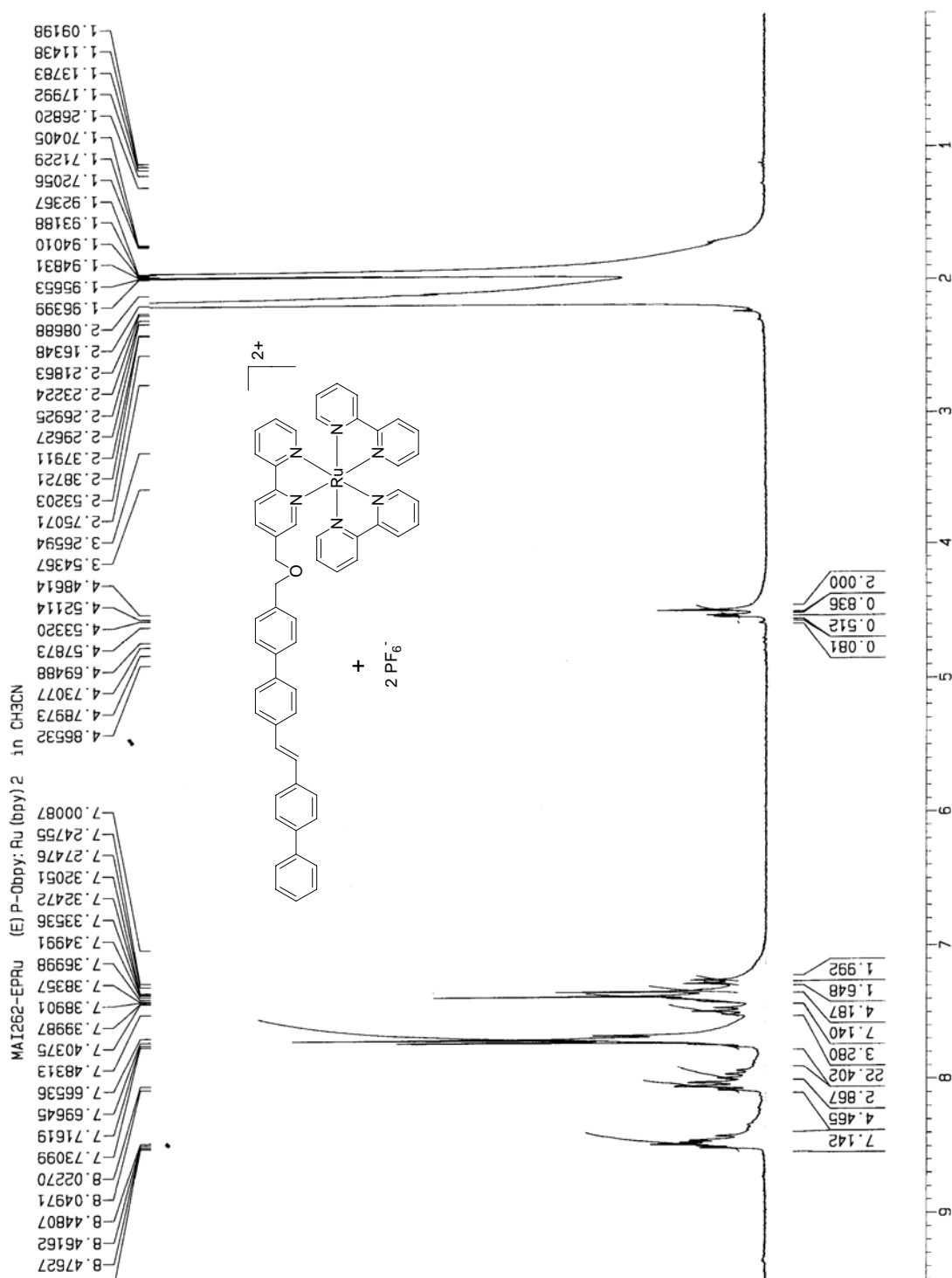


Figure 56.  $^1\text{H}$ - $^1\text{H}$  COSY of compound **17E**.

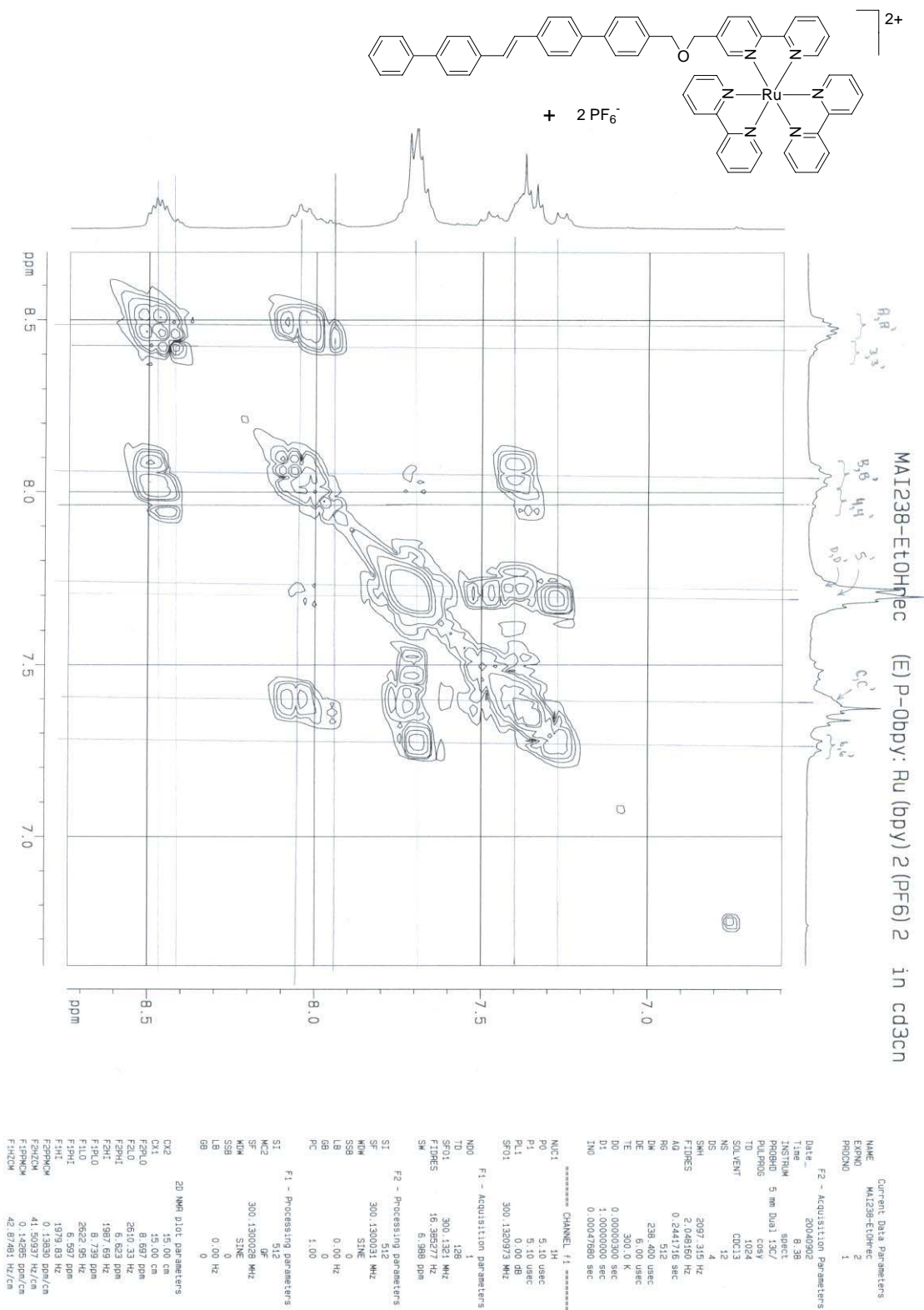


Figure 57.  $^{13}\text{C}$  NMR spectra of compound **17E**.

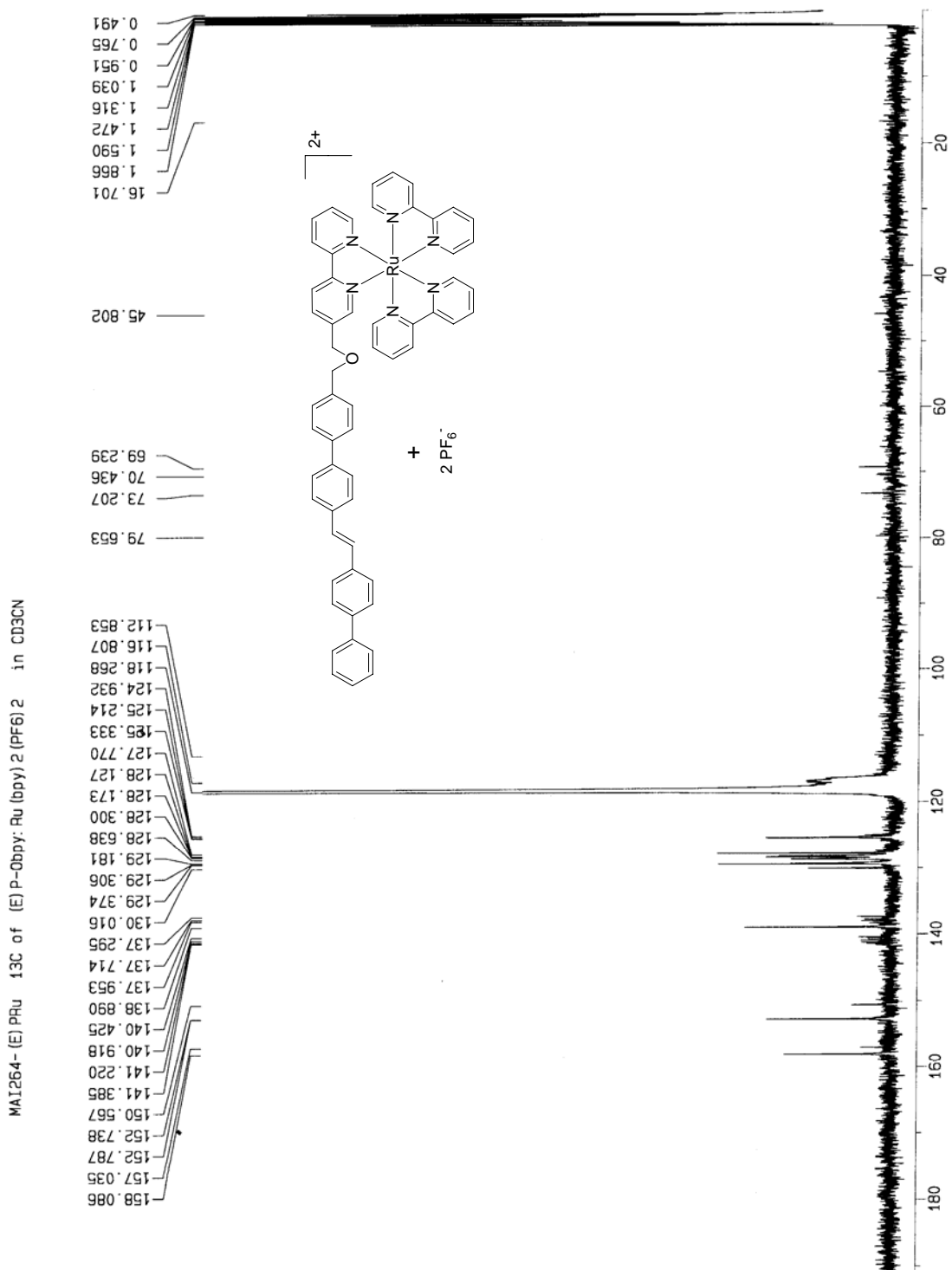


Figure 58. <sup>1</sup>H NMR spectra of compound 18Z.

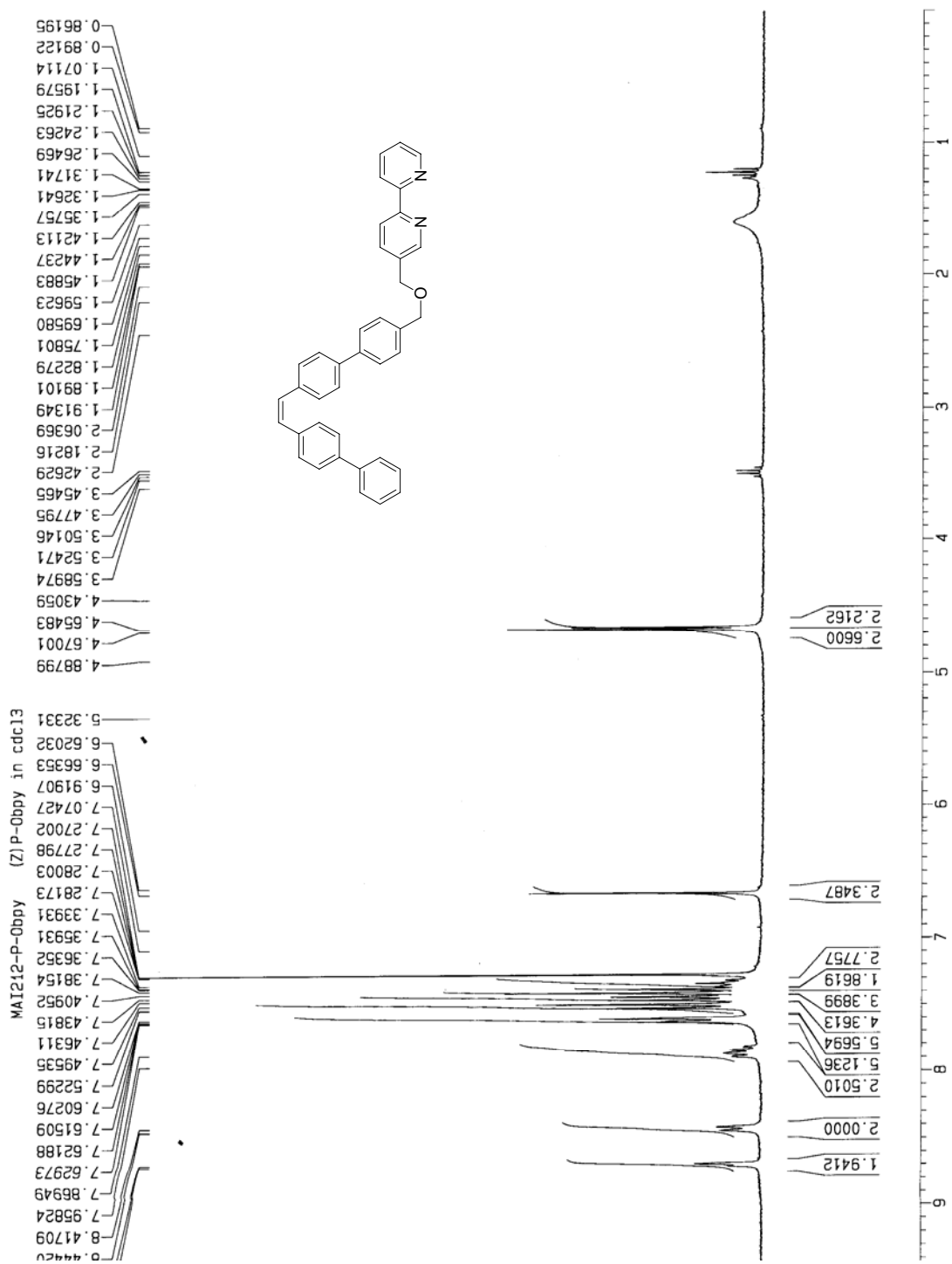


Figure 59.  $^1\text{H}$ - $^1\text{H}$  COSY of compound 18Z.

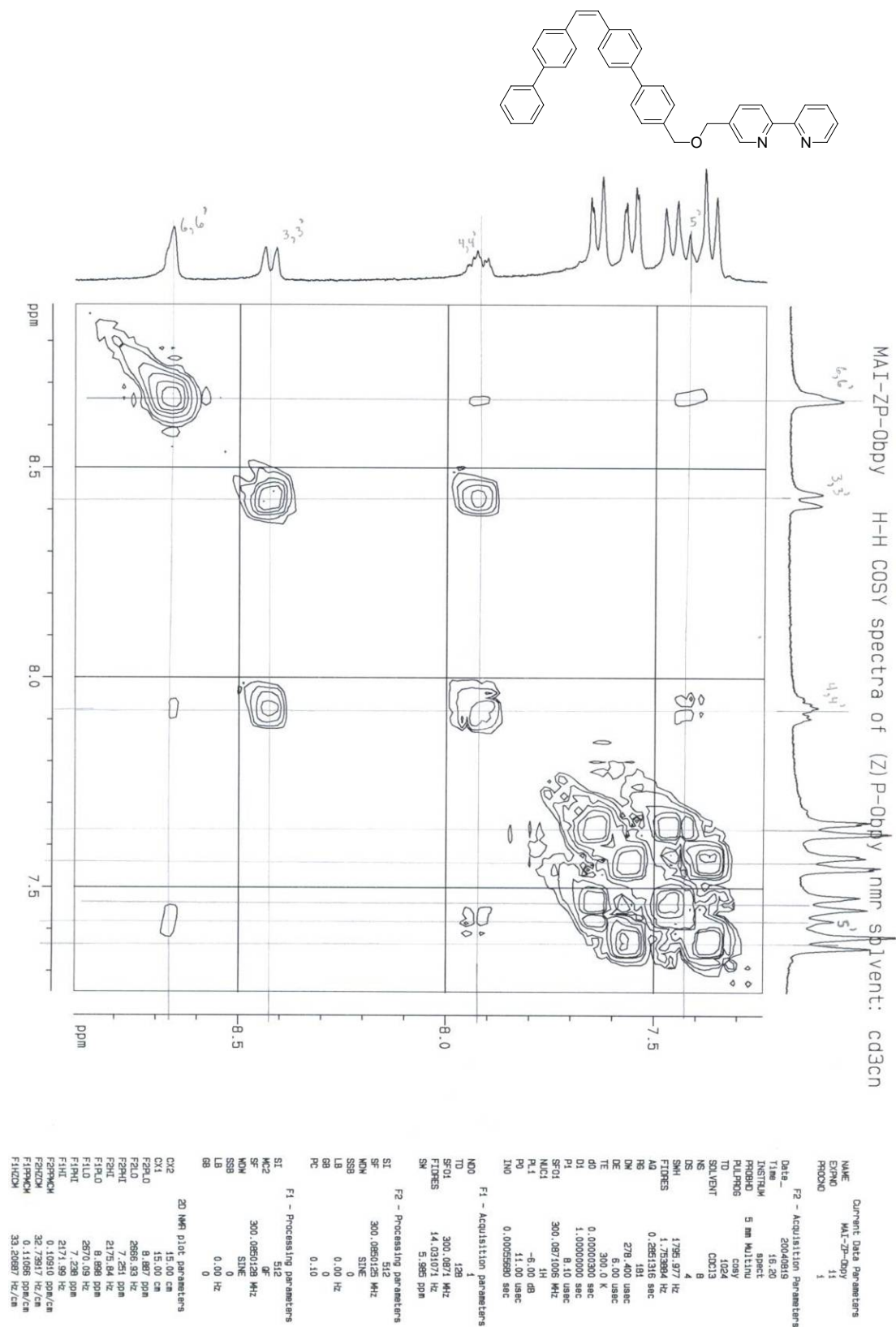


Figure 60.  $^{13}\text{C}$  NMR spectra of compound 18Z.

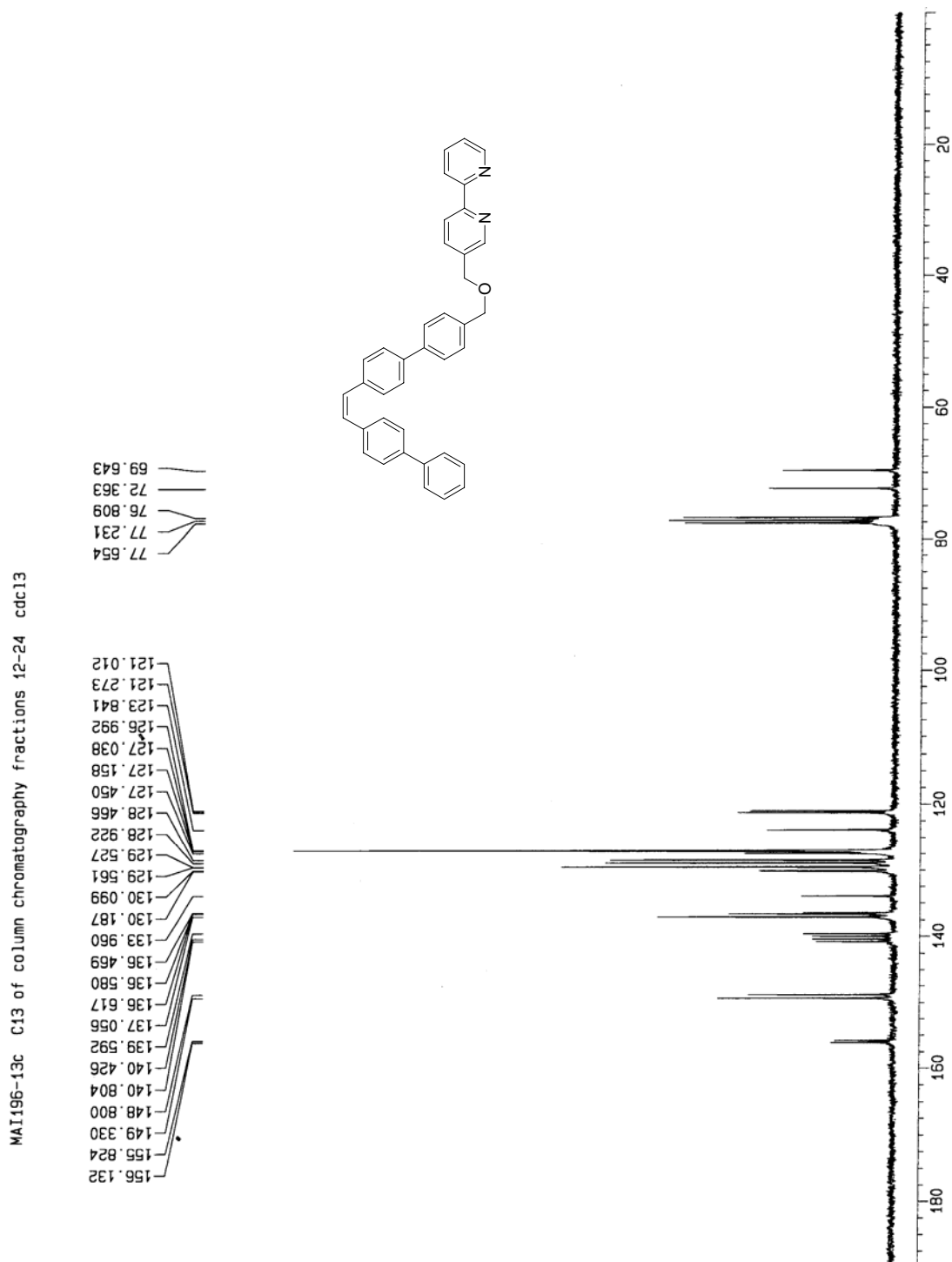


Figure 61.  $^1\text{H}$  NMR spectra of compound 18Z.

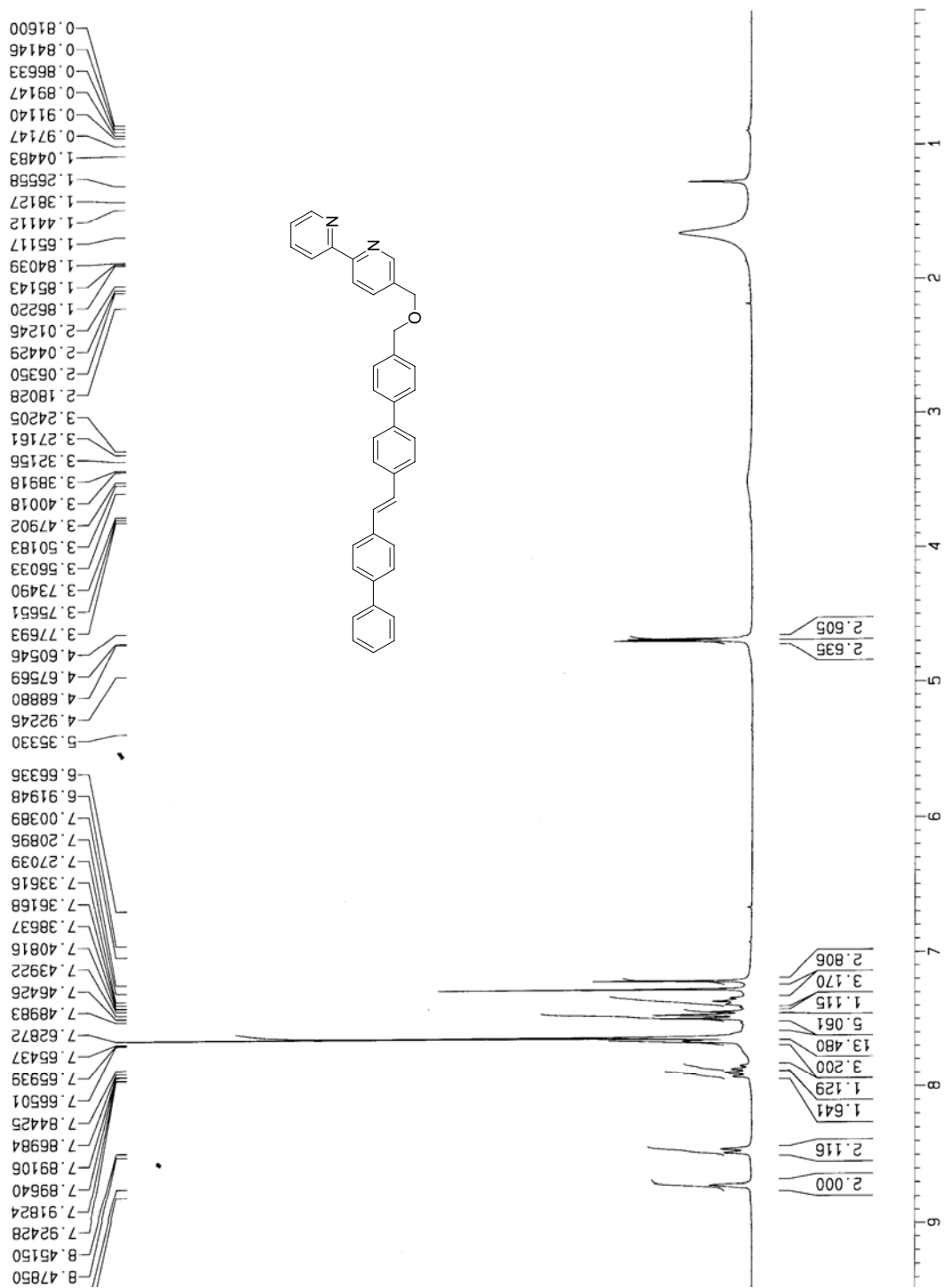
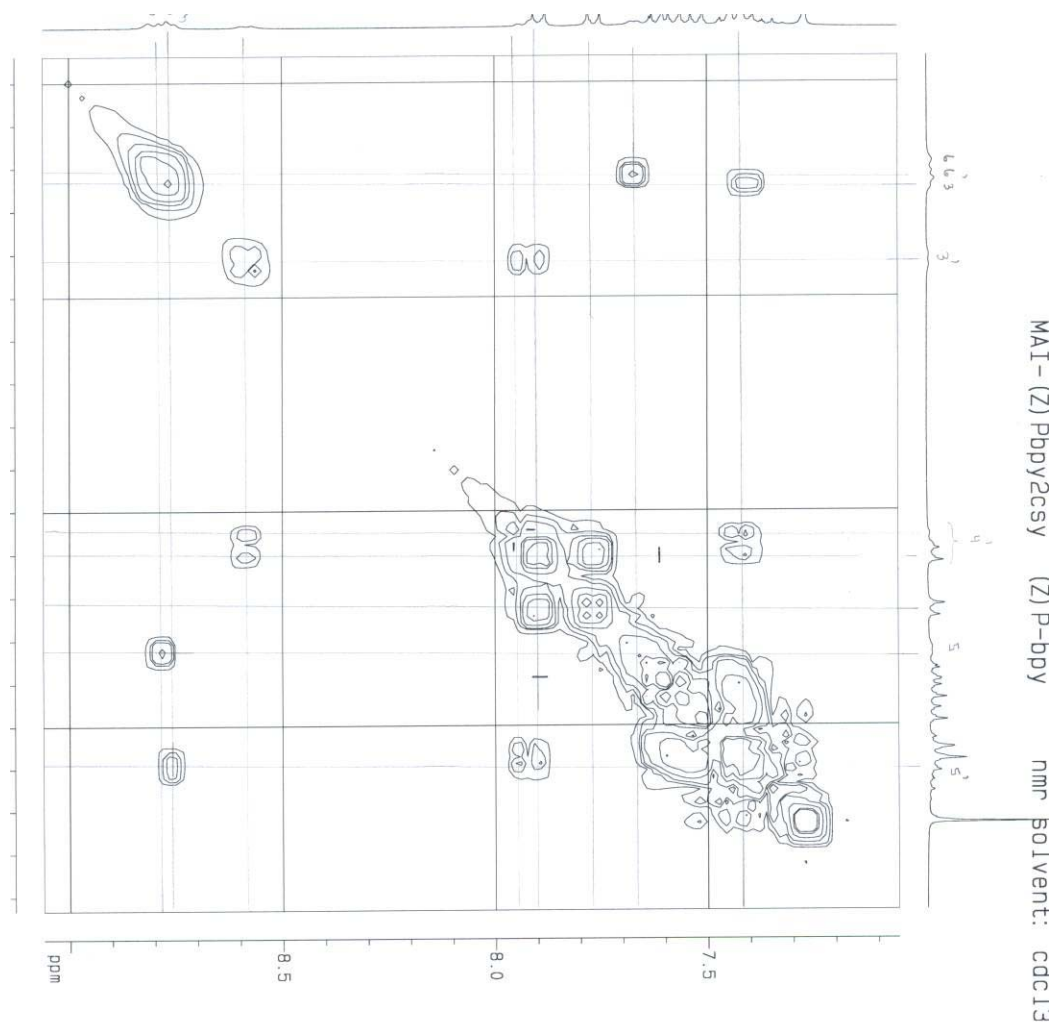
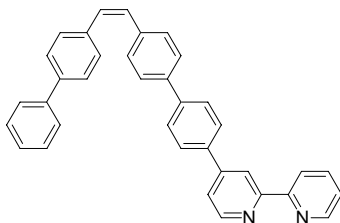


Figure 62.  $^1\text{H}$ - $^1\text{H}$  COSY of compound **20Z**.



Current Data Par  
 NAME MA1-(Z)Pbpy2csy  
 EXPNO 1  
 PROCNO 1

F2 - Acquisition F  
 Date\_ 20040825  
 Time 9:57  
 INSTRUM spect  
 PROBRW 5 mm BBO  
 PULPROG zgpg30  
 TD 1024  
 SOLVENT CDCl3  
 NS 12  
 DS 4  
 SMH 2394.636  
 FIDRES 2.338512  
 AQ 0.2138512  
 RG 574.7  
 DM 208.600  
 TE 300.0  
 DE 1.00000000  
 D0 0.00000000  
 D1 1.00000000  
 TMO 0.00041780

\*\*\*\*\* CHANNEL f  
 NUC1 1H  
 P0 5.10  
 P1 0.10  
 SFO1 300.132946

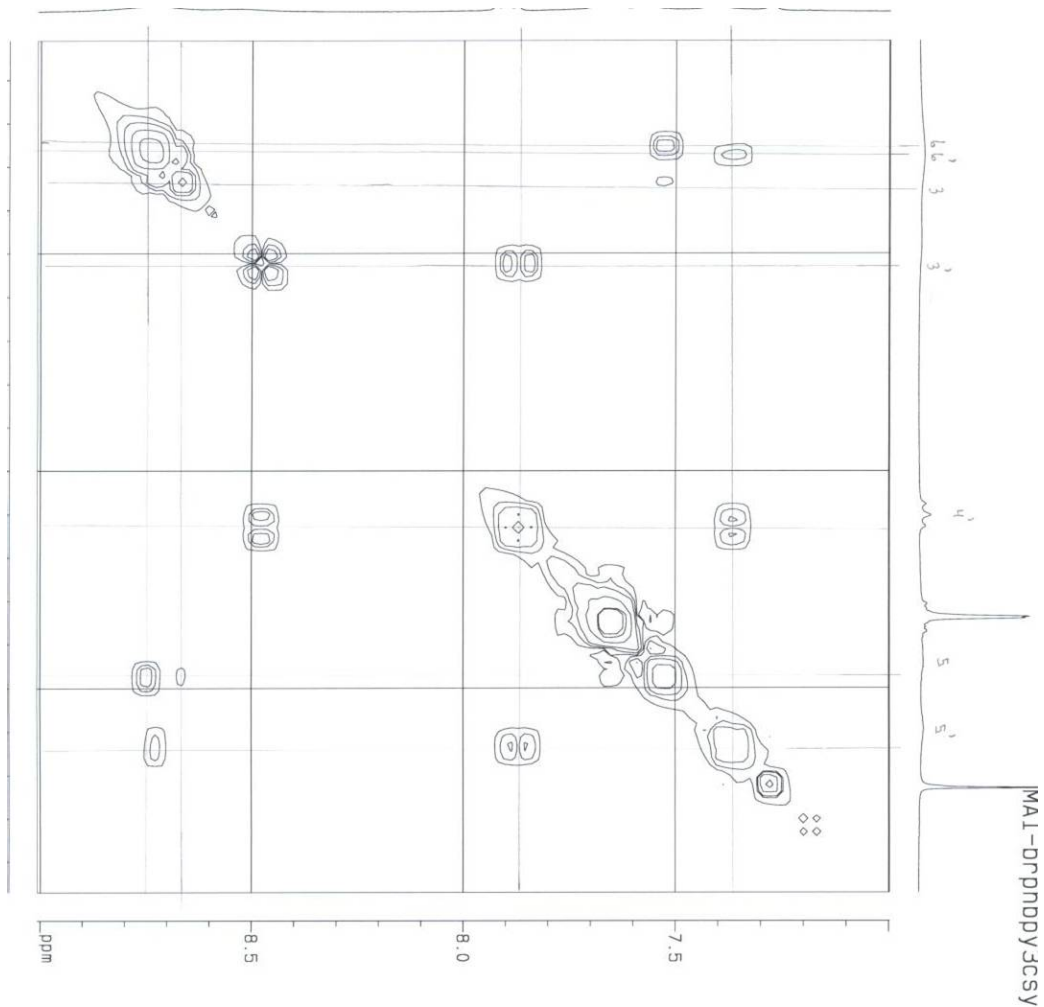
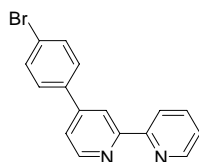
F1 - Acquisition f  
 NFO 1  
 TD 122  
 SFO1 300.1324  
 FIDRES 19.469596  
 SM 7.975

F2 - Processing f  
 SI 512  
 SF 300.130017  
 KW SINE  
 SSB C  
 LB 0.00  
 GB C  
 PC 1.00

F1 - Processing f  
 SI 512  
 SF 300.130017  
 KW SINE  
 SSB C  
 LB 0.00  
 GB C

2D NMR plot par  
 CX2 15.00  
 CX1 15.00  
 F2D0 0.00  
 F2D1 2270.00  
 F2S0 7.00  
 F2S1 2121.00  
 F1P0 9.00  
 F1L0 2719.70  
 F1PH 7.00  
 F1HT 2116.40  
 F2PR0 0.1328

Figure 63.  $^1\text{H}$ - $^1\text{H}$  COSY of compound 22.



```

Current Data Parameters
NAME      MA1-07ppbpy3csy
EXPNO    1
PROCNO   1

F2 - Acquisition Parameters
Date_    20040826
Time     8.33
INSTRUM spect
PROBHD   5 mm Dual 13C/
PULPROG zgpg30
TD       1024
SOLVENT  CDCl3
NS       16
DS       4
SWH      3264.858 Hz
AQ       2.338612 s
RG       0.2138642 s/s
AQ       574.7
DM       208.800 us
DE       6.00 us
TE       300.0 K
D0       0.00000300 s/c
DO       1.00000000 s/c
SFO1     0.00041760 s/c
SFO2
SFO3

***** CHANNEL f1 *****
NUC1     13C
PQ1      5.10 us
PL1      5.10 us
PL2      0.00 dB
SFO1     300.1323946 MHz

MNO
MNO1     13C
MNO2     13C
SFO1     300.1323946 MHz
F1F0ES   18.708094 Hz
SM       7.3799 DC

F2 - Processing parameters
SI       512
SF       300.1300094 MHz
WDW      SINE
SSB      0
LB       0.00 Hz
GB       0
PC       1.00

F1 - Processing parameters
SI       512
SF       300.1300092 MHz
WDW      SINE
SSB      0
LB       0.00 Hz
GB       0
PC       1.00

2D NMR 1D 1D 1D Parameters
CX2      15.00 cm
CX1      15.00 cm
F2PULP0  8.392 DC
F2AL0    2698.62 Hz
F2PHI0   7.028 DC
F2M1     2108.31 Hz
F2PULP1  9.108 DC
F2AL1    2703.892 Hz
F2PHI1   2100.10 Hz
F2P0     0.13090 DC
  
```

Figure 64.  $^1\text{H}$  NMR spectra of compound 24.

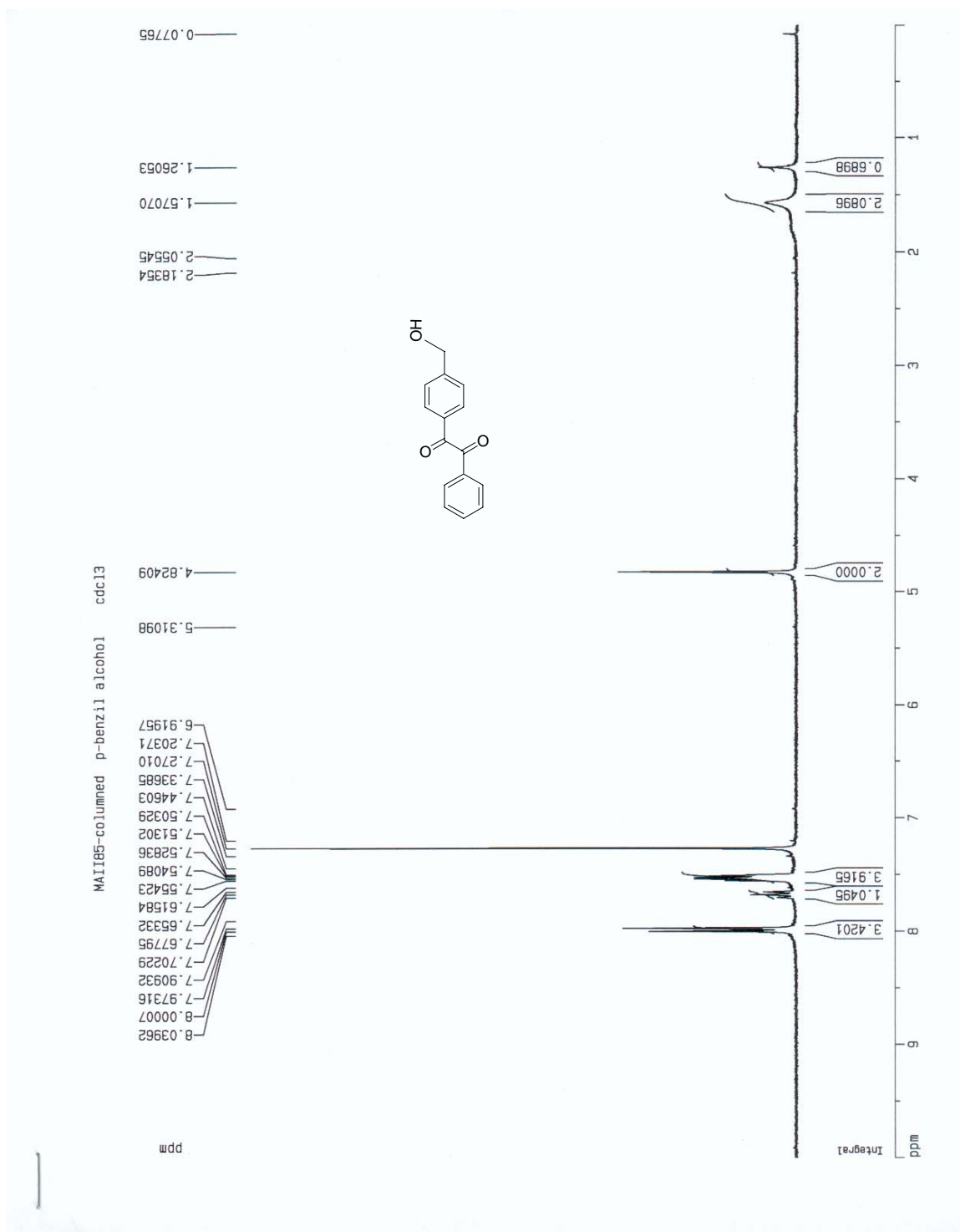


Figure 65.  $^{13}\text{C}$  NMR spectra of compound 24.

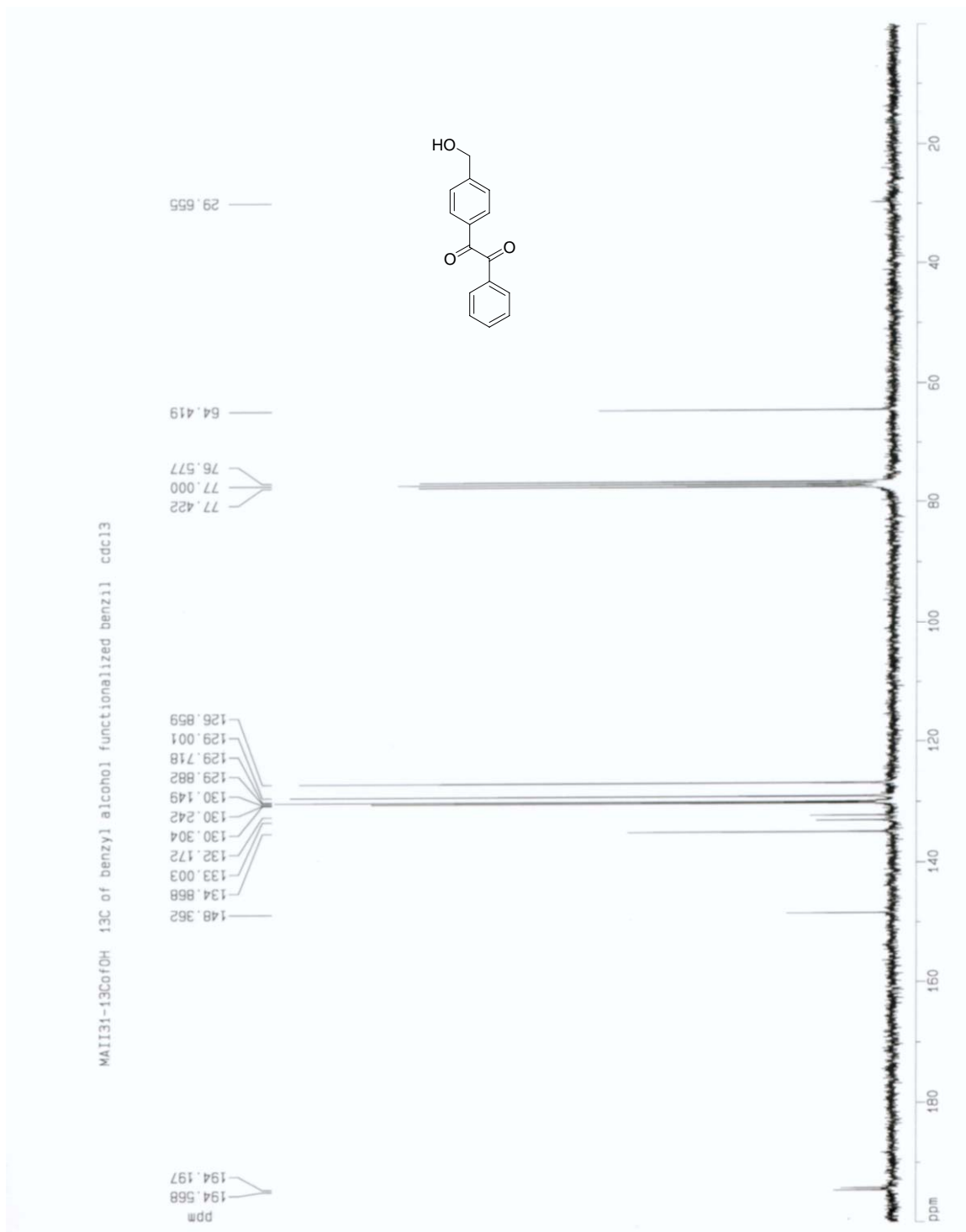




Figure 67.  $^{13}\text{C}$  NMR spectra of compound 25.

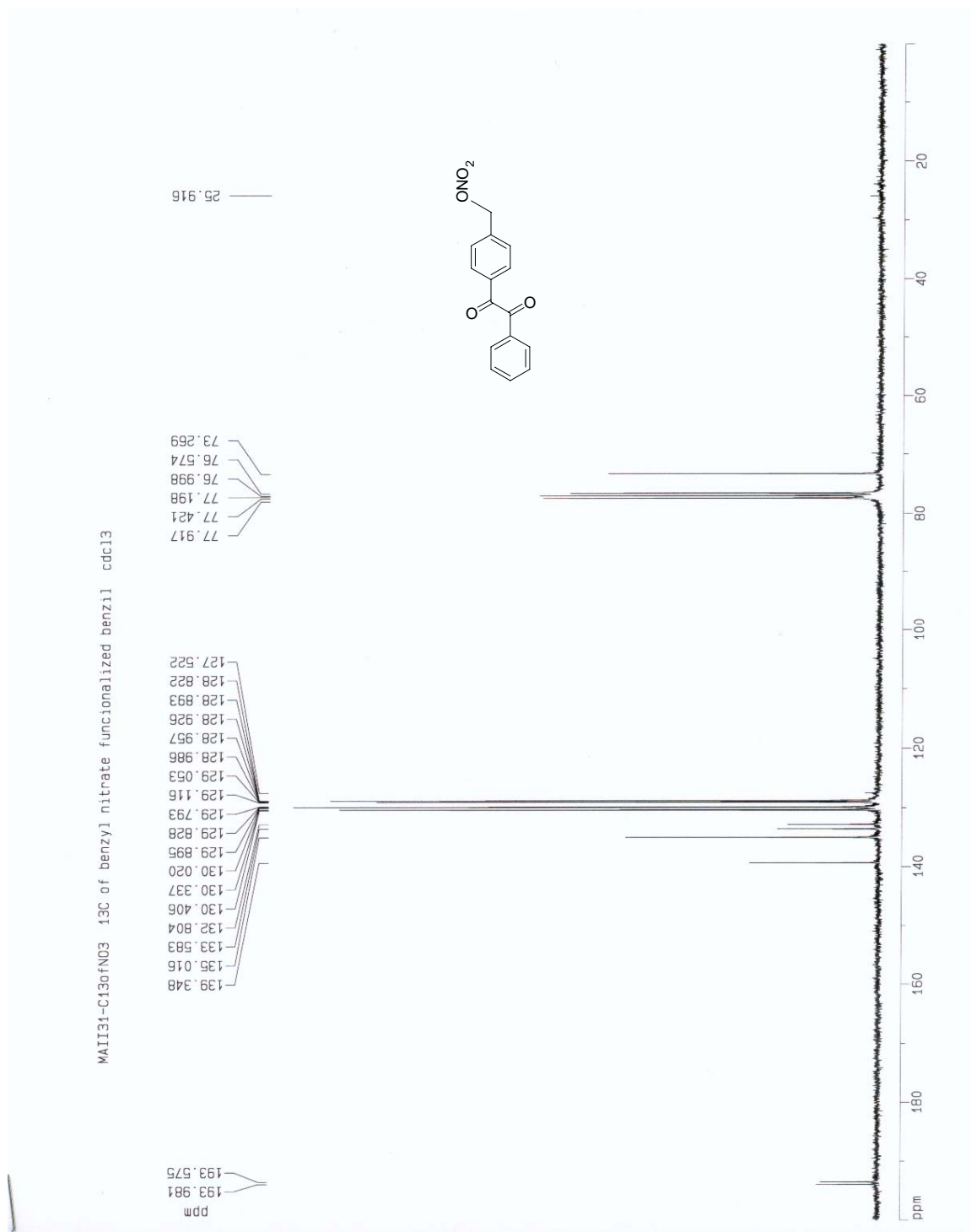


Figure 68.  $^1\text{H}$  NMR spectra of compound 31.

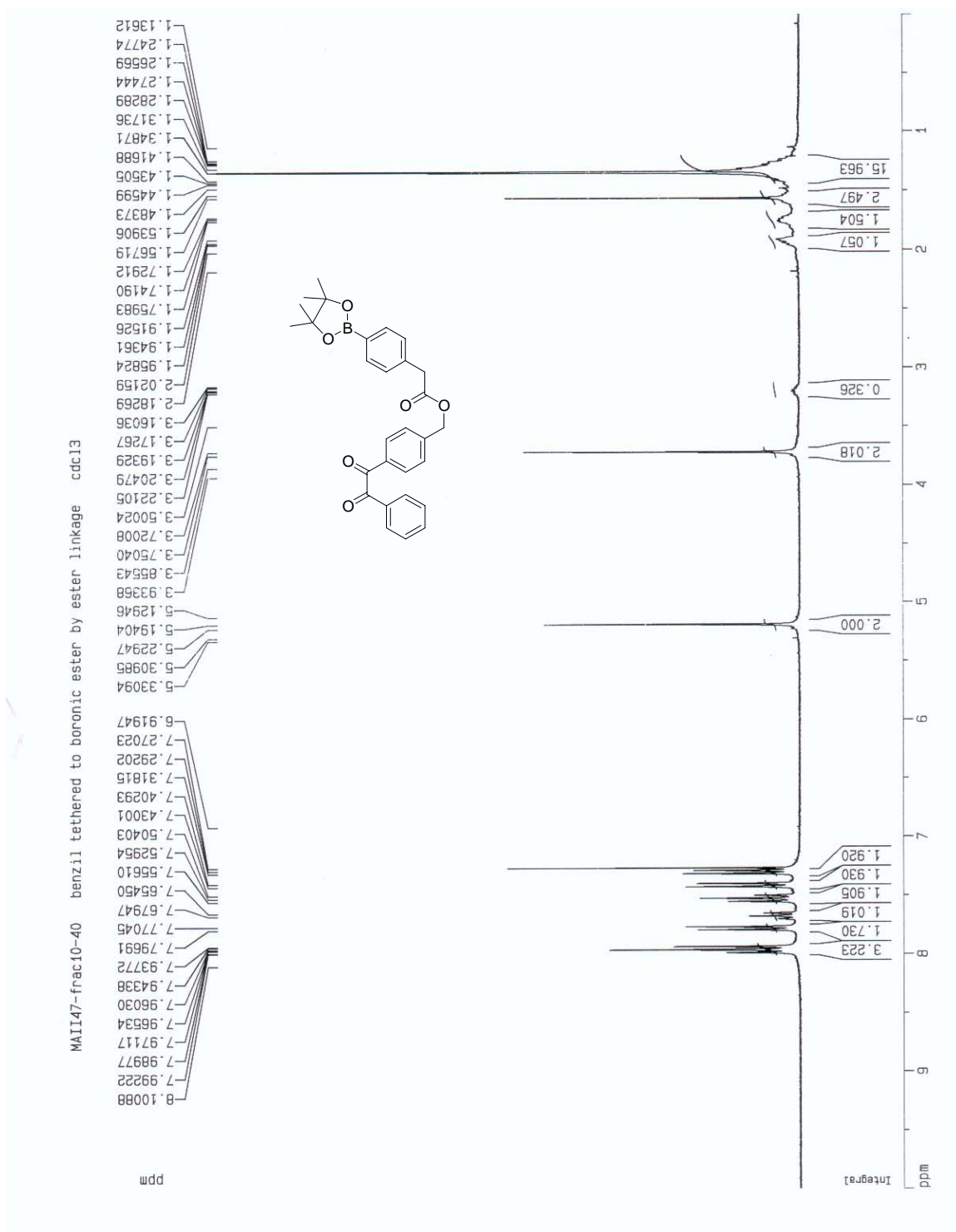




Figure 70.  $^1\text{H}$  NMR spectra of compound 34.

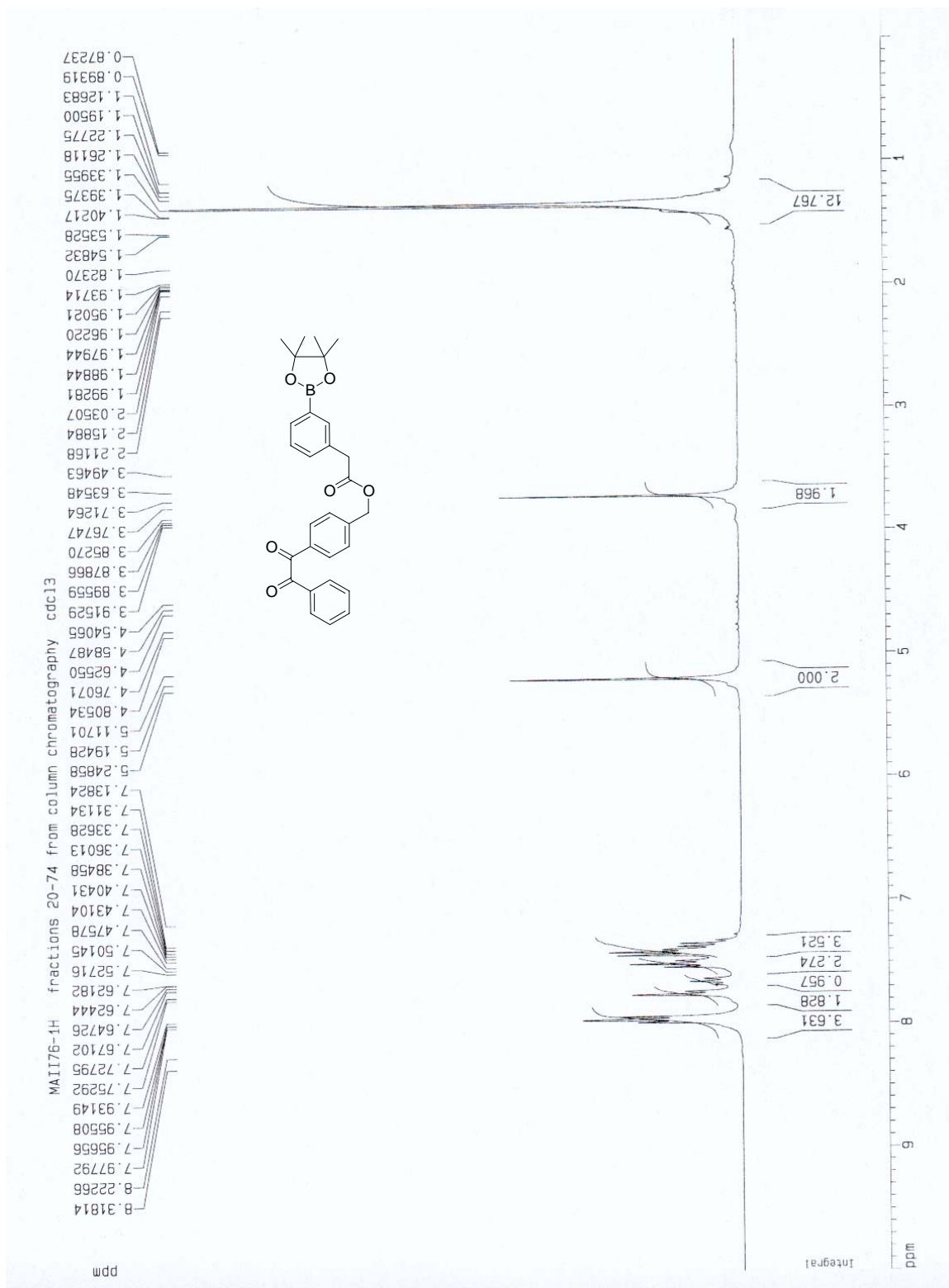


Figure 71.  $^{13}\text{C}$  NMR spectra of compound 34.

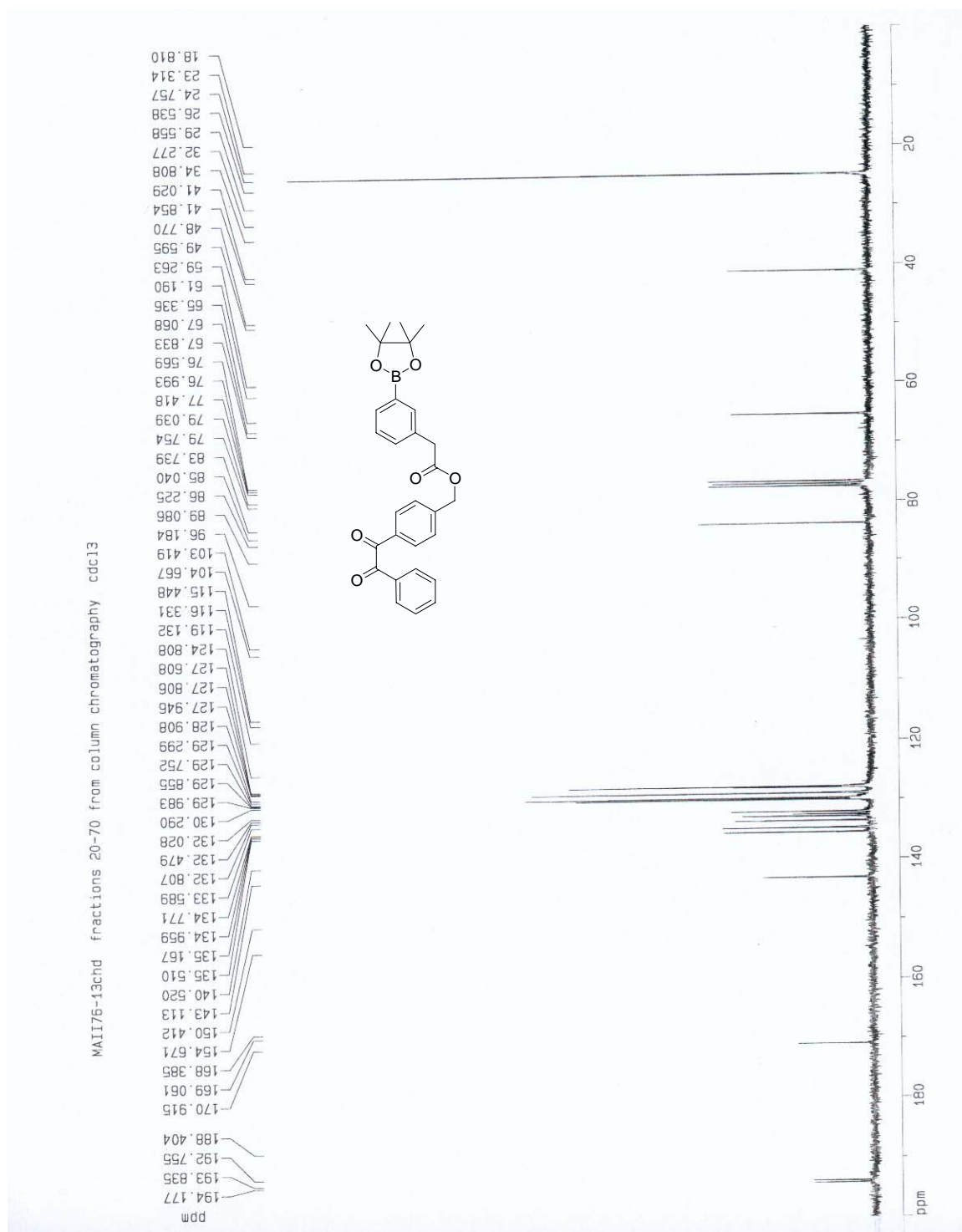


Figure 72.  $^1\text{H}$  NMR spectra of compound 28Z.

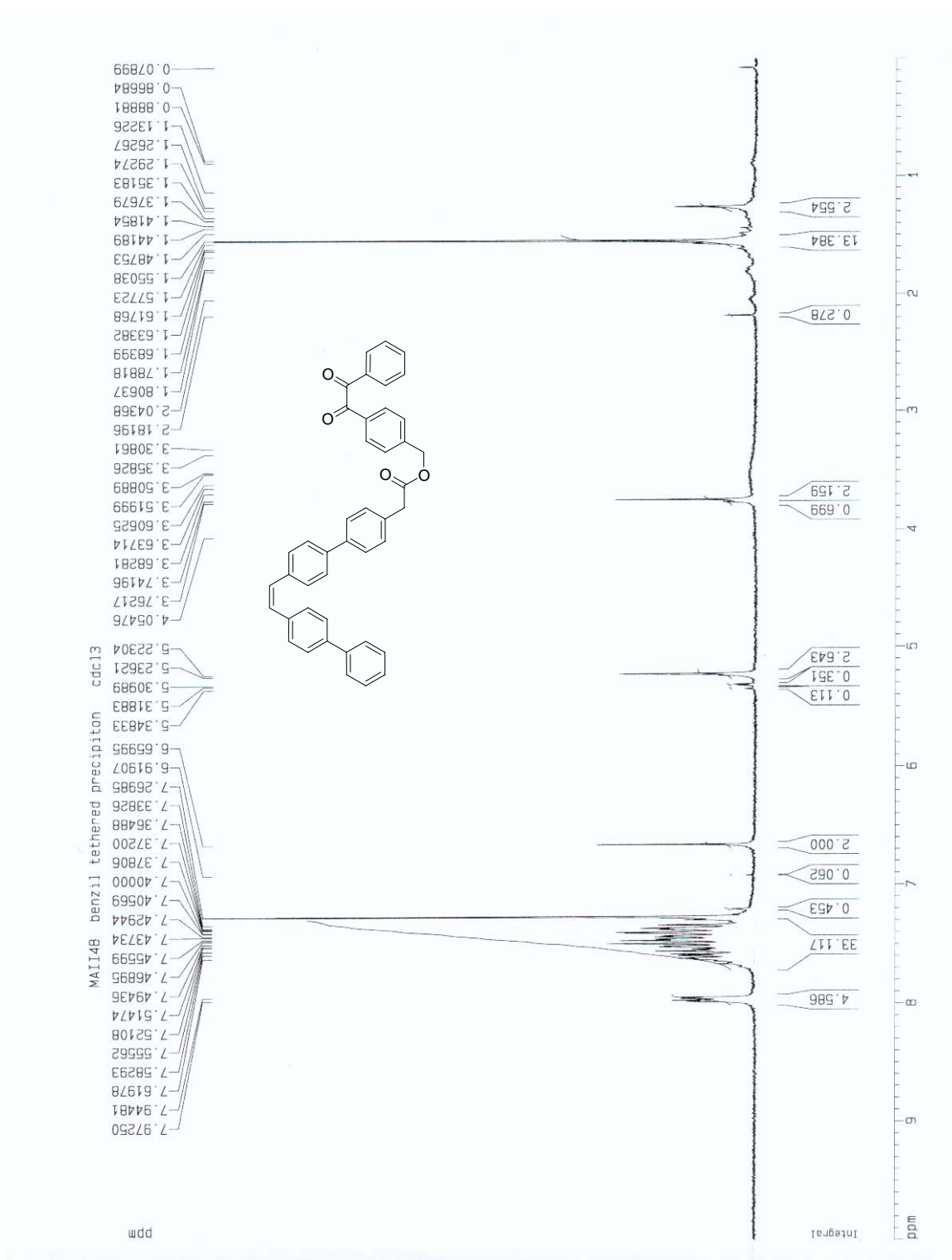


Figure 73.  $^{13}\text{C}$  NMR spectra of compound **28Z**.

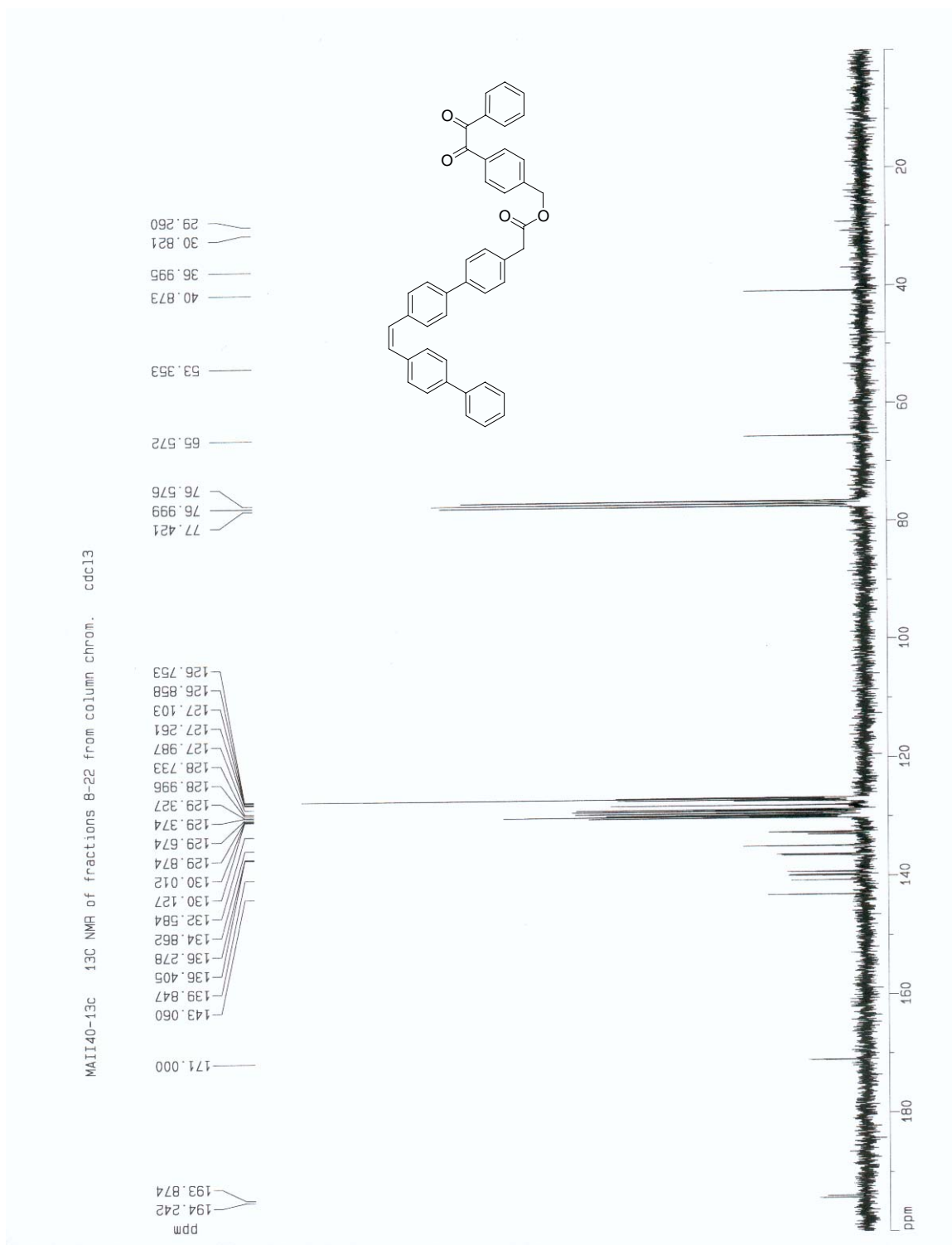


Figure 74.  $^1\text{H}$  NMR spectra of compound **28E**.

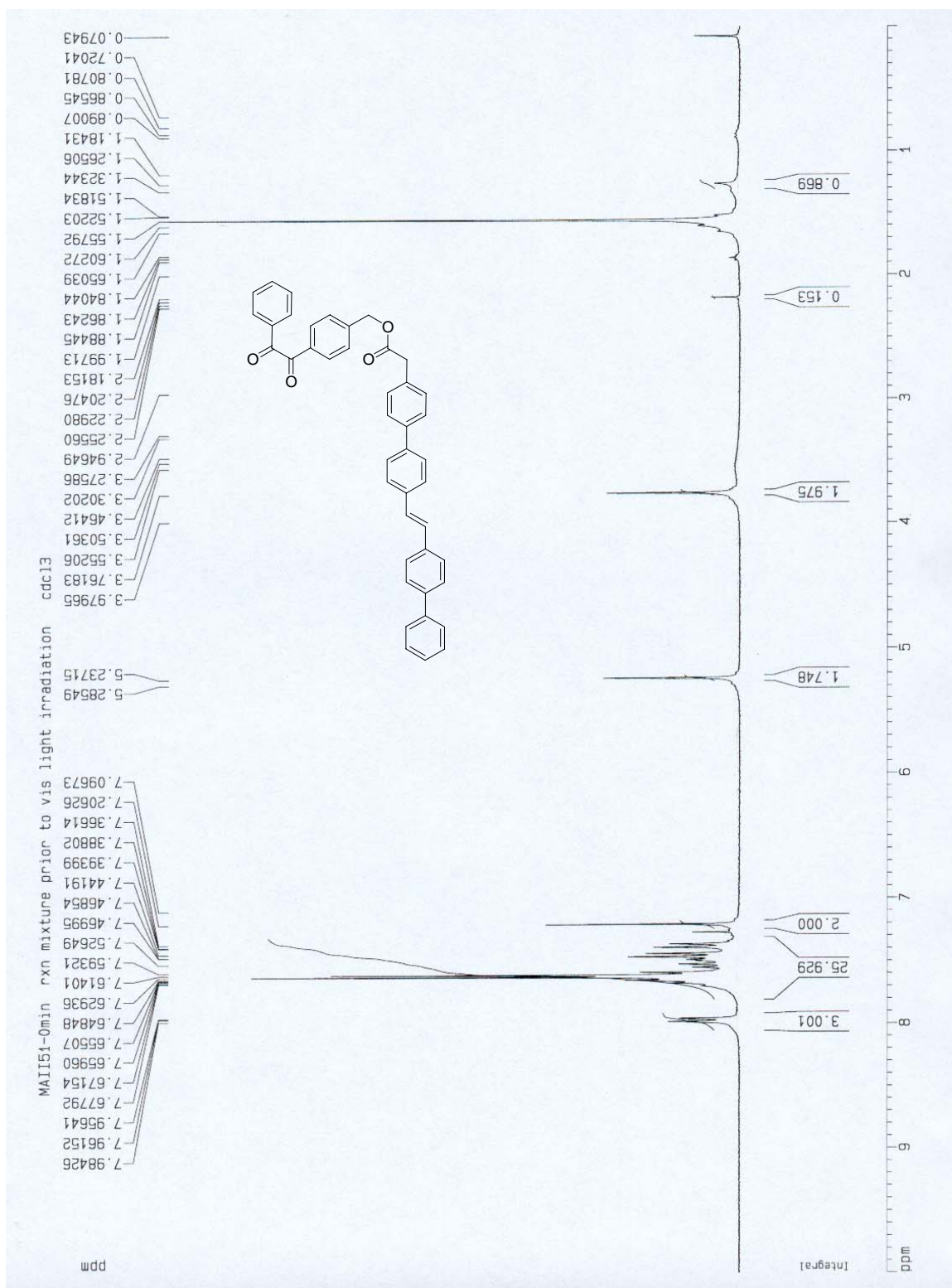


Figure 75.  $^1\text{H}$  NMR spectra of compound **29E**.

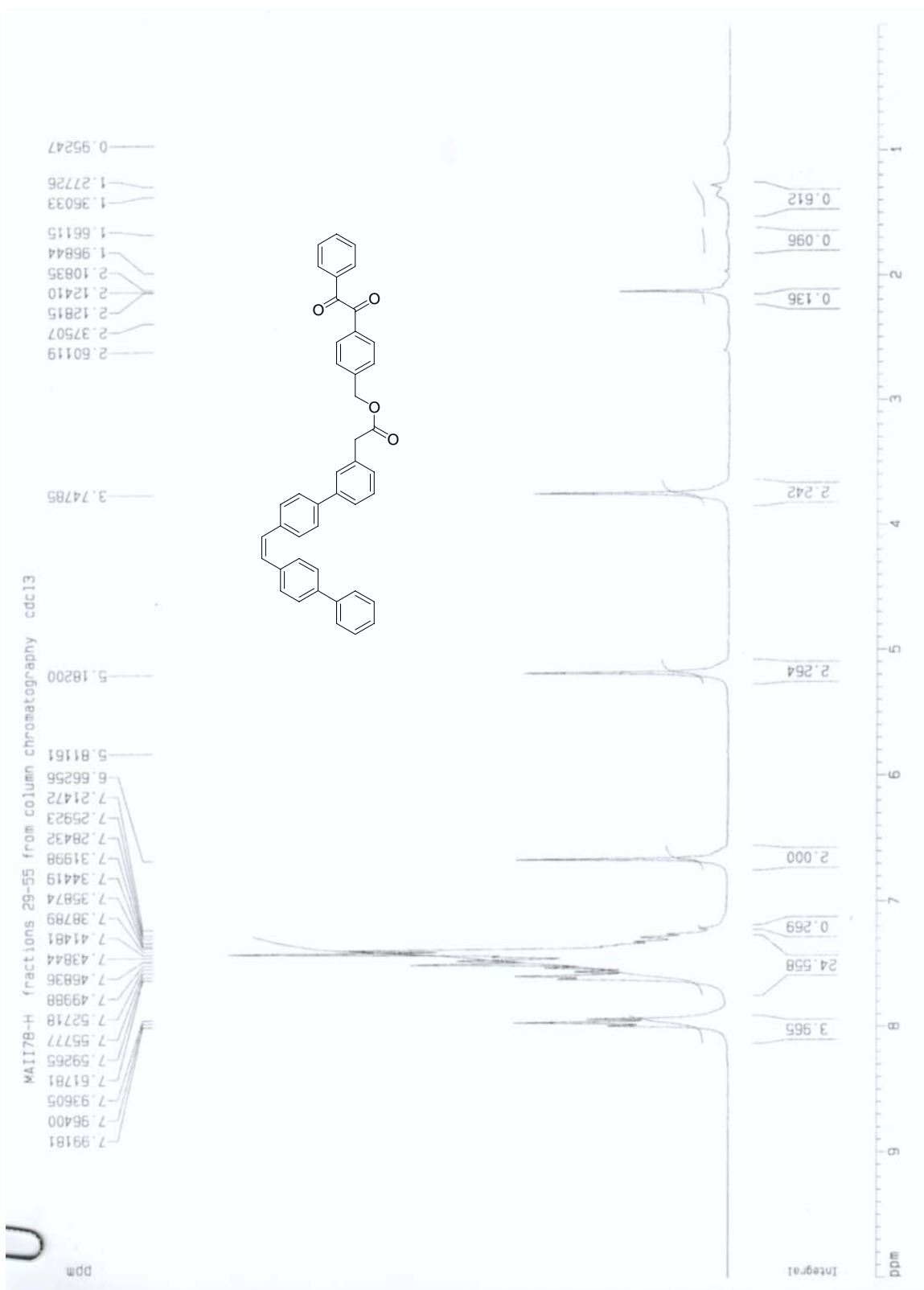
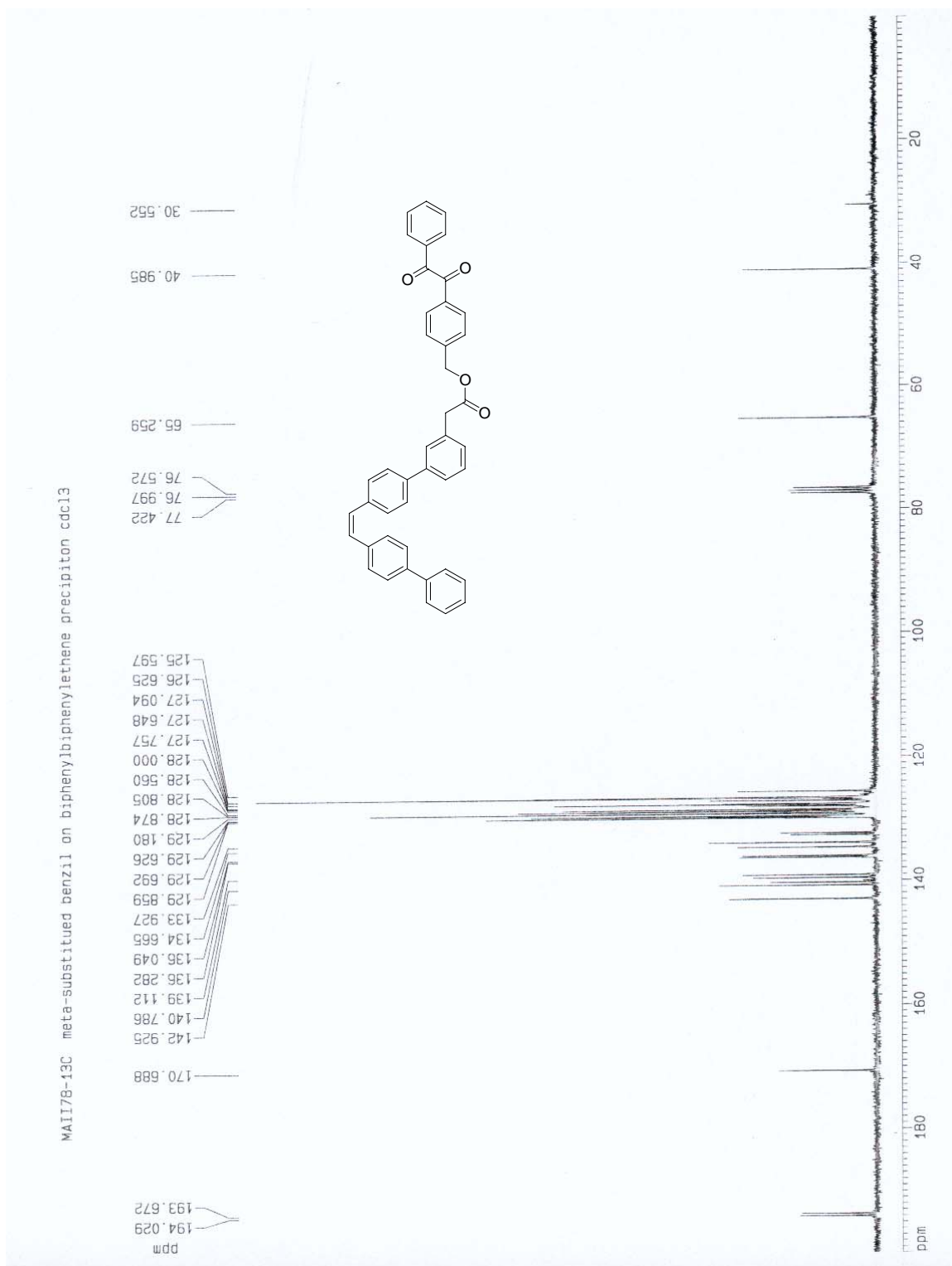


Figure 76.  $^{13}\text{C}$  NMR spectra of compound **29E**.





## 6.2.3 Photoisomerization Experiments

### 6.2.3.1 <sup>1</sup>H NMR Monitored Isomerizations

All isomerizations were performed in air-equilibrated solvent that was used as received, unless otherwise specified as degassed. In a typical <sup>1</sup>H NMR-monitored isomerization experiment, the chosen amounts of precipiton, triplet sensitizer, and isomenthol standard was dissolved in deuterated solvent and transferred by syringe into an NMR tube. The tube was capped and a <sup>1</sup>H NMR spectrum was recorded. If the reaction mixture was to be irradiated at  $\lambda_{\text{exc}} \geq 400$  nm, the tube was then placed within a pyrex water-cooling jacket to stabilize the reaction temperature at  $\sim 23$  °C. A 300 W incandescent lamp (allowed to warm up for 30 min), positioned 5 cm from the sample, irradiated the reaction mixture. Light above 400 nm was selected by wrapping the jacket with a 400 nm cutoff filter. The reaction mixtures were irradiated for specific time intervals, removed from the light source and their spectra recorded by <sup>1</sup>H NMR. If “disturbed” conditions were employed (Method A), the reaction mixture was irradiated again and the corresponding spectra recorded until the isomerization was complete. If “undisturbed” conditions were applied (Method B), the reaction mixture would not be irradiated further (see Section 3.1). If the reaction mixture was to be irradiated at  $\lambda_{\text{exc}} = 350$  nm, the tube was placed in a Rayonet photoreactor. The internal temperature of the photoreactor was 40 °C.

### 6.2.3.2 UV-Vis Monitored Isomerizations of 17Z/E

All of the measurements were performed at room temperature in degassed CH<sub>3</sub>CN or THF/CH<sub>3</sub>CN (70:30) solutions. UV-Vis absorption spectra were recorded with an Agilent 8453

spectrophotometer. Photoisomerization experiments were monitored by recording the UV-Vis absorption of **17Z/E** and **16Z/E** at 341 nm (exclusively) with a PerkinElmer Lambda 9 UV-Vis spectrometer. All experiments were performed in the dark or under red light due to the high sensitivity of the compounds to normal ambient lighting. Uncorrected luminescence spectra were recorded with a Cary Eclipse fluorescence spectrometer equipped with Varian software. The excitation light used for all photoisomerization experiments was produced by a 25 W Bausch & Lomb microscope lamp positioned 5 cm from the sample. The light emitted was filtered by using a cutoff filter ( $\lambda \leq 400$  nm).

### **6.2.3.3 UV-Vis Monitored Isomerizations of **28Z/E** and **29Z/E****

All of the photochemical measurements were performed in degassed THF. UV-Vis absorption spectra were recorded with a PerkinElmer Lambda 9 UV-Vis spectrophotometer. Photoisomerization experiments were monitored by recording the UV-vis absorption of **16Z/E**, **28Z/E**, and **29Z/E** at 345 nm exclusively. All experiments were performed in the dark or under red light due to the high sensitivity of the compounds to normal ambient lighting. Emission spectra were recorded with a 1680/1681 Spex Fluorolog spectrometer. The excitation light used for all photoisomerization experiments was produced by a 25 W incandescent lamp positioned 5 cm from the degassed cuvette which contained the sample.

## REFERENCES

- 
- 1) Smith, M. B.; March, J. *March's Advanced Organic Chemistry*; John Wiley & Sons, Inc.: United States of America, **2001**.
  - 2) Bosanac, T. Ph. D. Dissertation, University of Pittsburgh, **2003**.
  - 3) Carroll, F. *Perspectives in Structure and Mechanism in Organic Chemistry*; Brooks/Cole Press: Pacific Grove, U.S., **1998**.
  - 4) (a) Rodier, J.; Myers, A. B. *J. Am. Chem. Soc.* **1993**, *115*, 10791-10795. (b) Vicinelli, V.; Ceroni, P.; Maestri, M.; Lazzari, M.; Balzani, V.; Lee, S.; Van Heyst, J.; Vögtle, F. *Org. Biomol. Chem.*, **2004**, *2*, 2207-2213.
  - 5) (a) Hammond, G. S.; Saltiel, J.; Lamola, A. A.; Turro, N. J.; Bradshaw, J. S.; Cowan, D. D.; Counsell, R. C.; Vogt, V.; Dalton, C. J. *J. Am. Chem. Soc.* **1964**, *86*, 3197. (b) Herkstroeter, W. G.; Hammond, G. S. *J. Am. Chem. Soc.* **1966**, *88*, 4769. (c) Hammond, G. S.; Saltiel, J. *J. Am. Chem. Soc.* **1963**, *85*, 2516. (d) Saltiel, J.; Charlton, J. L.; Mueller, W.B. *J. Am. Chem. Soc.* **1979**, *101*, 1347. (e) Saltiel, J.; Marchand, G. R.; Kirkor-Kaminska, E.; Smothers, W. K.; Mueller, W. B.; Charlton, J. L. *J. Am. Chem. Soc.* **1984**, *106*, 3144. (f) Saltiel, J. S.; Ganapathy, S.; Werking, C. *J. Phys. Chem.* **1987**, *91*, 2755. (g) Waldeck, P. H. *Chem. Rev.* **1991**, *91*, 415. (h) Saltiel, J.; Waller, A. S.; Sears, D. F. *J. Photochem. Photobiol. A: Chem.* **1992**, *65*, 29. (i) Saltiel, J.; Waller, A. S.; Sears, D. F. *J. Am. Chem. Soc.* **1993**, *115*, 2453.
  - 6) Coyle, J. D. *Introduction to Organic Photochemistry* 14, John Wiley & Sons, Inc.: United

- 
- States of America, 1986.
- 7) Caldwell, R. A.; Riley, S. J.; Gorman, A. A.; McNeeney, S.P.; Unett, D. J. *J. Am. Chem. Soc.* **1992**, 114, 4424-4426.
  - 8) Saltiel, J.; Marchand, G. R.; Kirkor-Kaminska, E.; Smothers, W. K.; Mueller, W. B.; Charlton, J. L. *J. Am. Chem. Soc.* **1984**, 106, 3144-3151.
  - 9) (a) Gorman, A. A.; Beddoes, R.; Hamblett, I.; McNeeney, S. P.; Prescott, A. .; Unett, D. J. *J. Chem. Soc., Chem. Commun.* **1991**, 963-964. (b) Caldwell, R. A.; Riley, S. J.; Gorman, A. A.; McNeeney, S. P.; Unett, D. J. *J. Am. Chem. Soc.* **1992**, 114, 4424-4426.
  - 10) (a) Gorman, A. A.; Hamblett, I.; Jensen, N. H. *Chem. Phys. Lett.* **1984**, 111, 293. (b) Gorman, A. A.; Hamblett, I.; Irvine, M.; Raby, P.; Standen, M. C.; Yeates, S. *J. Am. Chem. Soc.* **1985**, 107, 4404. (c) Gorman, A. A.; Hamblett, I.; Lambert, C.; Prescott, A. L. *Photochem. Photobiol.* **1990**, 51, 29.
  - 11) (a) Tour, J. M. *Acc. Chem. Res.* 2000, 33, 791-804. (b) Wagner, R. W.; Lindsey, J. S. *J. Am. Chem. Soc.* **1994**, 116, 9759.
  - 12) (a) Otsuki, J. ; Tsujino, M. ; Lizaki, T.; Araki, K.; Seno, M.; Takatera, K. ; Watanabe, T. *J. Am. Chem. Soc.* **1997**, 119, 7895. (b) Hush, N. S.; Wong, A. T.; Bacskay, G. B.; Reimers, J. R. *J. Am. Chem. Soc.* **1990**, 112, 4192. (c) Deans, R.; Niemz, A.; Breinlinger, E. C.; Rotello, V. M. *J. Am. Chem. Soc.* **1997**, 119, 10863.
  - 13) (a) Anelli, P. L. *J. Am. Chem. Soc.* **1991**, 113, 5131. (b) Ashotn, P. R.; Douglas, P.; Spencer, N.; Stoddart, J. F. *Chem. Commun.* **1992**, 1124.
  - 14) Ballardini, R.; Balzani, B.; Gandolfi, M. T.; Prodi, L.; Venturi, M.; Philp, D.; Ricketts, H. G.; Stoddart, J. F. *Angew. Chem. Int. Ed. Engl.* **1993**, 32, 1301.
  - 15) Katayama, H.; Ito, S.; Yamamoto, M. *J. Phys. Chem.* **1992**, 96, 10115-10119.

- 
- 16) Tan, Z.; Kote, R.; Samaniego, W. N.; Weininger, S. J.; McGimpsey, W. G. *J. Phys. Chem. A* **1999**, 103, 7612-7620.
- 17) Haggquist, G. W.; Katayama, H.; Tsuchida, A.; Ito, S.; Yamamoto, M. *J. Phys. Chem.* **1993**, 97, 9270-9273.
- 18) Morales, A. F., Accorsi, G.; Armaroli, N.; Barigelletti, F.; Pope, S. J. A.; Ward, M. D. *Inorg. Chem.* **2002**, 41, 6711-6719.
- 19) Lamola, A. A.; Leermakers, P. A.; Byers, G. W.; Hammond, G. S. *J. Am. Chem. Soc.* **1965**, 2322-2331.
- 20) Castellano, R. K.; Craig, S. L.; Nuckolls, C.; Rebek, J. *J. Am. Chem. Soc.* **2000**, 122, 7876-7882.
- 21) Benedikt, S.; Belser, P.; De Cola, L.; Sabbioni, E.; Balzani, V. *J. Am. Chem. Soc.* **1999**, 121, 4207-4214.
- 22) (a) Calcaterra, L. T.; Closs, G. L.; Miller, J. R. *J. Am. Chem. Soc.* **1983**, 105, 670. (b) Miller, J. R.; Calcaterra, L. T.; Closs, G. L. *J. Am. Chem. Soc.* **1984**, 106, 3047. (c) Closs, G. L.; Calcaterra, L. T.; Green, N. J.; Penfield, K. W.; Miller, J. R. *J. Phys. Chem.* **1986**, 90, 3673.
- 23) Zimmerman, H. E.; Goldman, T.D.; Hirzel, T. K.; Schmidt, S. P. *J. Org. Chem.* **1980**, 45, 3933-3951.
- 24) Kszynski, P.; Friedl, A. C.; Michl, J. *J. Am. Chem. Soc.* **1992**, 114, 601-620. (b) Paddon-Row, M. N.; Jordan, K. D. *J. Am. Chem. Soc.* **1993**, 115, 2952-2960.
- 25) Stein, C. A.; Lewis, N. A.; Seitz, G. *J. Am. Chem. Soc.* **1982**, 104, 2596.
- 26) (a) Kroon, J.; Oliver, A. M.; Paddon-Row, M. N.; Verhoeven, J. W. *J. Am. Chem. Soc.* **1990**, 112, 4868-4873. (b) Paddon-Row, M. N. *Acc. Chem. Res.* **1994**, 27, 18-25. (c) Shephard, M. J.; Paddon-Row, M. N.; Jordan, K. D. *J. Am. Chem. Soc.* **1994**, 116, 5328-5333. (d) Ren, Y.;

- 
- Wang, Z.; Zhu, H.; Weininger, S. J.; McGimpsey, W. G. *J. Am. Chem. Soc.* **1995**, 117, 4367-4373.
- 27) Sun, S.; Lees, A. J. *Organometallics* **2002**, 21, 39.
- 28) Sun, S.; Robson, E.; Dunwoody, N.; Silva, A.; Brinn, I.; Lees, A. J. *Chem. Commun.* **2000**, 201.
- 29) Zarnegar, P.; Bock, C. R.; Whitten, D. G. *J. Amer. Chem. Soc.* **1973**, 95, 4367.
- 30) Agyin, J. K.; Morrison, H.; Siemiarczuk, A. *J. Am. Chem. Soc.* **1995**, 117, 3875-3876. (b) Agyin, J. K.; Timberlake, L. D.; Morrison, H. *J. Am. Chem. Soc.* **1997**, 119, 7945-7953.
- 31) (a) Kim, S.; Kim, K.; Stuben, D. J. *Environ. Eng.* **2002**, 128, 705-715. (b) Agrawal, A.; Sahu, K. K.; Pandey, B. D. *Colloids Surf., A* **2004**, 237, 133-140. (c) Wingenfelder, U.; Hansen, C.; Furrer, G.; Schulin, R. *Environ. Sci. Technol.* **2005**, 39, 4606-4613. (d) Rahman, M. A.; Ahsan, S.; Kaneco, S.; Katsumata, H.; Suzuki, T.; Ohta, K. *J. Environ. Manage.* **2005**, 107-110.
- 32) (a) Rosso, V. W.; Lust, D. A.; Bernot, P. J.; Grosso, J. A.; Modi, S. P.; Rusowicz, A.; Sedergran, T. C.; Simpson, J. H.; Srivastava, S.K.; Humora, M. J.; Anderson, N. G. *Org. Process Res. & Dev.* **1997**, 1, 311-314. (b) Manley, P.; Acemoglu M.; Marterer, W.; Pachinger, W. *Org. Process Res. Dev.* **2003**, 7, 436-445. (c) Urawa, Y.; Miyazawa, M.; Ozeki, N.; Ogura, K. *Org. Process Res. Dev.* **2003**, 7, 191-195.
- 33) Manley, P.; Acemoglu M.; Marterer, W.; Pachinger, W. *Org. Process Res. Dev.* **2003**, 7, 436.
- 34) (a) Brown, J.; Mercier, L.; Pinnavaia, T. J. *Chem. Commun.* **1999**, 69-70. (b) Liu, A. M.; Hidajat, K.; Kawi, S.; Zhao, D.Y. *Chem. Commun.* **2000**, 1145-1146. (c) Nooney, R. I.; Kalyanaraman, M.; Kennedy, G.; Maginn, E. J. *Langmuir* **2001**, 17, 528-533. (d) Vieira, E. F. S.; Simoni, J. de A.; Airoidi, C.; *J. Mater. Chem.* **1997**, 7, 2249-2252.

- 
- 35) This requires the right relationship between rates of exchange and precipitation.
- 36) (a) Wrighton, M.; Giordano, P. *J. Am. Chem. Soc.* **1979**, *101*, 2888-2897. (b) Sakaki, S.; Okitaka, I.; Ohkubo, K. *Inorg. Chem.* **1984**, *23*, 198-203. (c) Balzani, V.; Juris, A.; Venturi, M. *Chem. Rev.* **1996**, *96*, 759-833. (d) Yam, V.; Chor-Yue, V.; Wu, L. *J. Chem. Soc., Dalton Trans.* **1998**, 1461-1468. (e) Schanze, K. S.; Lucia, L. A.; Cooper, M.; Walters, K. A., Ji, H.; Sabina, O. *J. Phys. Chem. A* **1998**, *102*, 5577-5584. (f) Vlcek, A. *Coord. Chem. Rev.* **2000**, *200-202*, 933-977. (g) Sun, S.; Robson, E.; Dunwoody, N.; Silva, A.; Brinn, I.; Lees, A. J. *Chem. Commun.* **2000**, 201-202. (h) Yam, V. W.; Yang, Y.; Zhang, J.; Chu, W.; Zhu, N. *Organometallics* **2001**, *20*, 4911-4918. (i) Sun, S.; Lees, A. J. *Organometallics* **2002**, *21*, 39-49.
- 37) Wrighton, M.; Markham, J. *J. Phys. Chem.* **1973**, *77*, 3042.
- 38) Sakaki, S.; Okitaka, I.; Ohkubo, K. *Inorg. Chem.* **1984**, *23*, 198.
- 39) (a) Zarnegar, P.; Bock, C. R.; Whitten, D. G. *J. Amer. Chem. Soc.* **1973**, *95*, 4367-4372. (b) Shaw, J. R.; Webb, R. T.; Schmehl, R. H. *J. Am. Chem. Soc.* **1990**, *112*, 1117-1123.
- 40) (a) Morales, A.; Accorsi, G.; Armaroli, N.; Barigelletti, F.; Pope, S.; Ward, M. D. *Inorg. Chem.* **2002**, *41*, 6711-6719. (b) Wilson, G. J.; Launikonis, A.; Sasse, W. H. F.; Mau, A. W. H. *J. Phys. Chem. A* **1997**, *101*, 4860-4866. (c) Juris, A.; Prodi, L. *New J. Chem.* **2001**, *25*, 1132-1135. (d) Wilson, G. J., Sasse, W. H. F., Mau, A. W. H. *Chem. Phys. Lett.* **1996**, *250*, 583-588. (e) Tyson, D.; Bignozzi, C.; Castellano, F. *J. Am. Chem. Soc.* **2002**, *124*, 4562-4563. (f) Tyson, D. S.; Castellano, F. N. *J. Phys. Chem. A* **1999**, *103*, 10955-10960. (g) Wilson, G. J.; Launikonis, A.; Sasse, W. H. F.; Mau, A. W. H. *J. Phys. Chem. A* **1998**, *102*, 5150-5156. (h) Tyson, D. S.; Henbest, K. B.; Bialecki, J.; Castellano, F. N. *J. Phys. Chem. A* **2001**, *105*, 8154-

- 
8161. (i) Harriman, A.; Hissler, M.; Khatyr, A.; Ziessel, R. *Chem. Commun.* **1999**, 735-736.
- 41) Morales, A.; Accorsi, G.; Armaroli, N.; Barigelletti, F.; Pope, S.; Ward, M. D. *Inorg. Chem.* **2002**, *41*, 6711.
- 42) (a) Bosanac, T.; Yang, J.; Wilcox, C. S. *Angew. Chem. Int. Ed.* **2001**, *40*, 1875-1879. (b) Bosanac, T.; Wilcox, C. S. *Chem. Commun.* **2001**, 1618-1619. (c) Bosanac, T.; Wilcox, C. S. *Tetrahedron Lett.* **2001**, *42*, 4309-4212. (d) Bosanac, T.; Wilcox, C. S. *J. Am. Chem. Soc.* **2002**, *124*, 4194. (e) Honigfort, M.; Brittain, W. J.; Bosanac, T.; Wilcox, C. S. *Macromolecules* **2002**, *35*, 4849-4851. (f) Honigfort, M.; Shingtza, L.; Rademacher, J.; Malaba, D.; Bosanac, T.; Wilcox, C. S.; Brittain, W. J. *ACS Symposium Series* **2003**, *854*, 250. (g) Bosanac, T.; Wilcox, C. S. *Org. Lett.* **2004**, *6*, 2321-2324.
- 43) 5-Bromomethyl-2,2'-bipyridine was synthesized according to the following reference:  
Ballardini, R.; Balzani, V.; Clemente-Leon, M.; Credi, A.; Gandolfi, M.; Ishow, E.; Perkins, J.; Stoddart, F.; Tseng, H.; Wenger, S. *J. Am. Chem. Soc.* **2002**, *124*, 12786-12796.
- 44) Saltiel, J.; Marchland, G.; Kaminska, E.; Smothers, W.; Meuller, W.; Charlton, J. *J. Am. Chem. Soc.* **1984**, *106*, 3144.
- 45) Schlicke, B.; Belser, P.; De Cola, L.; Sabbioni, E.; Balzani, V. *J. Am. Chem. Soc.* **1999**, *121*, 4207.
- 46) The irradiation light, however was reduced 51% using a neutral density filter.
- 47) <sup>1</sup>H NMR spectroscopy and elemental analysis of **2E** revealed that 12% of **18E** was present in the sample prior to irradiation. To account for this, the absorbance due to **18E** was subtracted from the observed absorbance. The correction simply displaces curve and has no affect on the derived rate constants.

- 
- 48) Balzani, V.; Juris, A.; Venturi, M. *Chem. Rev.* **1996**, *96*, 759.
- 49) Yamagishi, A.; Naing, K.; Goto, Y.; Taniguchi, M.; Takahashi, M. *Dalton Trans.* **1994**, 2085.
- 50) (a) Herkstroeter, W. G.; Lamola, A. A.; Hammond, G. S. *J. Am. Chem. Soc.* **1964**, *86*, 4537-4540. (b) Subhas, C. B.; Mukherjee, R.; Chowdhury, M. J. *Chem. Phys.* **1969**, *51*, 754-761. (c) Wrighton, M. S.; Pdungsap, L.; Morse, D. L. *J. Phys. Chem.* **1975**, *79*, 66-71. (d) Flamigni, L.; Barigelletti, F.; Dellonte, S.; Orlandi, G. *J. Photochem.* **1983**, *21*, 237-244. (e) Darmanyan, A. P.; Foote, C. S.; Jardon, P. *J. Phys. Chem.* **1995**, *99*, 11854-11859. (f) Tokunaga, Y.; Akasaka, K.; Hisada, K.; Shimomura, Y.; Kakuchi, S. *Chem. Commun.* **2003**, *17*, 2250-2251. (g) Lopes, S.; Gomez-Zavaglia, A.; Lapinski, L.; Chattopadhyay, N.; Fausto, R. *J. Phys. Chem. A* **2004**, *108*, 8256-8263.
- 51) Samsonova, L. G.; Kopylova, T. N.; Svetlichnaya, N. N.; Andrienko, O. S. *High Energy Chem.* **2002**, *36*, 276-279.
- 52) The coefficient approximations were calculated using The Simple Huckel Molecular Orbital Theory Calculator at [www.chem.ucalgary.ca/SHMO](http://www.chem.ucalgary.ca/SHMO).
- 53) Bortolus, P.; Monti, S. *J. Phys. Chem.* **1979**, *83*, 648-652.
- 54) Schuster, D. I.; Nuber, B.; Vail, S. A.; MacMahon, S.; Lin, C.; Wilson, S. R.; Khong, A. *Photochem. Photobiol. Sci.*, **2003**, *2*, 315-321.
- 55) Rothe, C.; Palsson, L. O.; Monkman, A. P. *Chem. Phys.* **2002**, *285*, 95-101.
- 56) (a) Förster, Th. H. *Disc. Faraday Soc.* **1959**, *27*, 7-17. (b) Dexter, D. L. *J. Chem. Phys.* **1953**, *21*, 836-850. (c) Mondal, J. A.; Ramakrishna, G.; Singh, A. K.; Ghosh, H. N.; Mariappan, M.; Maiya, B. G.; Mukherjee, T.; Palit, D. K. *J. Phys. Chem. A* **2004**, *108*, 7843-7852.
- 57) Bergamini, G.; Ceroni, P.; Maestri, M.; Balzani, V.; Lee, S. K.; Vogtle, F. *Photochem. Photobiol. Sci.* **2004**, *3*, 898-905.

- 
- 58) Horn, D.; Rieger, J. *Angew. Chem. Int. Ed.* **2001**, *40*, 4330.
- 59) LaMer, V. K.; Dinegar, R. H. *J. Am. Chem. Soc.* **1950**, 4847-4854.
- 60) Boistelle, R.; Astier, J.P. *J. Cryst. Growth* **1988**, *90*, 14.
- 61) Ostwald, W. *Z. Phys. Chem.* **1897**, *22*, 289.
- 62) Cordaro, J.; McCusker, J.; Bergman, R. G. *Chem. Commun.* **2002**, 1496.
- 63) Ams, M. R. Masters Thesis, University of Pittsburgh, **2004**.
- 64) Cordaro, J.; McCusker, J.; Bergman, R. G. *Chem. Commun.* **2002**, 1496.